AD-A089 147 PRINCETON UNIV NJ DEPT OF MECHANICAL AND AEROSPACE --ETC F/G 1/4
DIGITAL FLIGHT CONTROL RESEARCH USING MICROPROCESSOR TECHNOLOGY--ETC(U)
MAY 80 R F STENGEL, J C SEAT, G E MILLER N00014-78-C-0257
UNCLASSIFIED MAE-1425 ONR-CR-300-003-1 NL

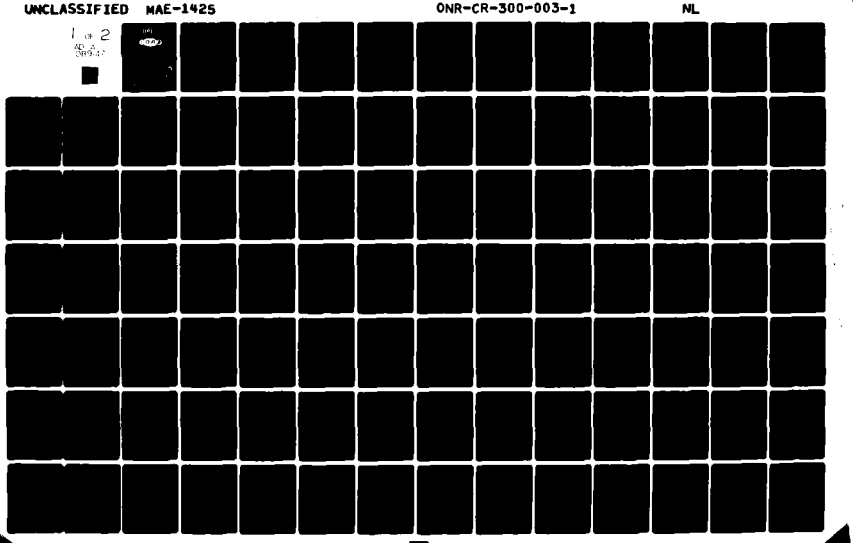

REPORT ONR-CR-300-003-1

LEVEL II

12

DIGITAL FLIGHT CONTROL RESEARCH USING MICROPROCESSOR TECHNOLOGY

ROBERT F. STENGEL
JAMES C. SEAT
GEORGE E. MILLER

FLIGHT RESEARCH LABORATORY
DEPARTMENT OF MECHANICAL AND AEROSPACE ENGINEERING
PRINCETON UNIVERSITY

PRINCETON, NEW JERSEY 08544
CONTRACT N00014-78-C-0257
ONR TASK 300-003

23 MAY 1980

ANNUAL TECHNICAL REPORT FOR PERIOD
1 FEBRUARY 1978 - 31 JANUARY 1979

PREPARED FOR THE
OFFICE OF NAVAL RESEARCH • 800 N. QUINCY ST. • ARLINGTON, VA. 22217

Organizations receiving reports on the initial distribution list should confirm correct address. This list is located at the end of the report. Any change of address of distribution should be conveyed to the Office of Naval Research, Code 211, Washington, D.C. 22217.

When this report is no longer needed, it may be transmitted to other authorized organizations. Do not return it to the originator or the monitoring office.

The findings in this report are not to be construed as an official Department of Defense or Military Department position unless so designated by other official documents.

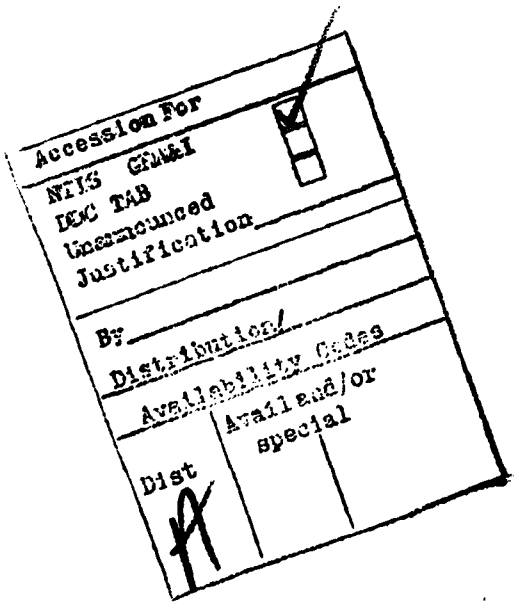

SECURITY CLASSIFICATION OF THIS PAGE (When Data Entered)

(19) REPORT DOCUMENTATION PAGE

READ INSTRUCTIONS BEFORE COMPLETING FORM

(18) 1. REPORT NUMBER: ONR-CR-300-003-1

2. GOVT ACCESSION NO.: AD-A089 147

3. RECIPIENT'S CATALOG NUMBER:

(1) 4. TITLE (and Subtitle): Digital Flight Control Research Using Microprocessor Technology,

(9) 5. TYPE OF REPORT & PERIOD COVERED: Annual Technical Report 1 Feb 78 - 31 Jan 79,

6. PERFORMING ORG. REPORT NUMBER: MAE Report No. 1425

(10) 7. AUTHOR(s): Robert F. Stengel, James C. Seat, George E. Miller

(15) 8. CONTRACT OR GRANT NUMBER(s): N00014-78-C-0257

9. PERFORMING ORGANIZATION NAME AND ADDRESS: Flight Research Laboratory, Department of Mechanical and Aerospace Engineering, Princeton University, James Forrestal Campus, Princeton, New Jersey 08544

10. PROGRAM ELEMENT, PROJECT, TASK AREA & WORK UNIT NUMBERS: ONR Task 300-003

11. CONTROLLING OFFICE NAME AND ADDRESS: Office of Naval Research, Code 211, 800 N. Quincy St., Arlington, VA 22217

(12) 1526 (11)

12. REPORT DATE: 23 May 80

13. NUMBER OF PAGES: 148

14. MONITORING AGENCY NAME & ADDRESS (if different from Controlling Office): (17) MAE-1425

15. SECURITY CLASS. (of this report): Unclassified

15a. DECLASSIFICATION/DOWNGRADING SCHEDULE:

16. DISTRIBUTION STATEMENT (of this Report)

Approved for public release; Distribution unlimited.

17. DISTRIBUTION STATEMENT (of the abstract entered in Block 20, if different from Report)

18. SUPPLEMENTARY NOTES

19. KEY WORDS (Continue on reverse side if necessary and identify by block number)

Aircraft flight control; digital control; aircraft flying qualities; modern control theory; atmospheric flight mechanics; flight testing techniques; microprocessor systems; variable-response research aircraft (VRA)

20. ABSTRACT (Continue on reverse side if necessary and identify by block number)

A digital flight control system based on microprocessor technology has been designed, developed, and flight tested in Princeton's Variable-Response Research Aircraft (VRA). The microprocessor-based digital flight control system (Micro-DFCS) works in conjunction with the VRA's existing fly-by-wire control system, and it is programmed to provide command and stability augmentation control laws formulated through modern control theory. The initial flight control computer program, CAS-1, provides

DD FORM 1 JAN 73 1473 EDITION OF 1 NOV 65 IS OBSOLETE S/N 0102-014-6601

Unclassified

SECURITY CLASSIFICATION OF THIS PAGE (When Data Entered)

A 10732 slk

direct, pitch rate, and normal acceleration command modes. The latter two closed-loop control laws are designed using sampled-data linear-quadratic regulator theory. The computer hardware and software are described, and initial flight test results are presented.

Flight test results are based on two longitudinal manual control tasks: tracking at altitude and approach and landing. They demonstrate the effects of varying sampling rate, computation delay, and control resolution on calibrated step response and on pilot opinion ratings. It is concluded that the human pilot can provide effective control with lower sampling rates and control resolution than might have been anticipated. The limiting values are task dependent, generally lying in the range of 5 to 10 samples per sec and 4- to 8-bit resolution. Flight test results with pure time delay tend to confirm earlier findings, i.e., that there is rapid degradation of pilot opinion as the delay increases beyond 0.2 sec. Further flight testing is warranted to improve statistical confidence and broaden the scope of these results.

ABSTRACT

A digital flight control system based on microprocessor technology has been designed, developed, and flight tested in Princeton's Variable-Response Research Aircraft (VRA). The microprocessor-based digital flight control system (Micro-DFCS) works in conjunction with the VRA's existing fly-by-wire control system, and it is programmed to provide command and stability augmentation control laws formulated through modern control theory. The initial flight control computer program, CAS-1, provides direct, pitch rate, and normal acceleration command modes. The latter two closed-loop control laws are designed using sampled-data linear-quadratic regulator theory. The computer hardware and software are described, and initial flight test results are presented.

Flight test results are based on two longitudinal manual control tasks: tracking at altitude and approach and landing. They demonstrate the effects of varying sampling rate, computation delay, and control resolution on calibrated step response and on pilot opinion ratings. It is concluded that the human pilot can provide effective control with lower sampling rates and control resolution than might have been anticipated. The limiting values are task dependent, generally lying in the range of 5 to 10 samples per sec and 4- to 8-bit resolution. Flight test results with pure time delay tend to confirm earlier findings, i.e., that there is rapid degradation of pilot opinion as the delay increases beyond 0.2 sec. Further flight testing is warranted to improve statistical confidence and broaden the scope of these results.

PREFACE

This investigation was conducted by the Flight Research Laboratory at Princeton University, Princeton, New Jersey from 1 February 1978 under Contract N00014-78-C-0257 for the Office of Naval Research, Washington, D. C. This report is the first annual technical report, and it includes results through 31 January 1979. The sponsoring office was the Vehicle Technology Program headed by Mr. David Siegel. Mr. Robert von Husen served as the Navy Technical Monitor for the program.

The principal investigator for the study was Professor Robert F. Stengel. He was assisted by W. Barry Nixon, senior technical staff member, George E. Miller, technical staff member, James C. Seat, graduate student, Barton C. Reavis, technical associate, and Donald Carter, electronic technician. M. E. Sandvik and S. Matarese typed the final report.

TABLE OF CONTENTS

TABLE OF CONTENTS

(cont.)

LIST OF FIGURES

LIST OF FIGURES

(cont.)

LIST OF TABLES

LIST OF SYMBOLS

Variables	Description
C	Optimal Gains
e	Naperian base (2.71828. . . . .)
F	System dynamics matrix (continuous-time system)
f	Frequency, Hz
$\underline{f}$	Nonlinear functions for vehicle equations of motion
G	Control effects matrix (continuous-time system)
g	Gravitational acceleration
H	• Observation matrix • Hexadecimal number
I	Identity matrix
J	Scalar cost functional
$L_{( )}$	Lift force stability-and-control derivative
$M_{( )}$	Pitch moment stability-and-control derivative
M	State/control weighting matrix
n_z	Normal acceleration, g units
P	• Riccati equation solution • State covariance matrix
p	Roll rate, deg/sec
Q	State weighting matrix
q	Pitch rate, deg/sec
R	Control weighting matrix
r	Yaw rate, deg/sec
S_{12}	Command input state matrix
S_{22}	Command input control matrix
s	Laplace transform variable

T	Sampling interval, sec
$TD_{(\ )}$	Axial stability-and-control derivative
t	Time, sec
u	x-axis velocity, ft/sec
$\underline{u}$	Control vector
V	Total velocity, ft/sec
v	y-axis velocity, ft/sec
W	• Implicit model-following weighting matrix • Disturbance covariance matrix
w	z-axis velocity, ft/sec
x	Axial position, ft
$\underline{x}$	State vector
y	Lateral position, ft
$\underline{Y}$	Command vector
Z	Aerodynamic force along the z-axis
z	Vertical position, ft

Variables (Greek)

α	Angle of attack, deg
Γ	Control effects matrix (discrete-time system)
γ	Vertical flight path angle, deg
δA	Aileron deflection, deg
δE	Elevator deflection, deg
δF	Flap deflection, deg
δR	Rudder deflection, deg
δS	Longitudinal stick deflection, deg
δSF	Side-force panel deflection, deg
δT	Throttle deflection percent
ζ	Damping ratio
θ	Pitch attitude angle, deg
λ	Eigenvalue

Σ	Summation
Φ	State transition matrix (discrete-time system)
ϕ	Roll attitude angle, deg
ψ	Yaw attitude angle, deg
ω_n	Natural frequency, rad/sec

Subscripts

CL	Closed-loop
d	Desired value
i	Element index for vectors and matrices
k	Sampling instant index
M	Model
o	Nominal value
q	Sensitivity to pitch rate
SP	Short-period
V	Sensitivity to total velocity
α	Sensitivity to angle of attack
δE	Sensitivity to elevator deflection

Punctuation

$(\dot{})$	Derivative of quantity with respect to time
$(\underline{\ })$	Vector quantity
$\delta(\ )/\delta(\ )$	Partial derivative of one variable with respect to another
$\Delta(\ )$	Perturbation variable
$(\ )^*$	Steady-state value
$(\ )^T$	Transpose of a vector or matrix
$(\ )^{-1}$	Inverse of a matrix
$(\hat{})$	Discrete weighting matrix

Acronyms

A/D	Analog-to-Digital
APL	A Programming Language
ASCII	American Standard Code for Information Interchange
CAS	Command Augmentation System
CDU	Control Display Unit
CPU	Central Processing Unit
D/A	Digital-to-Analog
DFCS	Digital Flight Control System
FBW	Fly-By-Wire
FCCU	Flight Control Computer Unit
FRL	Flight Research Laboratory
IAS	Indicated Air Speed
I/O	Input/Output
KIAS	Knots, Indicated Air Speed
LQ	Linear-Quadratic
Micro-DFCS	Microprocessor-based Digital Flight Control System
MSL	Mean Sea Level
PDM	Pulse Duration Modulation
PROM	Programmable Read-Only Memory
RAM	Random Access Memory
RF	Radio Frequency
SBC	Single Board Computer
sps	Samples per Second
VRA	Variable-Response Research Aircraft

1. INTRODUCTION

1.1 BACKGROUND

Research which anticipates the capabilities of emerging flight control technologies and establishes corresponding flight control system criteria plays a vital role in maintaining aeronautical progress. The needed research can begin on paper, but experiment and demonstration in flight are necessary for a full understanding of the relationships between control theory and practice.

Modern control theory and digital microprocessors represent two emerging technologies in the flight control context, and both must be tested in flight as a logical step to acceptance. Although "modern" control theory -- which combines state space, time domain, and optimal control concepts with earlier frequency domain methods -- has been with us for about two decades, there have been few applications of this theory to the flight-critical control of actual aircraft. (References 1 to 4 document programs that have used modern control laws in flight, and there may be other examples not cited here.) The commercial availability of single-board microcomputers is sufficiently recent that the application of microprocessors to flight control still is in its infancy. Past digital flight control programs (e.g., Ref. 2 to 9) have used pre-LSI electronic technology, setting the stage for the developments which follow.

The Flight Research Laboratory at Princeton University is engaged in a multi-faceted program whose principal objectives are to develop new methodologies for the analysis, design, and flight evaluation of digital control laws, to define microcomputer architectures and software structures for reliable flight control, and to demonstrate

the operation of digital control laws in flight. Control laws are being developed using "direct digital synthesis", i.e., the application of optimal sampled-data control theory to the aircraft control problem, and are being implemented in a microprocessor-based digital flight control system (Micro-DFCS), which has been assembled from commercially available components. These control laws are being flight tested using the Micro-DFCS and Princeton's Variable-Response Research Aircraft (VRA), Navion N91566 (Fig. 1). This report describes the Model 1 Micro-DFCS and its software, as well as presenting some results from the VRA's first flights using the Micro-DFCS for longitudinal control.

1.2 ORGANIZATION OF THE REPORT

Chapter 2 presents the sampled-data linear-quadratic regulator theory that has been used to design the CAS-1 control laws, as well as examples of the VRA's predicted closed-loop response. The effects of various cost function weights are noted, and an implicit model-following example is presented. Implementation of the control laws and hybrid simulation results are presented in Chapter 3. Micro-DFCS equipment and CAS-1 software are described, and the results of controlling an analog computer simulation of the VRA with the Micro-DFCS are shown. Chapter 4 treats flight test results, including the effects of sampling rate, time delay, and quantization during two manual control tasks: tracking at altitude, as well as approach and landing. Conclusions and recommendations are contained in Chapter 5. Five Appendices describe the VRA, Micro-DFCS hardware, Micro-DFCS software, APL control design programs, and the discrete-time implicit model-following algorithm.

2. DEVELOPMENT OF THE CONTROL LAW

This chapter describes the optimal control theory, control design objectives, and analytical results for the Micro-DFCS. Pitch rate and normal acceleration command control laws are developed with a second-order reduced model of the VRA, and an implicit model following example is presented.

2.1 DERIVATION OF THE TYPE 0 DIGITAL CAS

The development of the digital CAS in this report used sampled-data regulator theory. In this case, the selected control law drives a continuous system using piecewise-constant inputs that change only at the sampling intervals (zero-order hold). The objective of the sampled-data regulator is to control the system to be as close as possible to the trajectory obtained by using a continuous controller (Ref. 10). The derivation proceeds as follows.

The design of the digital CAS starts with specification of the continuous-time system dynamics. Neglecting disturbance inputs, the non-linear equations of motion for the flight vehicle can be written as a vector differential equation:

$$\dot{\underline{x}}(t) = \underline{f}[\underline{x}(t), \underline{u}(t)] \qquad (1)$$

The n-dimensional state vector $\underline{x}(t)$ specifically contains three components each of translational rate, translational position, angular rate, and angular attitude,

$$\underline{x}^T = [u\ v\ w\ x\ y\ z\ p\ q\ r\ \phi\ \theta\ \psi] \qquad (2)$$

where (u, v, w) are body-axis velocities, (x, y, z) are earth-relative

positions, (p, q, r) are body-axis rotational rates, and (ϕ, θ, ψ) are Euler angles of the body-axes with respect to the earth-fixed frame. The m-dimensional control vector $\underline{u}(t)$ includes deflections of the elevator, throttle, flaps, ailerons, rudder, and side force panels;

$$\underline{u}^T = [\delta E \ \delta T \ \delta F \ \delta A \ \delta R \ \delta SF] \tag{3}$$

In order to linearize the equations for use in designing the control laws, it is necessary to divide the states and controls into nominal and perturbation components,

$$\underline{x}(t) = \underline{x}_o(t) + \Delta\underline{x}(t) \tag{4}$$

$$\underline{u}(t) = \underline{u}_o(t) + \Delta\underline{u}(t) \tag{5}$$

The linearization is accomplished by expanding Eq. 1 in a Taylor series and retaining only first-degree terms:

$$\dot{\underline{x}}_o(t) = \underline{f}\,[\underline{x}_o(t), \underline{u}_o(t)\,] \tag{6}$$

$$\Delta\dot{\underline{x}}(t) = F(t)\ \Delta\underline{x}(t) + G(t)\ \Delta\underline{u}(t) \tag{7}$$

where

$$F(t) = \frac{\partial}{\partial\underline{x}}\,\underline{f}\,[\underline{x}_o(t), \underline{u}_o(t)] \tag{8}$$

$$G(t) = \frac{\partial}{\partial\underline{u}}\,\underline{f}\,[\underline{x}_o(t), \underline{u}_o(t)] \tag{9}$$

The F matrix is (n x n) and is referred to as the system dynamics matrix. G is (n x m) and is called the control effects matrix. The calculation of $\underline{x}_o$ is still a non-linear problem, so the CAS is designed with one specific $\underline{x}_o$ in mind. F(t) and G(t) are functions of $\underline{x}_o$ and $\underline{u}_o$; as long as the vehicle flies within close proximity to the

flight condition specified, F(t) and G(t) change very little (Ref. 11). This leads to control laws based on linear-time-invariant models which could be adapted to changing flight conditions by gain scheduling.

The linear differential equations of motion (Eq. 7) can be converted to difference equations, which take the form,

$$\Delta \underline{x}_{k+1} = \Phi \, \Delta \underline{x}_k + \Gamma \, \Delta \underline{u}_k \tag{10}$$

where Φ is the aircraft's state transition matrix and Γ is the discrete control effects matrix. Φ can be expressed as

$$\Phi = e^{FT} = I + FT + \frac{(FT)^2}{2} + \frac{(FT)^3}{6} + \ldots \tag{11}$$

Assuming that the control is fixed between sampling intervals,

$$\Gamma = \Phi F^{-1}(I - \Phi^{-1}) \, G$$

$$= \Phi[T(I\frac{FT}{2} + \frac{F^2T^2}{6} - \ldots.)] \, G \, , \; T = \text{sampling interval} \tag{12}$$

To complete the state-space representation of the aircraft's dynamics, the output of the system is defined as

$$\Delta \underline{y}_k = H_x \, \Delta \underline{x}_k + H_u \, \Delta \underline{u}_k \tag{13}$$

As shown below, the Type 0 control law takes the form

$$\Delta \underline{u}_k - \Delta \underline{u}_k^* = - C \, (\Delta \underline{x}_k - \Delta \underline{x}_k^*) \tag{14}$$

where a starred vector represents the steady-state value of the vector which corresponds to the pilot input at the k^{th} sampling instant. Examining Eq. 14, it is seen that when $\Delta \underline{x}_k$ reaches its steady-state value, the output of the controller, $\Delta \underline{y}_k$, will be equal to the proper steady-state

deflections. The steady-state vectors $\Delta\underline{x}^*$ and $\Delta\underline{u}^*$ are functions only of the pilot's commanded inputs and are independent of what feedback gains are used or how the loop is closed. They are simply the calculated values of $\Delta\underline{x}_k$ and $\Delta\underline{u}_k$ corresponding to a particular commanded input, $\Delta\underline{y}_k$.

The states or controls to be commanded by the pilot are specified in the control law by defining values for H_x and H_u of the output equation, Eq. 13. In this way, the pilot's inputs are defined as the system's outputs to be controlled by the CAS. In other words, the aircraft's motions are the variables commanded by the pilot's controls rather than the control surface positions. Since the pilot's inputs will be considered the system's outputs after the selection of H_x and H_u, Eq. 13 can be rewritten

$$\Delta\underline{y}_k^* = H_x\,\Delta\underline{x}_k^* + H_u\,\Delta\underline{u}_k^* \tag{15}$$

where $\Delta\underline{y}_k^*$ contains the pilot's commanded inputs.

The relations between $\Delta\underline{y}_k^*$, $\Delta\underline{x}^*$, and $\Delta\underline{u}^*$ are described by Eqs. 7 and 15 when $\dot{\underline{x}} = 0$, defining the trim point:

$$\begin{bmatrix} (\Phi-I) & \Gamma \\ H_x & H_u \end{bmatrix} \begin{bmatrix} \Delta\underline{x}^* \\ \Delta\underline{u}^* \end{bmatrix}_k \simeq \begin{bmatrix} F & G \\ H_x & H_u \end{bmatrix} \begin{bmatrix} \Delta\underline{x}^* \\ \Delta\underline{u}^* \end{bmatrix}_k = \begin{bmatrix} 0 \\ \Delta\underline{y}_k \end{bmatrix} \tag{16}$$

If the number of commands and controls is equal, and the compound matrix in Eq. 16 is nonsingular, then it can be inverted, and $\Delta\underline{x}^*$ and $\Delta\underline{u}^*$ are defined by

$$\begin{bmatrix} \Delta\underline{x}^* \\ \Delta\underline{u}^* \end{bmatrix}_k = \begin{bmatrix} F & G \\ H_x & H_u \end{bmatrix}^{-1} \begin{bmatrix} 0 \\ \Delta\underline{y}_k^* \end{bmatrix} = \begin{bmatrix} S_{11} & S_{12} \\ S_{21} & S_{22} \end{bmatrix} \begin{bmatrix} 0 \\ \Delta\underline{y}_k^* \end{bmatrix} \tag{17}$$

or

$$\Delta \underline{x}_k^* = - F^{-1}G(-H_x F^{-1}G + H_u)^{-1} \Delta \underline{y}_k^* \tag{18}$$

$$\Delta \underline{u}_k^* = (-H_x F^{-1}G + H_u)^{-1} \Delta \underline{y}_k^* \tag{19}$$

Equations 18 and 19 also can be expressed as

$$\Delta \underline{x}_k^* = S_{12} \Delta \underline{y}_k^* \tag{20}$$

$$\Delta \underline{u}_k^* = S_{22} \Delta \underline{y}_k^* \tag{21}$$

Substituting Eqs. 20 and 21 into Eq. 14 and rearranging, the control inputs (as functions of the pilot's inputs) are

$$\Delta \underline{u}_k = S_{22}\Delta \underline{y}_k^* - C(\Delta \underline{x}_k - S_{12}\Delta \underline{y}_k^*) \tag{22}$$

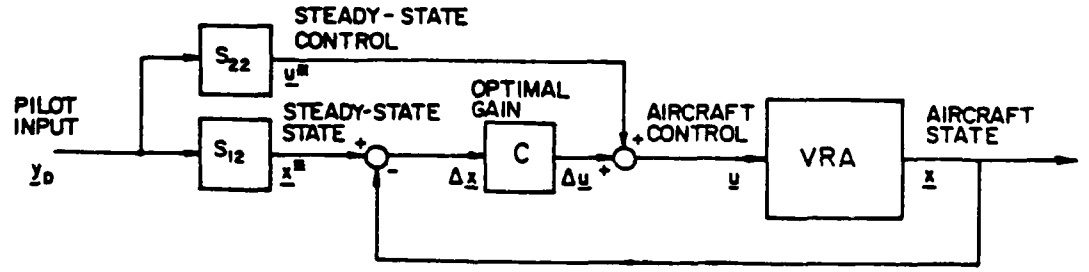

Figure 2-1. Type 0 CAS Structure obtained from the LQ Regulator.

It is interesting to note that due to the feedforward of $\Delta \underline{y}_k^*$ through S_{22}, it is possible to have zero "hang-off" (or steady-state) error even though this is a Type 0 system. A condition of zero hang-off depends, however, on there being no disturbances and knowing the exact system parameters when calculating S_{12} and S_{22}.

The gains, C, are calculated using LQ regulator theory. The objective of this method is to find the feedback gains which allow the control law to minimize the continuous-time quadratic cost functional (Ref. 12),

$$J = \int_0^\infty (\Delta\underline{x}^T Q \Delta\underline{x} + \Delta\underline{u}^T R \Delta\underline{u})\, dt \tag{23}$$

where Q is a positive semi-definite symmetric matrix and R is a positive definite symmetric matrix. Q and R weight the importance of suppressing perturbations from the commanded (i.e., steady-state) values of states and controls; therefore, Q and R can be used as design parameters to provide flexible and efficient means of changing closed-loop response to satisfy the response criteria.

An equivalent discrete-time cost functional can be written as

$$J = \sum_{k=0}^{N-1} (\Delta\underline{x}_k^T Q \Delta\underline{x}_k + \Delta\underline{u}_k^T R \Delta\underline{u}_k) \tag{24}$$

This cost functional observes the state and control only at discrete instants; the system response between samples is neglected, leading to the possibility of "intersample ripple" in the closed-loop response. Reference 12 outlines a method of picking continuous-time weighting matrices that minimize the continuous-time cost functional even though a discrete-time regulator is used. In this case, the cost functional for the sampled-data case penalizes the system continuously in time, i.e., not just at the sampling instances, by taking into account the state transition properties expressed by Eq. 10. Minimizing a continuous cost functional with a sampled-data regulator is equivalent to making the state trajectory obtained from the digital CAS as close as possible to that obtained with a continuous controller. Using the method of Ref. 12, Eq. 23 is set equal to the sampled-data cost functional

$$J = \sum_{k=0}^{\infty} (\Delta\underline{x}_k^T \hat{Q} \Delta\underline{x}_k + Q \Delta\underline{x}_k^T \hat{M} \Delta\underline{u}_k + \Delta\underline{u}_k^T \hat{R} \Delta\underline{u}_k) \tag{25}$$

The discrete weighting matrices are found to be

$$\hat{Q} = \int_{t_k}^{t_{k+1}} \Phi^T(T)\ Q\ \Phi(T)dt \tag{26}$$

$$\hat{M}^T = \int_{t_k}^{t_{k+1}} \Phi^T(T)\ Q\ \Gamma(T)dt \tag{27}$$

$$\hat{R} = \int_{t_k}^{t_{k+1}} [R + \Gamma^T(T)\ Q\ \Gamma(T)]\ dt \tag{28}$$

The matrices Q and R are, respectively, positive semi-definite and positive definite. The gain matrix, C, is given by

$$C = (\hat{R} + \Gamma^T P \Gamma)^{-1}(\Gamma^T P \Phi + \hat{M}) \tag{29}$$

where P is the steady-state solution of a discrete-time Riccati equation:

$$P = \Phi^T P \Phi - (\Gamma^T P \Phi + \hat{M})^T (\hat{R} + \Gamma^T P \Gamma)^{-1}(\Gamma^T P \Phi + \hat{M}) + \hat{Q} \tag{30}$$

To find C for a certain Q and R, $\hat{Q}$, $\hat{M}$ and $\hat{R}$ must be calculated using Eq. 26 - 28. The Riccati equation then is solved, and these results are used in Eq. 29 to compute C.

In summary, this section has presented a way to control a continuous-time system with a discrete-time Type 0 CAS. The weighting matrices Q and R can be specified for a continuous-time cost functional but implemented with a discrete-time control law (Eq. 22). This is easier than trying to specify $\hat{Q}$, $\hat{M}$, and $\hat{R}$ directly, because Q and R can be based on an intuitive understanding of the continuous-time problem. This feature is used to advantage in designing the present control law.

2.2 EFFECTS OF THE SAMPLING INTERVAL

One approach to digital control design is to formulate the equivalent analog controller and use its gains in the digital system. High sampling rates are required to minimize the phase lag associated with sampling and holding the continuous signals. Reference 13 presents a graph (Fig. 2-2) that shows the relation between phase lag and sampling frequency when the signal is first passed through a second-order low-pass filter with 20 dB attenuation at the sampling frequency, f_{sample}.

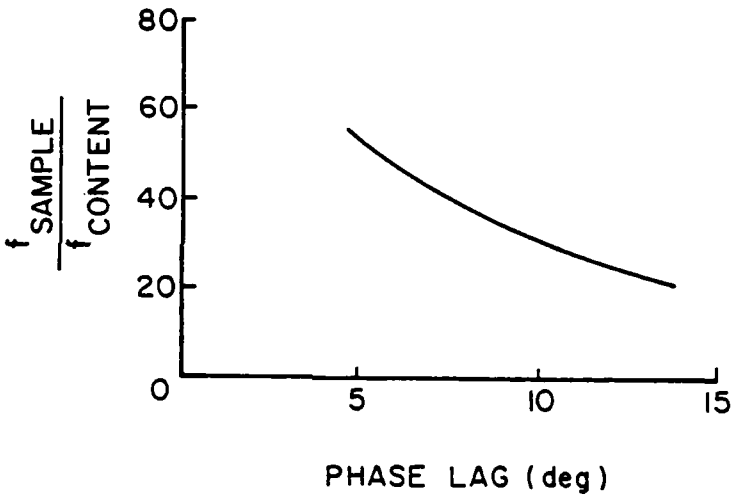

Figure 2-2. Frequency Ratio vs. Phase Lag for 20 dB Attenuation, (from Ref. 13).

For instance, if a phase shift of 10 deg is tolerable, the figure indicates that the sampling frequency should be approximately 30 times the highest frequency of interest.

The effects of phase lag due to sampling are considerably reduced by the sampled-data regulator because it is formulated using a discrete-time model of aircraft dynamics (Eq. 10) and its cost function accounts for response between samples (Eq. 25).

Nevertheless, there is a maximum value for the control sampling interval of any given system, which is largely dependent on error build-up between samples and pilot acceptance. These two limiting factors are explained below.

2.2.1 Error Build Up Between Samples

If there were no feedback measurement errors or disturbance inputs to the system and if the dynamic and control parameters of the system were known exactly, then the discrete-time model of the system would predict its response precisely for any sampling interval. With disturbances and parameter variations, errors between the predicted and actual states of the aircraft can build up while the system is running "open-loop" between the discrete control inputs. Therefore, the sampling interval should be selected so that intersample error growth is limited to acceptable values under "worst case" conditions (Ref. 14). Assuming that disturbances are gaussian with covariance matrix W, the error build up can be described by propagating the state covariance matrix, P, with the differential equation,

$$\dot{P}(t) = FP(t) + P(t)F^T + W \ , \ P(0) = 0 \qquad (31)$$

The sampling interval is chosen as the time at which the first element of P (t) reaches its maximum allowable value. Note that open-loop instability, turbulence or command levels, and estimation uncertainties can be introduced thru F, W, and P(0), respectively.

As a practical matter, too long a sampling interval can lead to large control change increments, which may be damaging to the control surface actuators and associated mechanisms. These large changes are commanded instantaneously, causing the actuators to deflect the controls at maximun rate. The quick, pulsing movements could set up vibrations

and high stresses on the actuators and linkage, effectively reducing the operating life of these components.

2.2.2 Pilot Acceptance

Because a DFCS changes its output only at discrete instants, aircraft response to pilot commands may not be instantaneous. The pilot may have a tendency to over-control because the time delay makes it seem that a certain stick movement is not enough, and he may experience difficulty in maintaining precise control. The lower limit on sampling rate for pilot acceptance can be found only by actual flight tests, in which the pilot can evaluate the aircraft's handling qualities for different DFCS sampling rates.

The one constraint of the two listed above which puts the lowest upper limit on the sampling interval determines the slowest allowable sampling rate for the system. In general, this rate is much lower than that dictated by the phase lag of a digitized analog system, appearing in the neighborhood of 10 sps for this study.

2.3 CONTROL OBJECTIVES AND FLYING QUALITIES CRITERIA

Several attributes of the control design procedure described in Section 2.1 are particularly useful in the flight control application. Linear algebra and the use of a general-purpose computer allows multi-input-output systems to be designed with the same level of ease regardless of the number of inputs and outputs (assuming observability and controllability criteria are met). Once the necessary computer programs are perfected, it is a straightforward process to design a controller, given the parameters and constraints on the system. LQ design is a time-domain procedure. Time histories are easy to obtain once the state transition and discrete control effects matrix are calculated. These are helpful because state and control trajectories can be evaluated directly. Decoupling of the pilot's inputs is another benefit;

minimizing the quadratic cost functional tends to suppress perturbations in states not commanded by the pilot. Because the control law minimizes a quadratic functional of state and control perturbations, it guarantees closed-loop stability when certain design criteria are met (Ref. 15).

The main difficulty of LQ control theory comes from the need to define what is "optimal". It is necessary to reduce performance requirements to a single index which is quadratic in states and controls. Direct relationships between these quadratic weightings and the more general control design specifications are not obvious (Ref. 16). As general control design specifications generally are not obvious (Ref. 16). As a result, it usually is necessary to go through a trial-and-error sequence until the time response and closed-loop eigenvalues are acceptable. This is not necessarily a time consuming or expensive process, but it is a limitation of the design approach.

improve the response of the commanded state to a step input from the pilot, as determined, for example, by comparison with the "Level 1" flying quality specifications for the short-period as defined by MIL-F-878SB(ASG) (Ref. 17). The specifications for short-period in the Military Specification on Flying Qualities are stated as constraints on the natural frequency and damping of that mode. For cruise, the minimum damping ratio is 0.3 and the maximum is 2.0. Natural frequency limitations are expressed in a graph with $\omega_{n_{sp}}$ related to normal acceleration (n_z) per angle of attack (α) (Fig. 2.3). The unaugmented VRA characteristic is seen to be in the Level 1 flying qualities area; hence, the design objectives for the current controller are to demonstrate the ability to shift characteristics within Level 1 boundaries using the digital controller. The LQ regulator presented in Section 2.1 tends to decrease rise time and overshoot, and it is this design approach which has been carried through flight test. Section 2.6 demonstrates that the opposite effects can be achieved using a technique known as LQ implicit model following.

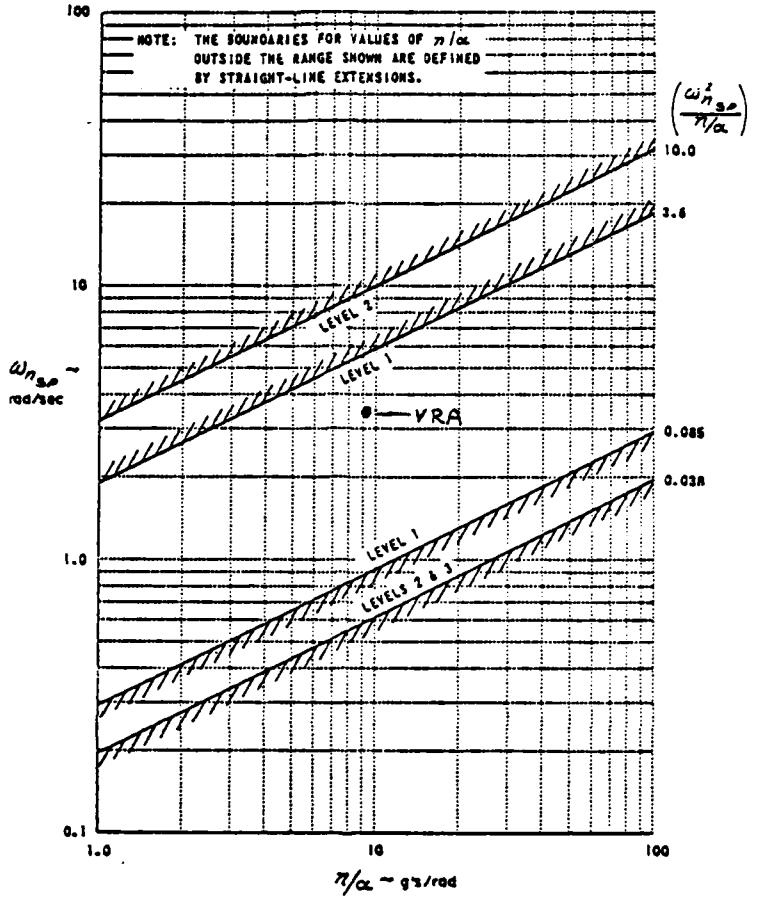

Figure 2-3. Short-Period Frequency Requirements - Category B Flight Phase.

2.4 PITCH RATE COMMAND CONTROL STRUCTURE

Pitch rate (q) is a desirable state for longitudinal stick (δS) to command because at low speeds, when performing a typical tracking task, q is the motion cue most apparent to the pilot in response to a deflection of δS. The simple Type 0 control law derived in Section 2.1 is now applied so that the response of Δq to $\Delta\delta S$ can be modified as required. The procedure begins by reviewing the dynamics which give rise to changes in q. The longitudinal and lateral-

directional dynamics can be assumed uncoupled in straight-and-level flight, so the perturbation state and control vectors derived from Eq. 2 and 3 reduce to

$$\Delta\underline{x}^T = [\Delta u \ \Delta w \ \Delta q \ \Delta\theta] \tag{32}$$

$$\Delta\underline{u}^T = [\Delta\delta E \ \Delta\delta T \ \Delta\delta F] \tag{33}$$

If $\underline{x}$ is redefined as

$$\Delta\underline{x}^T = [\Delta V \ \Delta\gamma \ \Delta q \ \Delta\alpha] \tag{34}$$

with velocity, ΔV, flight path angle, $\Delta\gamma$, and angle of attack, $\Delta\alpha$, a natural separation of long-period (phugoid mode) and short-period motions can be identified. The fundamental matrix associated with this state vector is

$$F = \begin{bmatrix} TD_V & -g\cos\gamma_o & TD_q & TD_\alpha \\ L_V/V_o & (g/V_o)\sin\gamma_o & L_q/V_o & L_\alpha/V_o \\ M_V & 0 & M_q & M_\alpha \\ -L_V/V_o & (-g/V_o)\sin\gamma_o & (1-L_q/V_o) & -L_\alpha/V_o \end{bmatrix} \tag{35}$$

At an airspeed of 105 kt in straight-and-level flight, the VRA's fundamental matrix is

$$F = \begin{bmatrix} -.073 & -32.2 & 0 & 26.2 \\ .002 & 0 & 0 & 2 \\ .002 & 0 & -2.08 & -8.35 \\ -.002 & 0 & 1. & -2. \end{bmatrix} \tag{36}$$

where angles are measured in radians, velocity in fps, and acceleration is in fps^2. F can be divided into four (2 x 2) matrices that contain

the parameters for the short period and phugoid modes:

$$F = \left[\begin{array}{c|c} \begin{array}{l}\text{Phugoid}\\ \text{Parameters}\end{array} & \begin{array}{c}\text{Short Period}\\ \text{-to-}\\ \text{Phugoid Coupling}\end{array} \\ \hline \begin{array}{l}\text{Phugoid-to-}\\ \text{Short Period}\\ \text{Coupling}\end{array} & \begin{array}{l}\text{Short Period}\\ \text{Parameters}\end{array} \end{array}\right] \qquad (37)$$

Since the off-diagonal matrices have elements with values near zero, the association of state variables with dynamic modes is apparent. The short period is described primarily by changes in Δq and $\Delta\alpha$, and the phugoid is described by changes in ΔV and $\Delta\gamma$. This implies that control of Δq response can be analyzed using a reduced second-order model of the VRA, defined by the (2 x 2) sub-matrix of Eq. 37 with the short period parameters. The controls vector is reduced to δE in order to simplify the initial control law design. The G matrix is (2 x 1) and has the elements

$$G = \begin{bmatrix} M_{\delta E} \\ -L_{\delta E}/V_o \end{bmatrix} = \begin{bmatrix} -12.5 \\ -.125 \end{bmatrix} \qquad (38)$$

for the 105-KIAS flight condition. The resulting model used for the design of the pitch rate controller is

$$\begin{bmatrix} \Delta\dot{q} \\ \Delta\dot{\alpha} \end{bmatrix} = \begin{bmatrix} -2.08 & -8.35 \\ 1 & -2 \end{bmatrix} \begin{bmatrix} \Delta q \\ \Delta\alpha \end{bmatrix} + \begin{bmatrix} -12.5 \\ -.125 \end{bmatrix} \Delta\delta E \qquad (39)$$

$$\Delta\underline{y} = H_x\, \Delta\underline{x} + H_u\, \Delta\delta E \qquad (40)$$

The reduced-order VRA dynamics along with a choice of weighting matrices, Q and R, can be used to generate the feedback gains, C, and matrices, S_{12} and S_{22}. Appendix B contains an explanation of the APL functions used to find and evaluate C, S_{12}, and S_{22}. The procedure is as shown in Fig. 2-4. First, matrices H_x and H_u are defined to specify what variables the pilot will command with δS. In this case,

$$H_x = [1\ 0] \tag{41}$$

$$H_u = 0 \tag{42}$$

The sampling rate is chosen next because it is used in Eq. 11 and 12 to find Φ and Γ. S_{12} and S_{22} then are calculated from Eq. 18 and 19, as they depend on H_x, H_u, Φ, and Γ. For the pitch rate CAS, these matrices are

$$S_{12} = \begin{bmatrix} 1 \\ .5 \end{bmatrix}, \quad S_{22} = -.5$$

and they are independent of Q and R. Choosing Q and R sets the closed-loop response of the system, and changing the elements of these matrices allows the desired response to be attained. An appropriate starting choice for the weighting factors in Q and R is the inverse of the maximum allowable mean-square values of the states and control:

$$Q = \begin{bmatrix} 1/\Delta q^2 & 0 \\ 0 & 1/\Delta\alpha^2 \end{bmatrix}_{max}, \quad R = 1/\Delta\delta E^2_{max} \tag{43),(44}$$

In the iterative technique of developing the desired time response, the weighting factors can be made higher or lower than the initial set as necessary. Matrices $\hat{Q}$, $\hat{R}$, and $\hat{M}$ are found by performing an Euler integration of Eq. 26-28. The Riccati equation (Eq. 30) is solved,

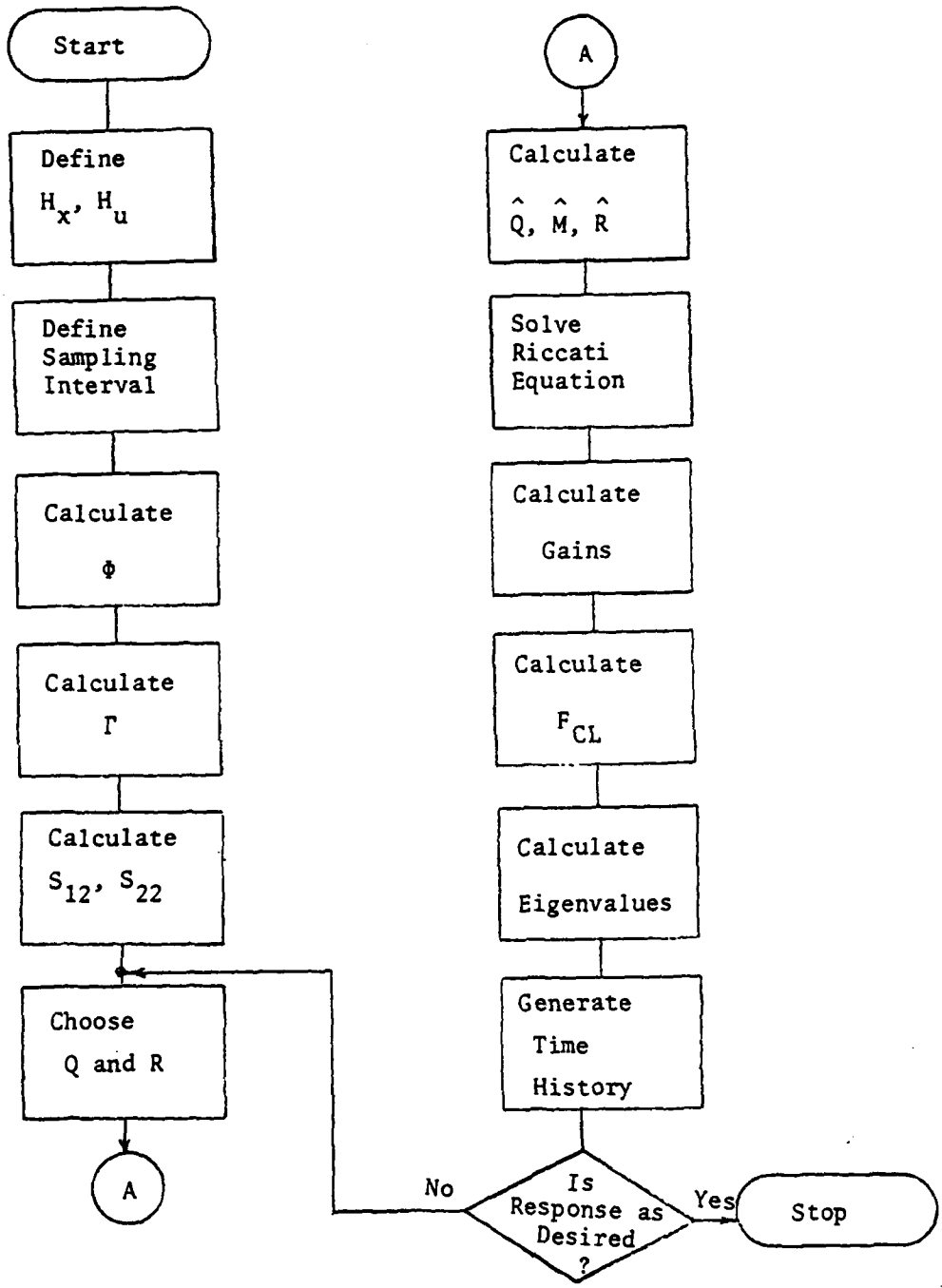

Figure 2-4. Sequence for Finding Optimal Gains.

yielding the matrix P necessary to derive the gains from Eq. 29. The closed-loop fundamental matrix, F_{CL}, is the continuous-time equivalent of Φ_{CL}; it can be calculated from the series expansion of the matrix logarithm of the closed-loop state (Ref. 14) transition matrix:

$$F_{CL} = \frac{1}{T} \ln \Phi_{CL} \tag{45}$$

or

$$F_{CL} = \frac{1}{T} [(\Phi_{CL}-I) - 1/2(\Phi_{CL}-I)^2 + 1/3 (\Phi_{CL}-1)^3 - \ldots] \tag{46}$$

where Φ_{CL} is simply

$$\Phi_{CL} = \Phi - \Gamma C \tag{47}$$

The equivalent continuous-time eigenvalues of the closed-loop system are the roots of the characteristic equation specified by the determinant

$$|sI - F_{CL}| = 0 \tag{48}$$

Time histories are generated using Eq. 10 and 14. If the time response and closed-loop eigenvalues do not show the desired response, it is necessary to revise the matrices Q and R.

It is possible to determine an empirical relationship between quadratic weightings and time response characteristics for a given dynamic system. The particular relationship between fourth-order VRA response to a step input (measured in time to rise to 95 percent of commanded value, and percent overshoot of commanded value) and the second-order weighting elements of Q is shown in Fig. 2-5. R is held constant, with a value of $1/(.17\text{rad})^2 = 32.8$, and the sampling rate is 10 sps. The curves radiating outward correspond to decreasing rise

times and increasing initial control deflections. The straight lines intersecting the origin represent decreasing overshoots when approaching the Δq axis. The dotted line represents the approximate boundary between closed-loop systems with complex eigenvalues (below the line) and real eigenvalues. Figure 2-5 was generated by crossplotting points from 25 design cases, so the information presented cannot be taken as exact; however, the general relationship is as shown. The relationship between weightings and response is virtually independent of sampling rate for rates above a few per sec; therefore, Fig. 2-5 can be used for sampling rates other than 10 sps. Control gains change with sampling rate to achieve this insensitivity, and effects of the control the sample-and-hold process become apparent at very low rates.

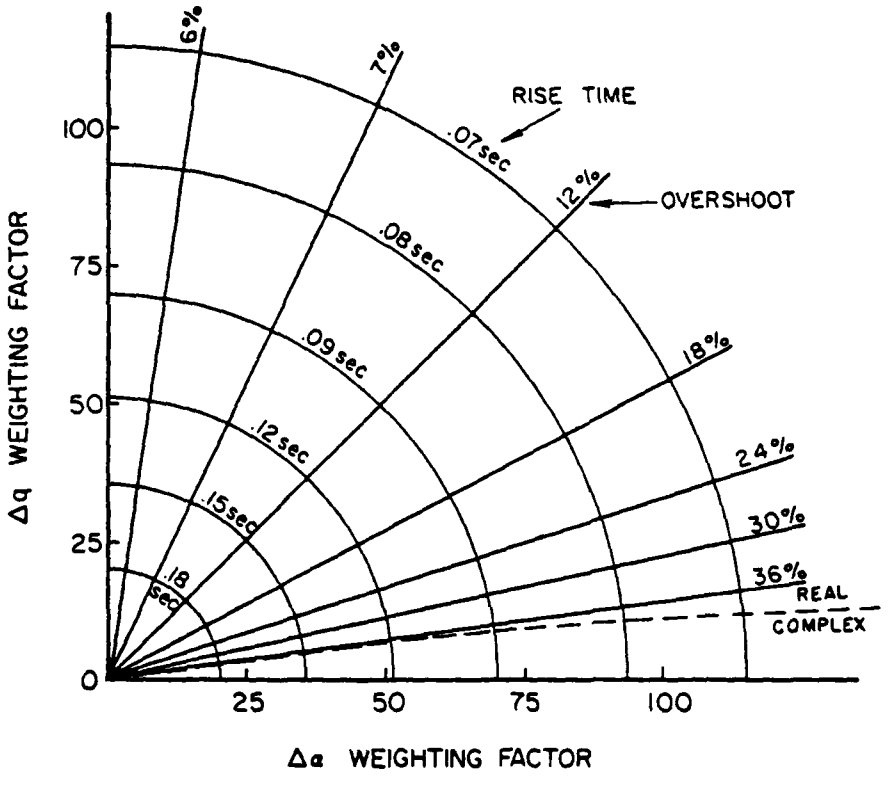

Figure 2-5. Relation Between Second-Order Weighting and Fourth-Order Time Response -- q CAS.

Time history plots for a few representative weightings have been generated using a digital computer (Figs. 2-6 through 2-11). In each case, a step input of 5 deg/sec is commanded; the two-state controller is used in conjuction with a fourth-order model of the VRA's longitudinal dynamics. The Δq response of the unaugmented aircraft (Fig. 2-6) has a 47.5-percent overshoot and 0.19-sec rise time. As the velocity decreases, Δq falls off because there is no throttle input. Angle of attack shows the expected initial increase as the phugoid oscillation sets in. Closed-loop control with a Q matrix of (25,25) causes a decrease in rise time and overshoot of the Δq response (Fig. 2-7). Because the CAS is Type 0 and there is no feedback to throttle, Δq eventually decreases, but not quite as much as in the open-loop case. The elevator initially attains a large deflection to improve rise time, then decreases to damp the transient.

The plots for weightings of (50,50) and (75,25) (Fig. 2-8 and 2-9) show quickened time response with increased initial elevator deflection. The time responses with weightings (25,25) and (75,25) also are plotted (Fig. 2-10 and 2-11) for a sampling rate of 20 sps. It can be seen that the pitch rate responses are virtually identical to the 10 sps plots of the same weightings.

The gains, resulting step responses, and closed-loop eigenvalues obtained from the simulation are given in Table 2-1. A negative gain implies negative feedback while positive gains give positive feedback. The phugoid eigenvalues change very little due to the weak coupling between short-period and phugoid modes and the absence of V-γ feedback. The $\omega_{n_{sp}}$ is increased from the open-loop value of 3.54 rad/sec (Table 2-2) for the 3 weightings examined. This increase is linked to the decrease in rise time for the commanded state, Δq. Figure 2-3 indicates that the closed-loop $\omega_{n_{sp}}$ for weightings of (50,50) and (75,75) is outside the Level 1 area for n/α constant at 9.3 g/rad.

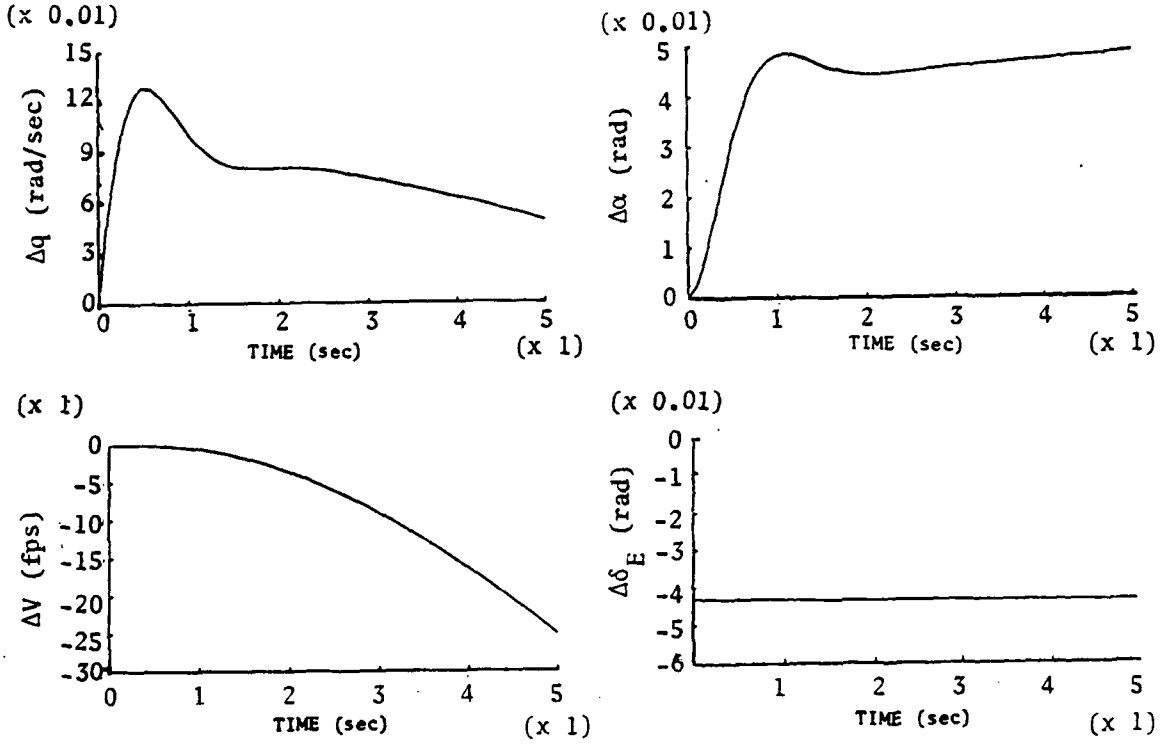

Figure 2-6. Open-Loop Step Response for $\Delta q^* = 5^o$/sec (105 KIAS).

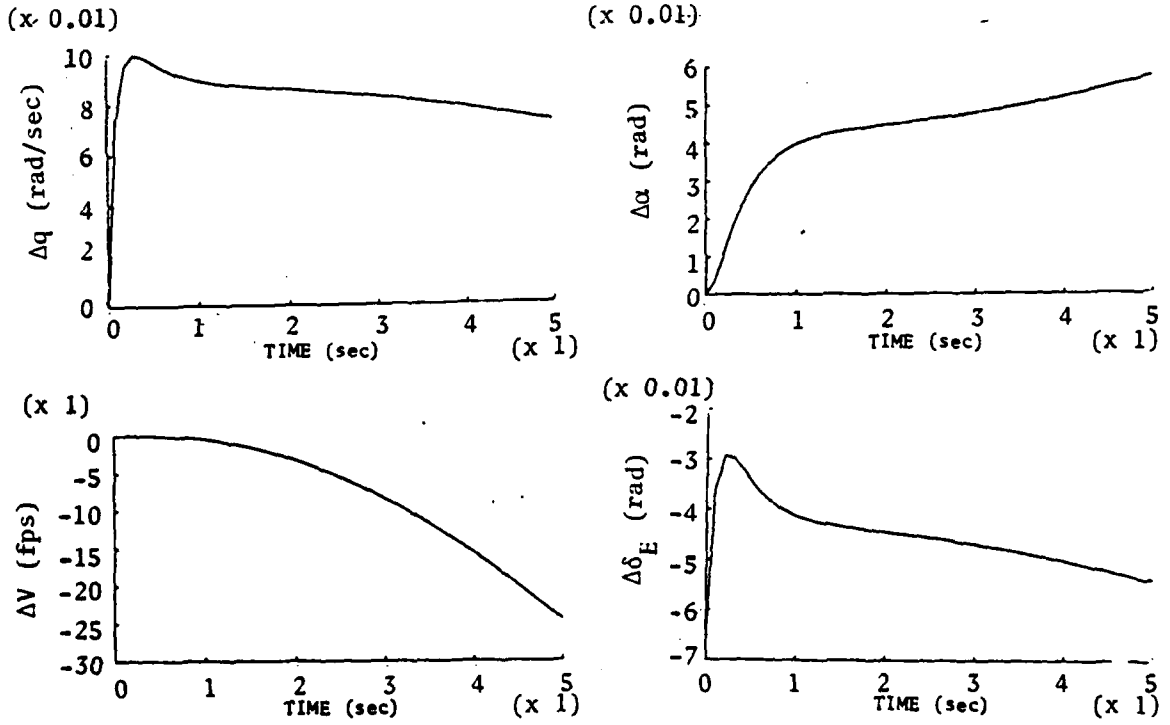

Figure 2-7. Pitch Rate Command Step Response for Diag Q = (25,25) ($q^* = 5^o$/sec, 10 sps, 105 KIAS).

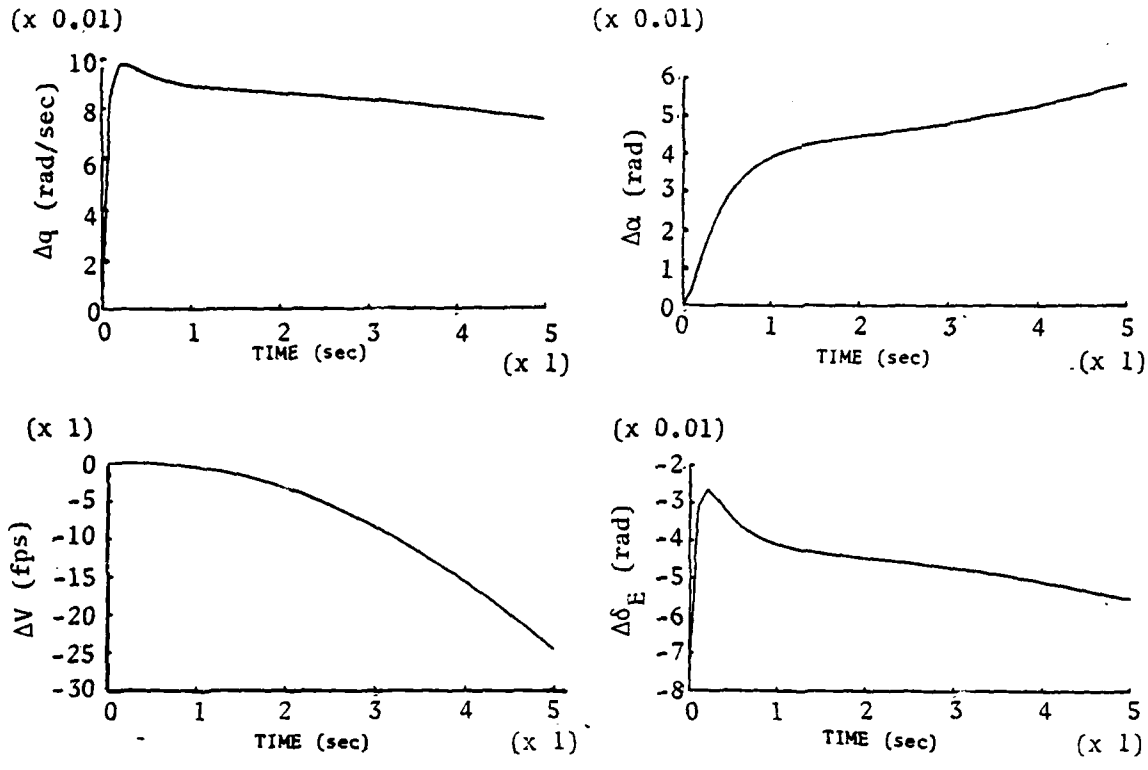

Figure 2-8. Pitch Rate Command Step Response for Diag Q = (50,50) (Δq^* = 5°/sec, 10 sps, 105 KIAS).

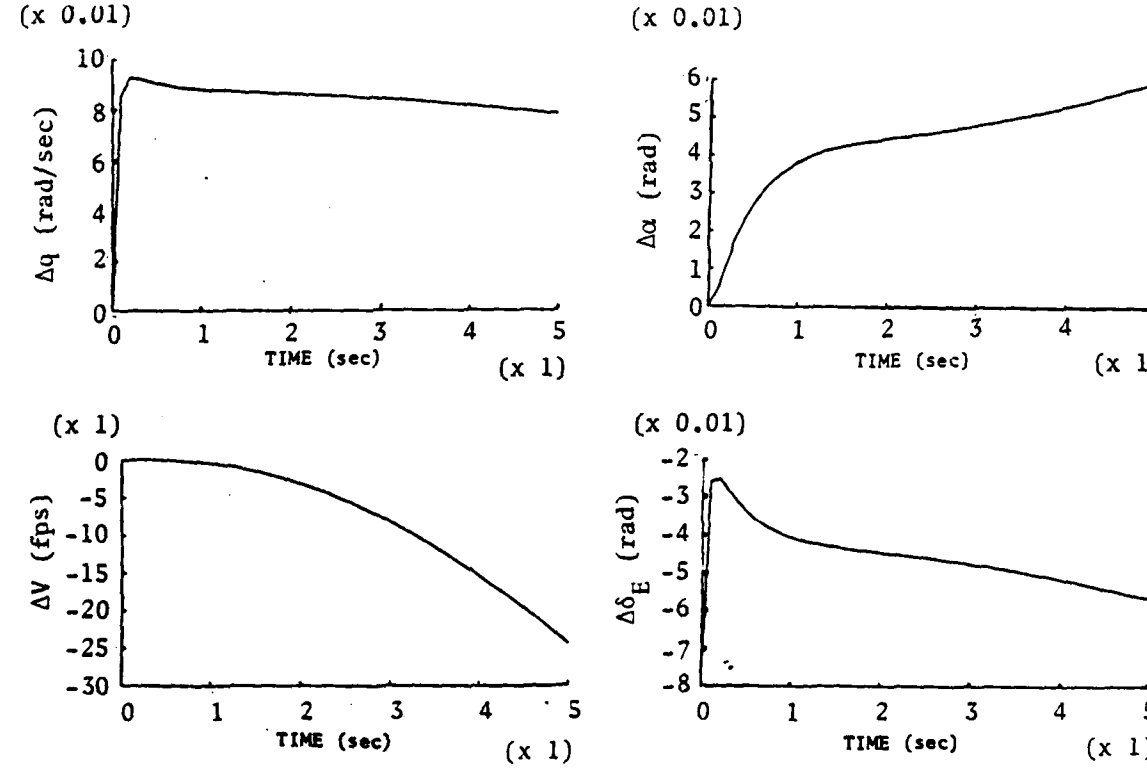

Figure 2-9. Pitch Rate Command Step Response for Diag Q = (75,25) (Δq^* = 5°/sec, 10 sps, 105 KIAS).

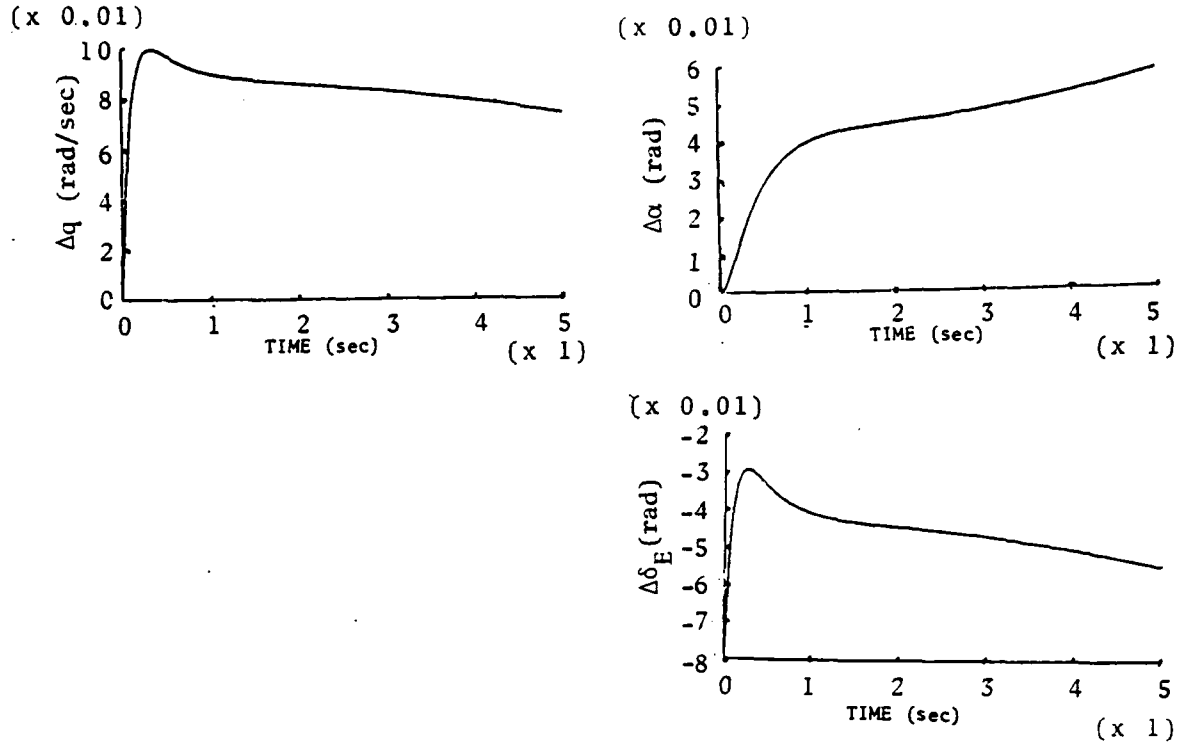

Figure 2-10. Pitch Rate Command Step Response for Diag Q = (25,25) ($\Delta q^* = 5°$/sec, 20 sps, 105 KIAS).

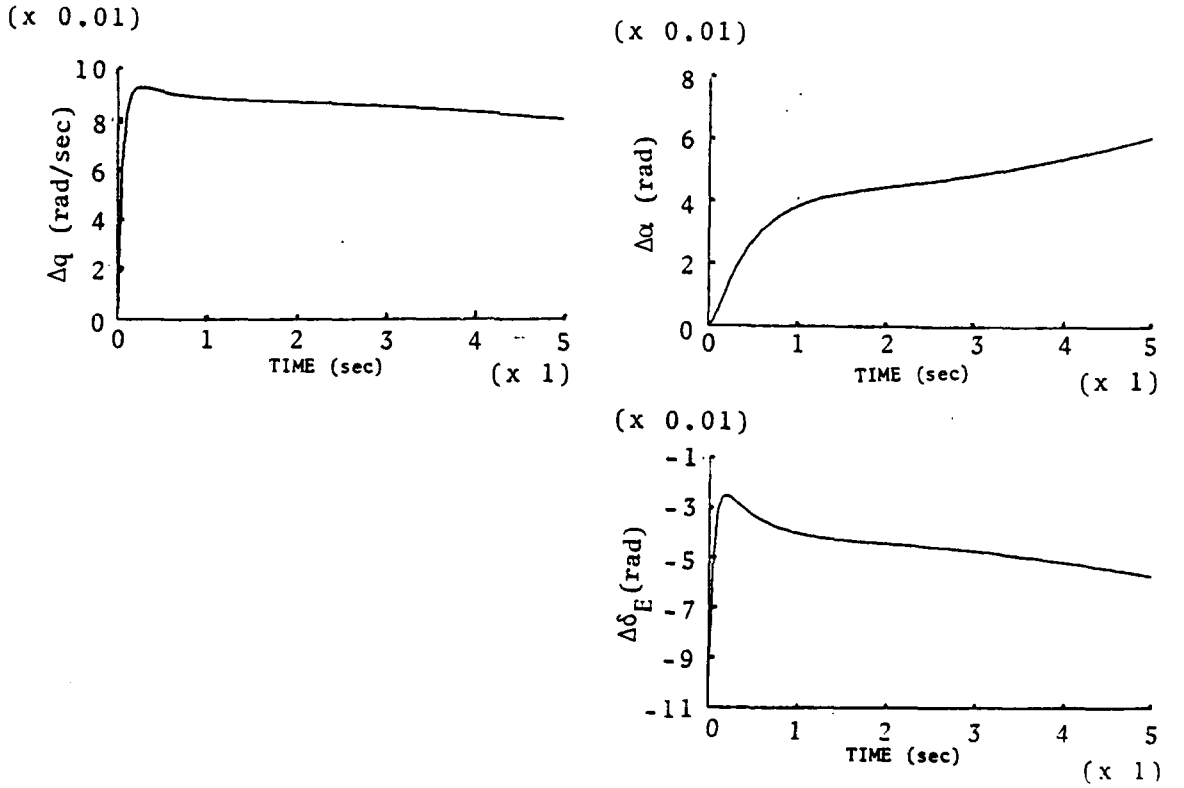

Figure 2-11. Pitch Rate Command Step Response for Diag Q = (75,25) ($\Delta q^* = 5°$/sec, 20 sps, 105 KIAS).

TABLE 2-1

Gains, Predicted Step Responses, and Eigenvalues for q CAS (105 KIAS)

	State Weightings	Gains q	Gains α	Eigenvalues (Short-Period, Phugoid)	Response Rise Time, Sec	Response Overshoot, %
Open-Loop	[-,-]	-	-	-2.04±j2.89 -.033±j.228	0.19	47.5
10 sps	[25,25]	-.427	.324	-10.74,-2.68 -0.45±j.139	0.15	14.7
	[50,50]	-.554	.360	-16.96,-2.43 -.046±j.123	0.09	11.8
	[75,25]	-.620	.468	-23.23,-2.20 -.048±j.104	0.08	6.7
20sps	[25,25]	-.541	.283	-10.30,-2.68 -.045±j.133	.14	14.3
	[75,25]	-.876	.439	-19.31,-2.20 -.049±j.092	0.1	6.4

This implies that the flying qualities of the control laws designed with higher weightings might be unsatisfactory in actual flight tests.

Examination of F_{CL}, calculated from Eq. 46, shows how the stability derivatives have been augmented for the particular weightings chosen. For example, the second-order F_{CL} for weightings of 75 and 25 is

$$\begin{bmatrix} M_q & M_\alpha \\ (1-L_q/V_o) & -L_\alpha/V_o \end{bmatrix} = \begin{bmatrix} -23.5 & -4.48 \\ 1.40 & -1.93 \end{bmatrix} \qquad (49)$$

TABLE 2-2

Closed-Loop $\omega_{n_{sp}}$ and ζ_{sp} for q CAS (105 KIAS)

State Weightings	$\omega_{n_{sp}}$, (rad/sec)	ζ_{sp}, (-)
Open Loop	3.54	0.576
[25,25]	5.39	1.25
[50,50]	6.45	1.51
[75,25]	7.19	1.77

Comparing this to the open-loop F matrix of Eq. 39, M_q has increased by approximately a factor of ten, M_α has decreased by a factor of two, and some negative lift due to q has developed. The stability derivative, L_α has not changed much because the only control surface used by the CAS is elevator and $L_{\delta E}$ is very small. To augment L_α, direct lift control from the flaps would be needed. For weightings of (25,25) and (50,50), the equivalent closed-loop matrices are

$$F_{CL} = \begin{bmatrix} -11.5 & -5.93 \\ 1.09 & -1.96 \end{bmatrix} \quad \text{and} \quad = \begin{bmatrix} -17.5 & -6.56 \\ 1.22 & -1.92 \end{bmatrix}$$

respectively.

2.5 NORMAL ACCELERATION COMMAND CONTROL STRUCTURE

Normal acceleration commanded by $\Delta\delta S$ is the next CAS structure examined. The development is very similar to that of the pitch rate CAS of Section 2.4; hence, only the principal differences are given here. The gains are again calculated with a second-order model but using the states Δq and Δn_z. Using the relation

$$\Delta n_z = -(Z_\alpha \Delta\alpha + Z_{\delta E} \Delta\delta E) \; / g \tag{50}$$

the model represented by Eq. 39 can be used if the correct substitution for $\Delta\alpha$ is made. Since the effects of $Z_{\delta E}$ are so small, the second term of Eq. 50 is neglected here. Since $Z_\alpha \simeq -L_\alpha$, the second-order fundamental matrix is

$$F = \begin{bmatrix} M_q & gM_\alpha/L_\alpha \\ L_\alpha(1-L/_q V_o)/g & -L_\alpha/V_o \end{bmatrix} = \begin{bmatrix} -2.08 & -.758 \\ 11.02 & -2 \end{bmatrix} \tag{51}$$

and the resulting model is given as

$$\begin{bmatrix} \Delta\dot{q} \\ \Delta\dot{n}_z \end{bmatrix} = \begin{bmatrix} -2.08 & -.758 \\ 11.02 & -2 \end{bmatrix} \begin{bmatrix} \Delta q \\ \Delta n_z \end{bmatrix} + \begin{bmatrix} -12.5 \\ -.125 \end{bmatrix} \Delta\delta E \tag{52}$$

with

$$\Delta \underline{y} = H_x \, \Delta \underline{x} + H_u \, \Delta\delta E \tag{53}$$

To select Δn_z as the state commanded by $\Delta\delta S$, H_x and H_u are given the values

$$H_x = [0 \quad 1] \tag{54}$$

$$H_u = 0 \tag{55}$$

Following the procedure of Section 2.4, gains, time responses, and eigenvalues are generated. The matrices S_{22} and S_{12} are found to be

$$S_{22} = -.091 \quad , \quad S_{12} = \begin{bmatrix} .181 \\ 1 \end{bmatrix} .$$

The general relationship between Q weightings for R = 32.8 and a sampling rate of 10 sps is presented in Fig. 2-12. The straight lines relate rise time to weightings and the curves, connected at the origin, relate overshoot to weightings. The dotted line separates closed-loop systems with complex short-period eigenvalues on the top and real eigenvalues on the bottom. The relations in Fig. 2-12 are not exact, but can be used to find good starting values for weightings. As explained in Section 2.4, Fig. 2-12 is the same for other sampling rates.

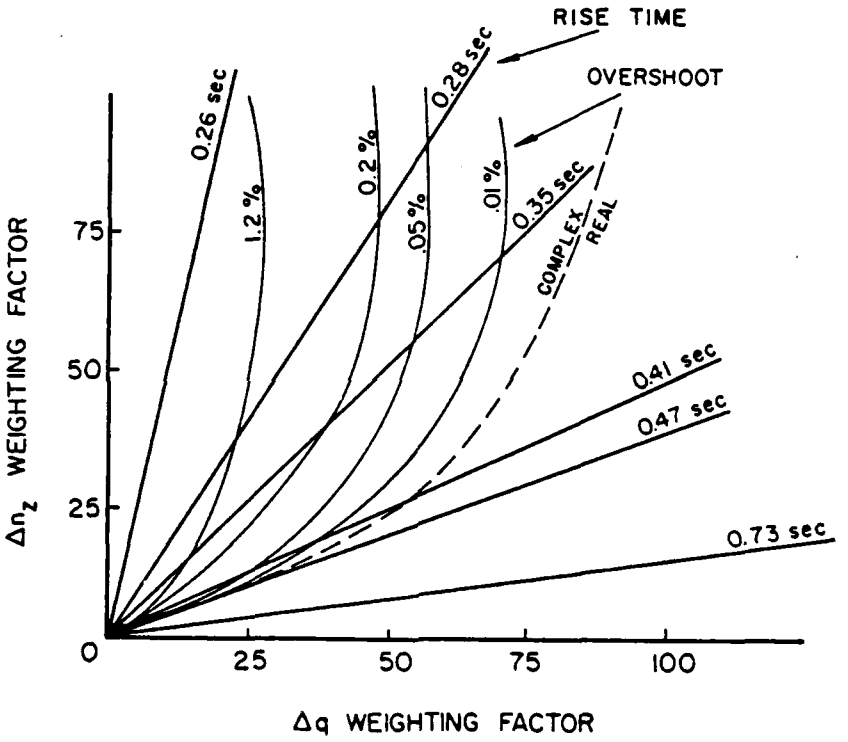

Figure 2-12. Relation Between Second-Order Weighting and Fourth-Order Time Response -- n_z CAS.

Time history plots for a few representative weightings are presented in Figs. 2-13 through 2-16. All plots are generated with a step command input of 0.25g using a two-state controller and fourth-order model of the VRA's longitudinal dynamics. The Δn_z response for

the open-loop aircraft (Fig. 2-13) has a 10.8-percent overshoot and 0.7-sec rise time. Velocity falls off, and $\Delta\delta E$ holds constant at 1.3 deg. Weightings of (5,10) in Q and R = 32.8 (Fig. 2-14) produce a controller with large improvement in rise time for Δn_z response. Δq overshoots its steady-state value quite a bit more than in the open-loop case. The elevator initially deflects more than 5 deg, implying that the FBW system of the VRA would disengage for a 0.25g step input. Figure 2-15 shows the response for a heavier weighting (R = 250) on $\Delta\delta E$. The initial step of $\Delta\delta E$ is less than 3 deg, but rise time of Δn_z has been slowed by 0.2 sec. The peak of the Δq overshoot also is less with the heavier control weighting. The time response for 20-sps sampling rate with diag Q = (5,10) shows once again that a change in sampling rate has negligible effect on command variable response if new gains are calculated to account for the different rate (Fig. 2-16).

The gains, resulting step responses, and closed-loop eigenvalues obtained from the computer simulation are given in Table 2-3.

TABLE 2-3

Gains, Predicted Step Responses, and Eigenvalues for n_z CAS (105 KIAS)

Weightings Q R	Gains q	Gains α	Eigenvalues, (Short Period, Phugoid)	Response Rise Time, Sec	Response Overshoot, %
Open Loop	-	-	$-2.04\pm j2.89$ $-.033\pm j.228$	0.7	10.8
[5,10] 33	-.533	-.181	$-6.47\pm j6.04$ $-.036\pm j.252$	0.35	3.0
[5,10] 250	-.238	-.0535	$-3.71\pm j4.09$ $-.0360\pm j.257$	0.52	5.6
[5,10] 33	-.620	-.250	$-6.52\pm j5.95$ $-.0364\pm j.252$	0.35	3.15

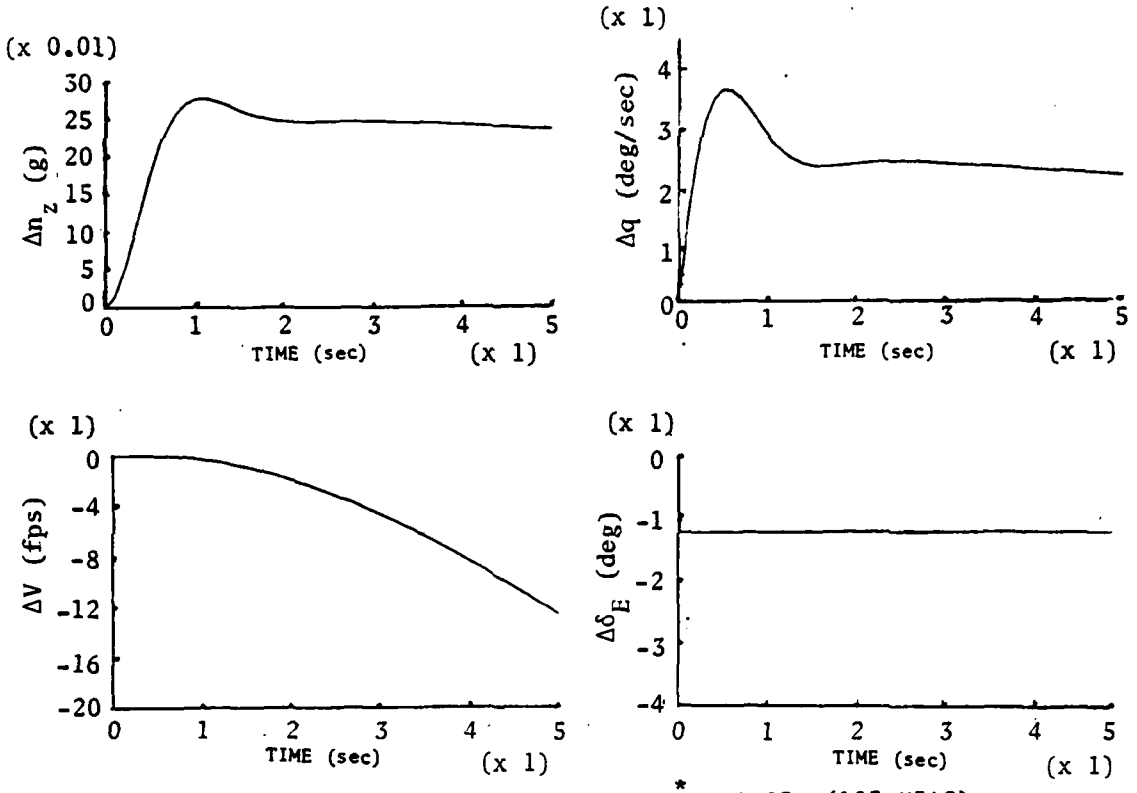

Figure 2-13. Open-Loop Step Response for $\Delta n_z^* = 0.25g$ (105 KIAS).

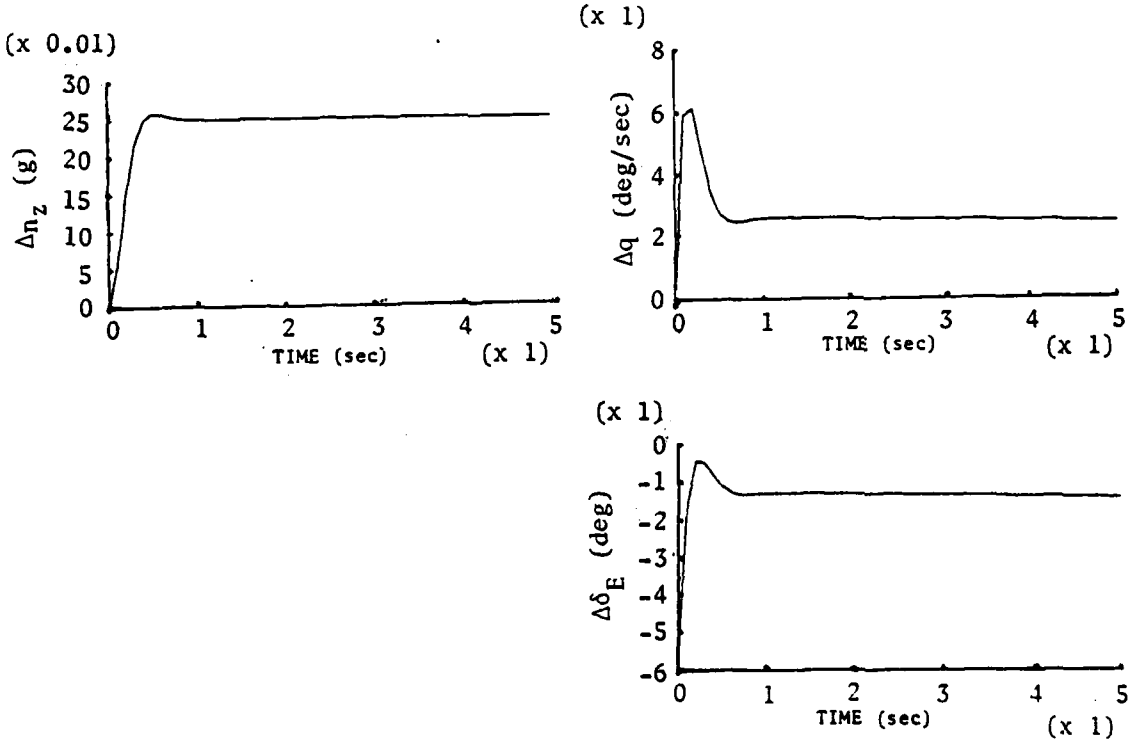

Figure 2-14. Normal Acceleration Step Response for Diag Q = (5,10), R = 33 ($\Delta n_z^* = 0.25g$, 10 sps, 105 KIAS).

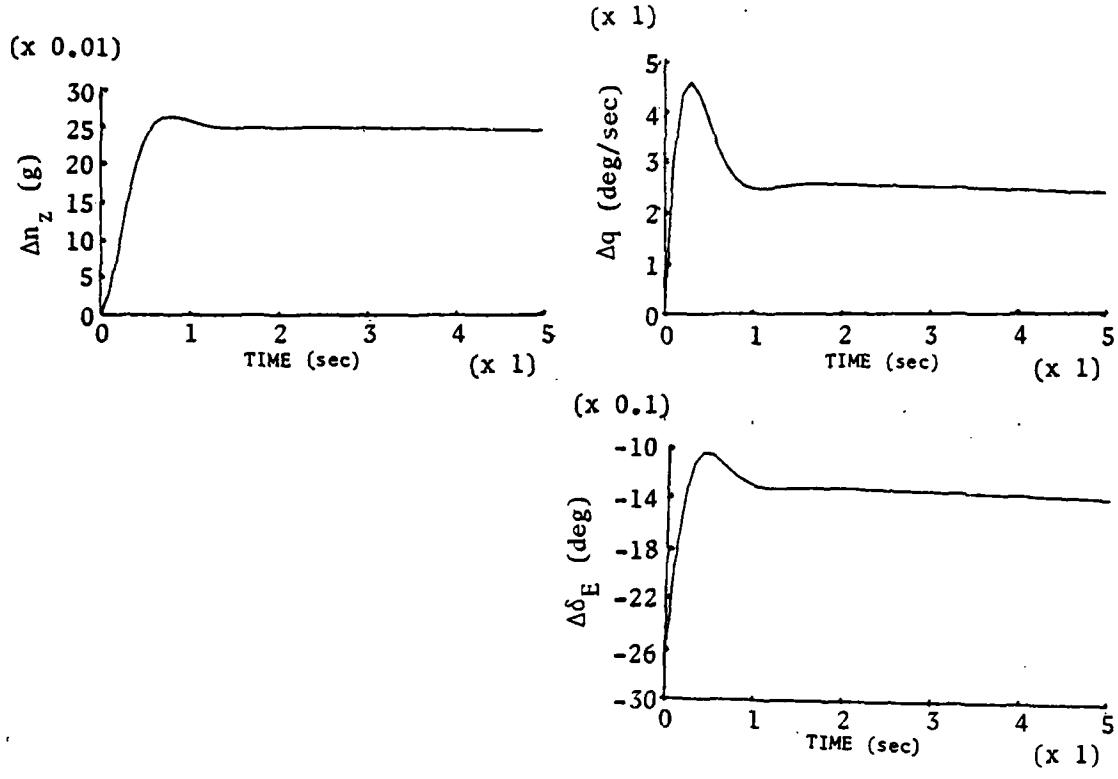

Figure 2-15. Normal Acceleration Step Response for Diag Q = (5,10), R = 250 (Δn_z^* = .25g, 10 sps, 105 KIAS).

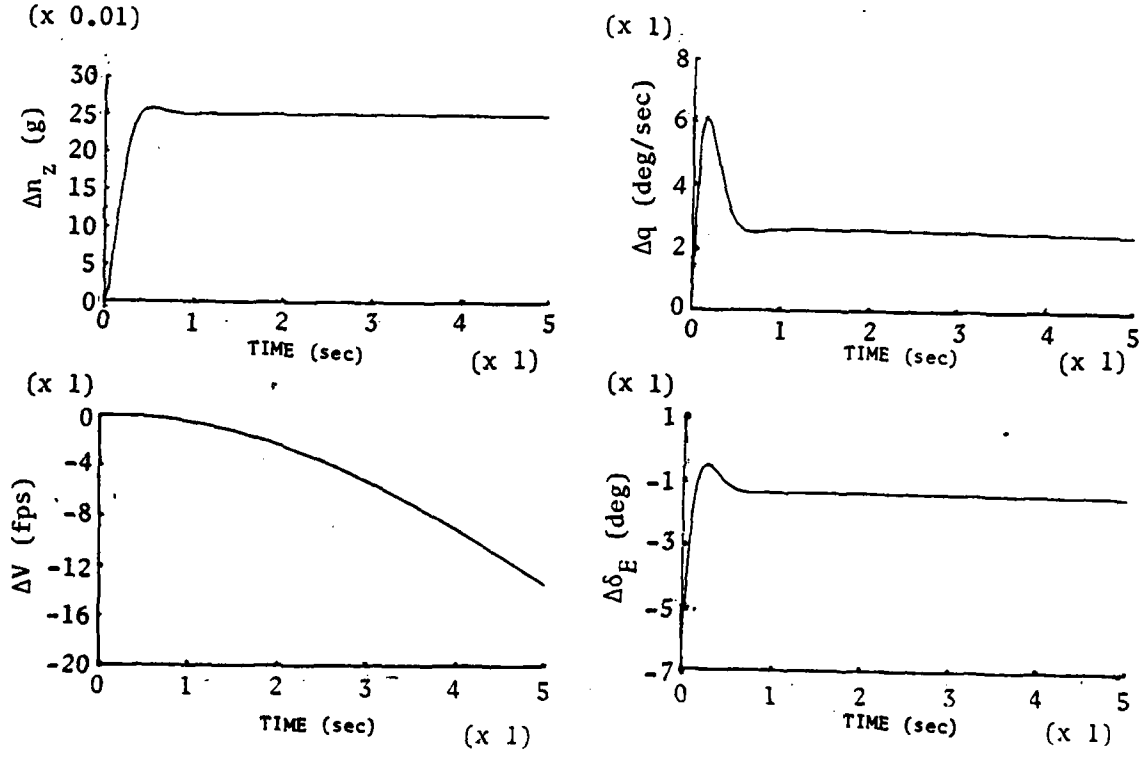

Figure 2-16. Normal Acceleration Step Response for Diag Q = (5,10), R = 33 (Δn_z^* = .25g, 20 sps, 105 KIAS).

The short-period natural frequencies for the weightings with R = 33 and 250 are 8.85 rad/sec and 5.52 rad/sec, respectively. This increase in $\omega_{n_{sp}}$ from the open-loop value (3.54 rad/sec) accounts for the decrease in Δn_z rise time. For the case where $\omega_{n_{sp}}$ = 8.35 rad/sec, the requirement set by the Military Specification on Flying Qualities (Ref. 17) is not satisfied. Referring to Fig. 2-3, the augmented $\omega_{n_{sp}}$ puts the aircraft in the Level 2 area of the chart for n/α = 9.3 g/rad. This implies that the control law, with gains calculated from weightings of Diag Q = (5,10) and R = 32.2, may not be satisfactory to the pilot in the actual flight tests.

The closed-loop stability derivatives may be examined by calculating F_{CL} from Eq. 46. With R = 33 and R = 250, the equivalent closed-loop matrices are

$$F_{CL} = \begin{bmatrix} -11.5 & -5.33 \\ 11.53 & -1.48 \end{bmatrix} \quad \text{and} \quad \begin{bmatrix} -5.49 & -1.80 \\ 11.09 & -1.93 \end{bmatrix}$$

respectively. These can be compared to the open-loop F of Eq. 52 to see how the stability derivatives have changed.

2.6 DYNAMIC MODEL MATCHING

The method of choosing weighting matrices Q and R described in the preceding two sections can result only in decreases in overshoot and rise time for the time response of the commanded state; however, it may be desirable to change the model characteristics of an aircraft in the opposite way if the basic plane's response is too fast or overly damped. This can be done with the previously described LQ control methods by using the method of implicit model-following to specify cost function weights.

The procedure begins by defining a model which the closed-loop system should emulate. By the method of implicit model-following, the cost functional weightings are chosen to weight errors between model and closed-loop responses (Ref. 18).

$$J = \int_0^\infty (\Delta\underline{x}^T Q \Delta\underline{x} + 2\,\Delta\underline{x}^T M \Delta\underline{u} + \Delta\underline{u}^T R \Delta\underline{u})\, dt \tag{56}$$

where

$$Q = (F-F_M)^T W\ (F-F_M) \tag{57}$$

$$M = (F-F_M)^T\ W\ G \tag{58}$$

$$R = G^T\ W\ G \tag{59}$$

The matrix W is a diagonal weighting matrix, and F_M is the F matrix to be modeled.

If the modeling were to be done in continuous-time, the Riccati equation would be solved next and the feedback gains calculated. However, in the discrete-time case, the weightings must be modified to account for effects of the sampling process. Unlike the cost functional of Eq. 23, there is a cross weighting, M, in Eq. 56 which cannot be transformed to its discrete counterpart just by using Eqs. 26-28 of the procedure outlined in Section 2.1. Following the development in Ref. 12, a transformation from the continuous-time weighting matrices (Q, M, and R) to the discrete-time matrices ($\hat{Q}$, $\hat{M}$, and $\hat{R}$) is derived (see Appendix A). The discrete weighting matrices are found to be

$$\hat{Q} = \int_{t_k}^{t_{k+1}} \Phi^T\ Q\ \Phi\ dt \tag{60}$$

$$\hat{M} = \int_{t_k}^{t_{k+1}} (\Gamma^T Q\Phi + M\Phi)\, dt \tag{61}$$

$$\hat{R} = \int_{t_k}^{t_{k+1}} (R + \Gamma^T Q\Gamma + 2M\Gamma)\, dt \tag{62}$$

The gains are calculated (Eq. 29) from the solution of the Riccati equation (Eq. 30), and F_{CL} is found with Eq. 46. APL functions to perform these calculations are listed and explained in Appendix B.

For example, consider a model with $\omega_{n_{sp}} = 1.56$ rad/sec and $\zeta_{sp} = 0.76$; the corresponding eigenvalues are $-1.18 \pm j1.02$. Since L_q and L_α are augmented weakly by $\Delta\delta E$, assume that they are fixed in F_M. M_q and M_α are varied to achieve an F_M with the desired eigenvalues:

$$F_M = \begin{bmatrix} -.36 & -1.71 \\ 1 & -2 \end{bmatrix}$$

Choosing the diagonal weighting matrix W initially to be I_2 and completing the rest of the method outlined in Fig. 2-17,

$$F_{CL} = \begin{bmatrix} -.375 & -1.68 \\ 1.00 & -2.01 \end{bmatrix}$$

With a few iterations of F_M, it is found that

$$F_M = \begin{bmatrix} -.34 & -1.73 \\ 1 & -2 \end{bmatrix}$$

yields

$$F_{CL} = \begin{bmatrix} -.360 & -1.71 \\ 1.01 & -2.01 \end{bmatrix}$$

The corresponding weighting matrices and resulting gains are listed in Table 2-4.

The next chapter outlines the hardware and software aspects of the Micro-DFCS. It describes how the control laws derived in this chapter are actually implemented, and gives test results and analysis for a hybrid simulation.

TABLE 2-4

Weighting Matrices and Gains for Implicit Model-Following Example

Continuous-Time Weightings	Discrete-Time Weightings and Gains
$Q = \begin{bmatrix} 3.03 & 11.5 \\ 11.5 & 43.7 \end{bmatrix}$	$\hat{Q} = \begin{bmatrix} .338 & .965 \\ .965 & 2.83 \end{bmatrix}$
$M = [21.8 \quad 82.6]$	$\hat{M} = [2.08 \quad 6.03]$
$R = 156.3$	$\hat{R} = 12.9$
	$C = [.161 \quad .467]$

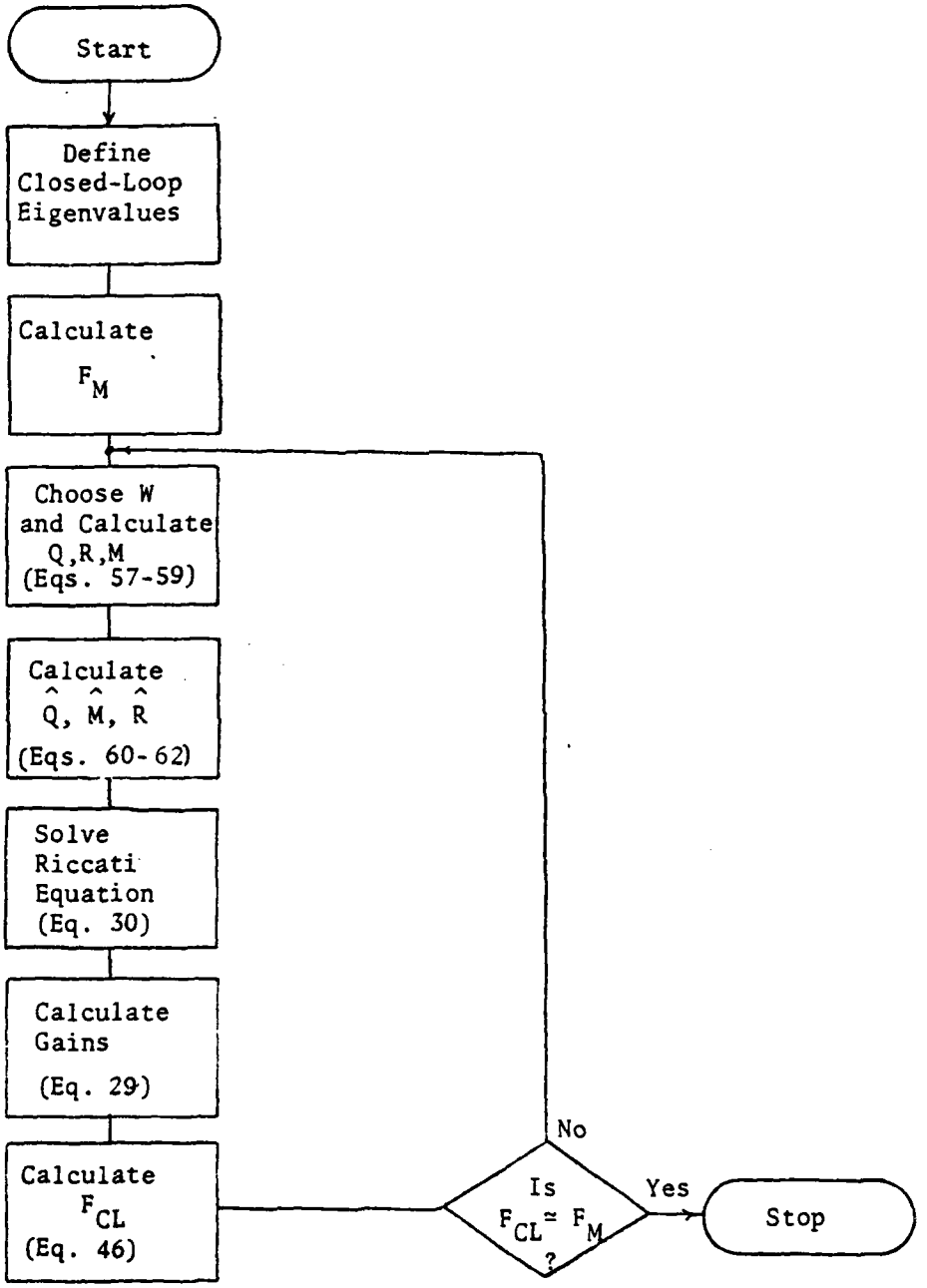

Figure 2-17. Sequence for Implicit Model-Following.

3. CONTROL LAW IMPLEMENTATION AND HYBRID TESTING

The control law developed in Chapter 2 is coded in the software of the Micro-DFCS for implementation on board the VRA. The type and configuration of the Micro-DFCS equipment specifies, to a large extent, in what manner and how well these control laws will operate with the existing VRA FBW system. The efficiency and versatility of the equipment and software determines the complexity of control laws that may be used. Therefore, the control law design has an impact on the equipment selected and organization of the software. This chapter outlines some of the specific aspects of the Micro-DFCS that support the implementation of the control design. The equipment and software are tested with an analog simulation of the VRA as a logical step before actual flight tests.

3.1 EQUIPMENT CONFIGURATION OF THE MICRO-DFCS

The primary task of the Micro-DFCS hardware is to accept analog information, to calculate the control laws, and to generate commands for aircraft controls at periodic instants in time. This definition of the computer's main function suggests some desirable characteristics for the hardware to possess. Since the control law must be calculated in short intervals of time, the computations must not only be fast but also have precision at least as great as the resolution of the digital data words generated by the analog-to-digital (A/D) converter. The computational speed is determined by the instruction cycle time, the bit length of the data word, and the speed of the mathematical operations themselves. Resolution of the A/D and digital-to-analog (D/A) converters should be consistent with the measurable resolution of the sensors and the control actuators. A computer with at least one interrupt that can be triggered by a resetable timer is

needed to initiate the control law calculation at precise instants in time. Other factors to consider include the cost, the range of compatible components which may be used to expand or upgrade the computer at a later date, the standardization and flexibility of the bus structure (which determines the availability of components compatible with the system), the power requirements, and the software available to support the microcomputer.

The Micro-DFCS for this study is based on the Intel Single Board Computer (SBC) using the Intel 8085 Central Processing Unit (CPU). The SBC system has a modular design, with the main functions of the computer being executed on separate circuit boards. These boards can be combined to configure the system for a particular application. Multiple CPUs may be used in a system, either for increased "throughput" or for increased reliability. The multiple CPU feature is not used in this application. As shown in Fig. 3-1, the Model 1 Micro-DFCS is built around the SBC 80/05 central processing board.

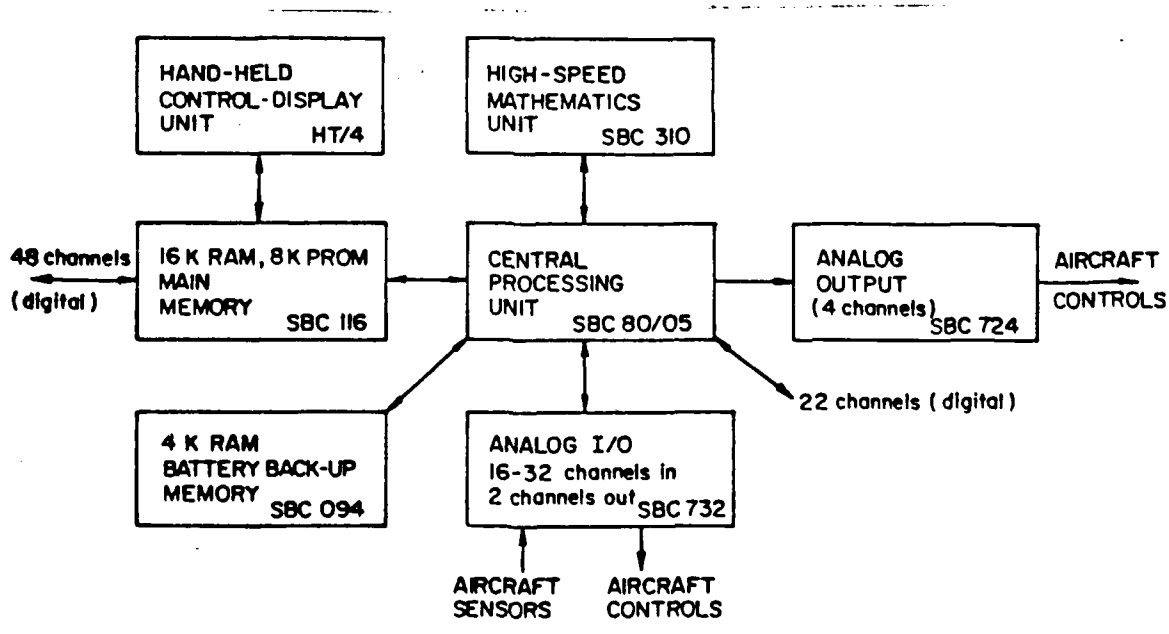

Figure 3-1. Model 1 Micro-DFCS Microcomputer Configuration.

This is supported by a high-speed mathematics unit, random-access and programmable read-only memory (RAM and PROM), A/D and D/A conversion boards, and a hand-held control-display unit (CDU). The CPU works with 80 different machine instructions; it has an 8-bit data word length, and instruction cycle times ranging from 2 to 6.1 μsec (depending on the instruction). A detailed description of the microcomputer components is contained in Appendix D.

The Micro-DFCS is functionally related to the VRA's FBW system as shown in Fig. 3-2. The Micro-DFCS can operate in series or parallel with the existing analog system; it is possible to model another aircraft with the VRA using the analog system and test a digital control design (for the modeled aircraft) using the Micro-DFCS. Two pilots fly the VRA for reasons of safety and experimental efficiency. The safety pilot has conventional aircraft controls with mechanical linkages to the control surfaces. The evaluation pilot operates the experimental controls, which in this case, include a center control stick and the CDU.

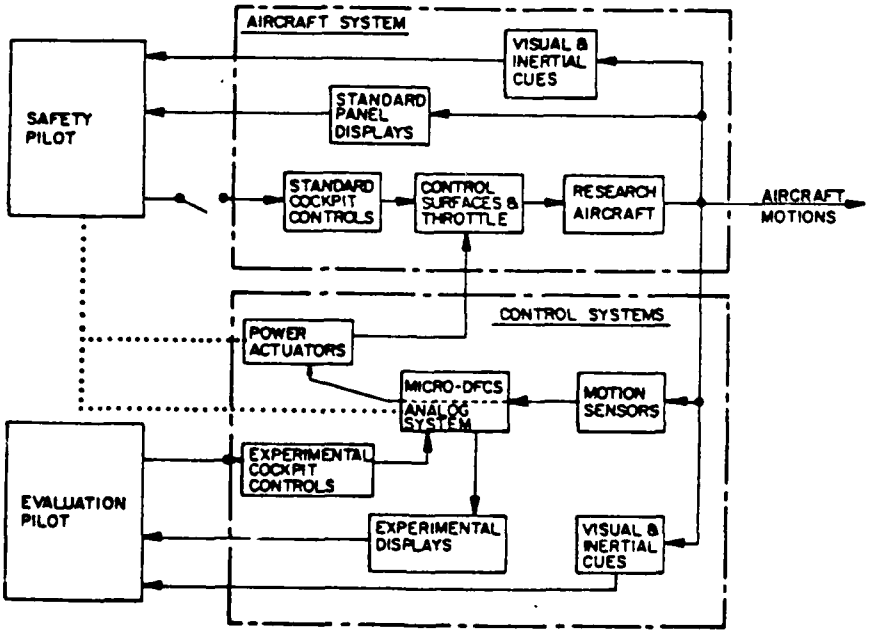

Figure 3-2. Overview of the VRA/Micro-DFCS System.

The VRA's motion is measured by various air data and inertial sensors and sent to a ground station via 42 channels of telemetry. A more detailed explanation of the VRA's systems and ground station is contained in Appendix A.

3.2 THE OPERATIONAL MICROCOMPUTER SOFTWARE

The calculations for the control laws are performed by a set of software programs that execute every sampling instant. These flight control routines are coded to minimize the execution duty cycle. The flight control routines are supported by two sets of programs called the executive and utility routines, which are designed to allow new flight control routines to be added easily. Together, these routines form the operational software for the first command augmentation system program, entitled CAS-1. The routines of CAS-1, arranged in chapter format, are listed with memory requirements in Table 3-1. The executive routines handle initialization, CDU interface, and one of the three error detection methods used in CAS-1. The executive error detection routine checks the contents of memory every 50 samples to insure that the coding of CAS-1 has not been changed. A second error detection method checks for mathematical errors on every operation. The third method indicates when a flight control routine is executing properly by flashing a light at a steady rate on the pilot's panel. A more detailed description of the error detectors and a brief description of all routines are given in Appendix C.

The flexibility of the executive and utility routines is derived mainly from the modular construction of the program. Major and often-performed tasks are divided into subroutines that are very general in nature. All user-definable parameters and variables that change in the operation of CAS-1 are stored in RAM outside the body of CAS-1. Therefore, any part or all of CAS-1 may be stored in PROM. Developing new flight control programs for the Micro-DFCS can be done quickly and

TABLE 3-1

CAS-1 PROGRAM TABLE OF CONTENTS AND MEMORY REQUIREMENTS

	Memory Words
1. EXECUTIVE ROUTINES	
1.1 INITIALIZATION	118
1.2 CDU INTERFACE AND COMMAND RECOGNITION	154
1.3 MEMORY CHECK	89
2. UTILITY ROUTINES	
2.1 ANALOG TO DIGITAL CONVERSION	19
2.2 ENTRY ERROR	68
2.3 BLINK	24
2.4 CLEAR LINE	24
2.5 CONSOLE OUTPUT	11
2.6 COUNT-UP DISPLAY	76
2.7 DECIMAL TO HEX CONVERSION	25
2.8 ERASE BLOCK MEMORY	8
2.9 MATH ERROR PROCESSOR	112
2.10 HEX TO DECIMAL CONVERSION	61
2.11 NUMERIC INPUT	67
2.12 INTERRUPT COUNT	20
2.13 LIMIT ANALOG OUTPUT	46
2.14 MATH UNIT DRIVER	47
2.15 MODE CHANGE	143
2.16 MOVE 4 WORDS	13
2.17 SERIAL OUTPUT	13
2.18 CALIBRATED STEP INPUT	295
2.19 SET DELAY	274
2.20 HEX INPUT	76
2.21 TIMER	137
2.22 CONSOLE IN	12
2.23 16 BIT DECIMAL TO HEX CONVERSION	75
2.24 DELAY	143
2.25 SLOW	24
2.26 RESOLUTION	126
3. FLIGHT CONTROL ROUTINES	
3.1 DIRECT CONTROL SET UP (MODE 19)	78
3.2 PITCH RATE CONTROL SET UP (MODE 0)	135
3.3 PITCH RATE CONTROL SET UP (MODE 1)	
3.4 PITCH RATE CONTROL SET UP (MODE 2)	96
3.5 PITCH RATE CONTROL SET UP (MODE 3)	
3.6 NORMAL ACCELERATION CONTROL SET UP (MODE 10)	136
3.7 DIRECT INTERRUPT SERVICE ROUTINE	99
3.8 PITCH RATE INTERRUPT SERVICE ROUTINE	328
3.9 NORMAL ACCELERATION INTERRUPT SERVICE ROUTINE	394
3.10 DIRECT LATERAL CONTROL SET UP (MODE 18)	92
3.11 DIRECT LATERAL ONLY SET UP (MODE 13)	40
3.12 DIRECT LATERAL SERVICE ROUTINE	149
TOTAL =	3847

efficiently by using these existing routines. A detailed explanation on defining new keyboard commands and flight control modes is contained in Appendix C.

The selected control mode (Pitch Rate, Normal Acceleration, or Direct) determines which control law will be calculated at each sampling instant. The control law calculation has the highest priority over all other tasks because the sampling interval must be kept constant. Figure 3-3 presents a diagram of this priority structure and a description of the duty cycle for a nominal sampling interval of 0.1 sec.

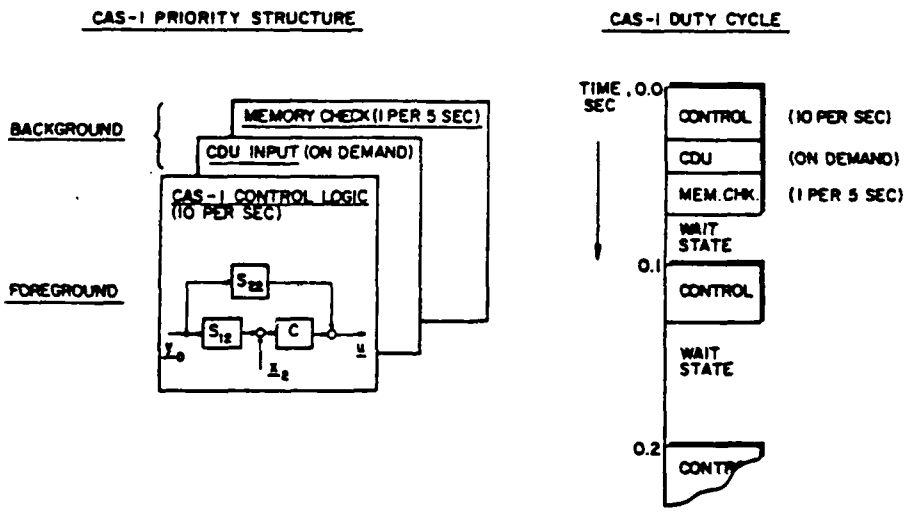

Figure 3-3. CAS-1 Program Organization.

The control law calculation operates in the "foreground", and all other tasks are performed in the remaining available time (in the "background"). The duty cycle shows again that the routine containing the control logic is executed exactly every 0.1 second, and any other routines fill in the available "wait state" time.

The components of the software development system (Fig. 3-4) allow programs to be entered and tested efficiently. The ground chassis

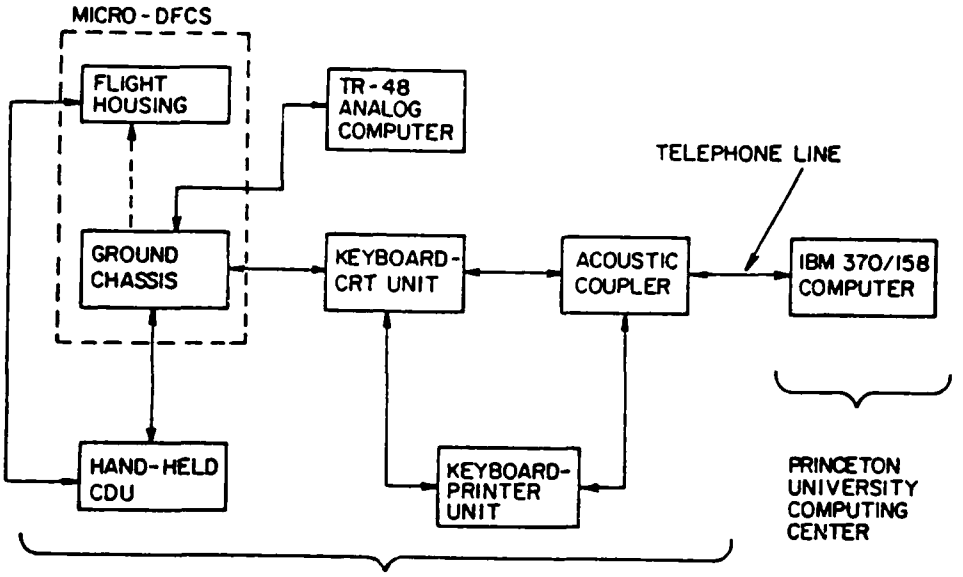

Figure 3-4. Equipment Layout for Micro-DFCS Software Development.

holds the microcomputer boards and provides them with power. The routines, when first coded in assembly language, can be entered into the microcomputer through the keyboard-CRT unit. The text of the routine can be edited to a limited extent on the microcomputer before it is sent to Princeton University's IBM 370/158 computer via an acoustic coupler and the telephone lines. The IBM computer provides more sophisticated text editing, cross-assembly of Micro-DFCS code, and permanent storage of all routines. The assembled routines can be loaded to the microcomputer from the IBM computer and then debugged using the keyboard-CRT unit. A further description of the software development system is contained in Appendix D.

For actual flight tests, the programs are transferred from the development system to the Flight Control Computer Unit (FCCU) mounted in the VRA. The programs can be transferred either on PROM

or on a battery back-up 4K RAM board. The battery back-up RAM is the most convenient method, because program modifications made in RAM are much easier and quicker than programming a new PROM. CAS-1 presently occupies approximately 3.5K words of memory. When CAS-1 is expanded past the 4K limit, the routines that will require no changes (the executive and most of the utility routines) should be relocated in PROM. Flight control routines that are likely to be modified quite often can be kept in battery back-up RAM.

3.3 HYBRID SIMULATION TESTS AND RESULTS

As a logical step between the analytic development and the flight tests, the Micro-DFCS hardware, software, and implemented control laws were tested by simulating the VRA's longitudinal dynamics on an EAI TR-48 analog computer. The voltage levels of the signals interfacing the analog computer to the A/D and D/A channels of the microcomputer were scaled to be of the same magnitude and sign as the outputs from the actual sensors in the VRA. This allows a "real-time" simulation of the Micro-DFCS, which insures that all scalings, gains, and other parameters within the software have been set correctly. The analog computer diagram for the longitudinal dynamics of the VRA and a table of potentiometer settings is given in Appendix C (Fig. C-5 and Table C-2).

The simulation used the fourth-order longitudinal equations of motion that give the effects of both the short-period and phugoid modes. The simulated Δq, $\Delta \alpha$, Δn_z, and $\Delta \delta S$ signals were connected to the analog input channels of the Micro-DFCS. The $\Delta \delta E$ signal generated by the Micro-DFCS was connected to the control input of the modeled VRA. The states of the VRA and the $\Delta \delta E$ output from the Micro-DFCS were recorded on a strip chart recorder.

The three flight control modes -- Direct, Pitch Rate, and

Normal Acceleration -- were tested with different feedback gains and sampling rates (called control configurations). Each was investigated by generating a step input on $\Delta\delta S$ and examining the response of the state variables. Specifically, the rise time and overshoot of the commanded state were compared to those predicted by the numerical results of Chapter 2. The $\Delta\delta S$ step was generated internally in the microcomputer using the calibrated step routine explained in Appendix C. This insures that a true step was made for each input, and it eliminated differences in resulting plots that could be due to the input of $\Delta\delta S$.

The control law calculations were timed during these tests, and it was found that the Direct Mode routine takes 5 msec to execute, the Pitch Rate Mode takes 19 msec, and the Normal Acceleration Mode takes 6 msec. The Normal Acceleration Mode routine executes faster than the Pitch Rate Mode because the former is coded more efficiently to save execution time and not memory space. The Pitch Rate Mode could be recoded to execute in 6 msec, as detailed in Appendix C.

Step responses for fifteen configurations of the three basic flight modes were generated. The control modes which were evaluated are listed in Table 3-2, which, together with sampling rate variations, resulted in the fifteen configurations listed in Table 3-3. Whenever a control mode is used at a different sampling rate, the gains are recalculated to account for the new sampling interval.

The time histories are shown in Fig. 3-5. All plots assume a nominal condition of straight-and-level flight at 105 KIAS. For each run, the six variables Δq, $\Delta\theta$, Δn_z, $\Delta\alpha$, ΔV, and $\Delta\delta E$ are plotted. The $\Delta\delta S$ step input is released after approximately two seconds.

TABLE 3-2

Command Modes Used in Hybrid Tests

CAS Mode	Sub-Mode	Q (q_{11} , q_{22})	R
Direct	-	-	-
Pitch Rate	A	3,20	33
"	B	25,25	33
"	C	50,50	33
"	D	75,25	33
Norm. Acc.	A	5,10	33
"	B	10,5	33
"	C	5,10	250

The Direct Mode (Fig. 3-5a) demonstrates the predicted open-loop response of the aircraft. Pitch rate overshoots and decays, $\Delta\alpha$ reaches a new steady state, and ΔV decreases as the aircraft starts to climb. When Δy^*, scaled to a pitch rate input, is set to zero, $\Delta\alpha$ returns to its original value; the decreased ΔV leads to a negative Δq and a rapidly decreasing $\Delta\theta$.

Pitch Rate Mode A has little effect on the step response (Fig. 3-5b), but provides quicker Δq response with less overshoot. The Δq decay is reduced, but it is not eliminated because the control law is not Type 1 and there is no throttle augmentation to control the decrease in ΔV. Upon releasing the stick, Δq returns closer to the original value than the previous case, and the rate of $\Delta\theta$ decrease is reduced. Comparing these plots to those generated in the all-digital simulation (Fig. 2-7), it is seen the Micro-DFCS is operating as predicted. The initial control deflection is approximately 3.5 deg on both plots,

TABLE 3-3

Optimal Gains for the Fifteen Control Configurations

Control Mode	Sampling Rate (sps)	Gains q	Gains $\alpha(n_z)$
a) Direct	10	-	-
b) q Mode A	10	-.150	.036
c) q Mode B	10	-.427	.324
d) q Mode C	10	-.554	.360
e) q Mode D	10	-.620	.469
f) q Mode C	8	-.484	.377
g) q Mode D	8	-.532	.475
h) q Mode B	7	-.358	.347
i) q Mode B	6	-.324	.355
j) q Mode B	5	-.282	.362
k) q Mode B	4	-.232	.366
l) n_z Mode A	10	-.533	(-.181)
m) n_z Mode B	10	-.474	(-.106)
n) n_z Mode C	10	-.238	(-.054)
o) n_z Mode A	8	-.494	(-.154)

and the responses of Δq, $\Delta\alpha$, and ΔV are similar. Increasing the Q weighting for Pitch Rate Modes C and D (Fig. 3-5d and e) shows the expected decrease in rise time for Δq, with about the same amount of overshoot. To obtain the faster rise time, the magnitude of the initial $\Delta\delta E$ deflection has increased. Effects of slower sampling rates are shown in Fig. 3-5f-k. The optimal gains are recalculated for each set of weightings, taking into account the change in sampling interval. Runs with the same continuous-time weightings but different sampling rates show essentially identical state trajectories. In all control configurations, the zero-order-hold steps in $\Delta\delta E$ become more visible as sampling rate decreases. The state responses to these control inputs are smooth because the rigid-body dynamics of the VRA filter out the higher frequency content of the sharp-edged steps.

The Normal Acceleration Mode A (Fig. 3-5 1) forces a large Δq overshoot to obtain rapid, well-damped Δn_z response. The $\Delta\delta E$ deflection begins with a large impulse; this is followed by a gradual deflection which increases $\Delta\alpha$ to minimize Δn_z decay as ΔV decreases. Figure 3-5n gives the response for R = 250. The weighting R increases the importance of suppressing perturbations in $\Delta\delta E$ in the cost functional. Comparing Fig. 3-5m to Fig. 3-5n, the $\Delta\delta E$ deflection is initially less for R = 250, even though the step input used ($\Delta n_z^* = .25g$) is greater. Figure 3-5o illustrates that changing the sampling rate to 8 sps with corresponding gain changes has negligible effect on the step response.

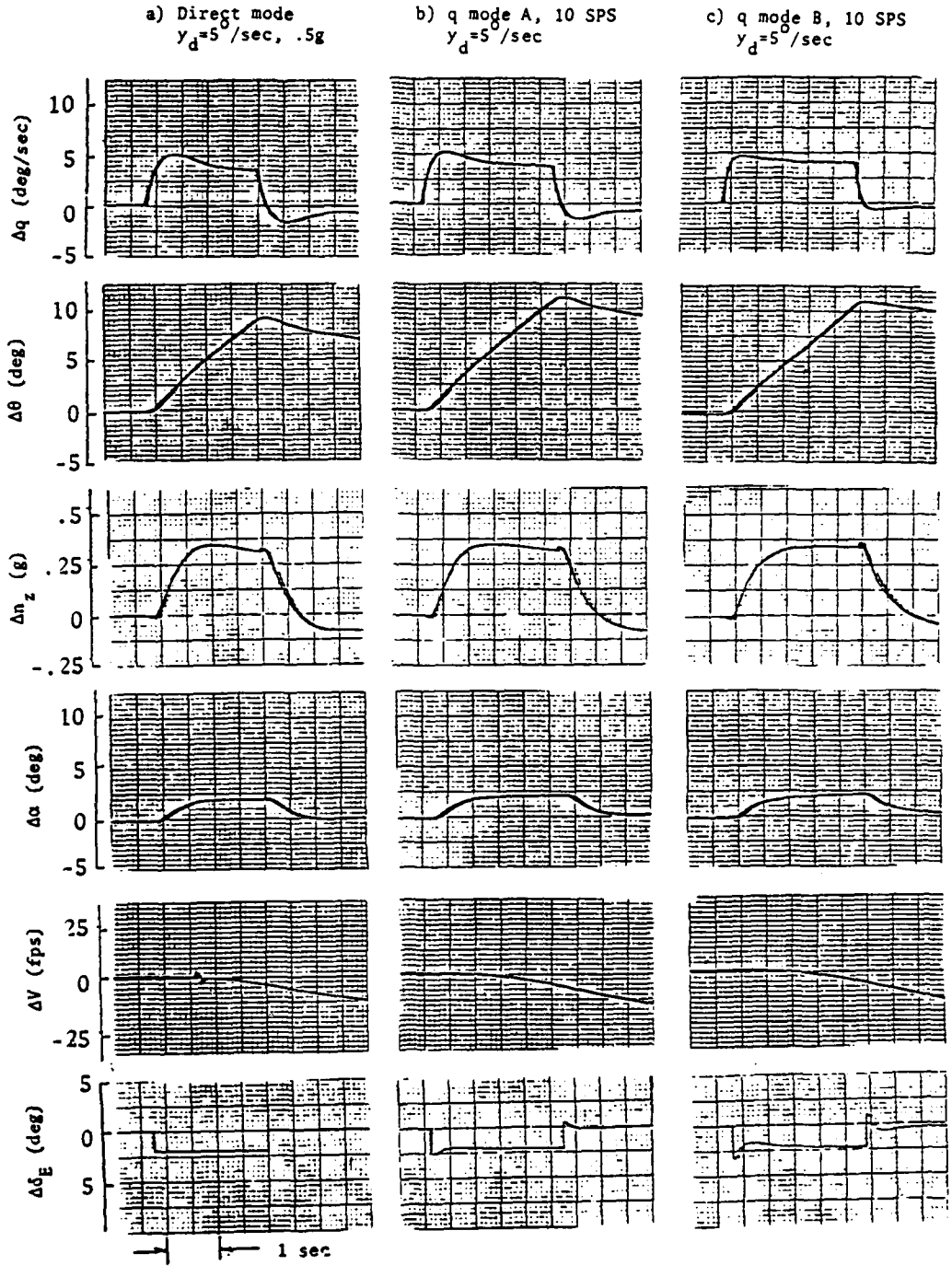

Figure 3-5. Hybrid Simulation Step Responses.

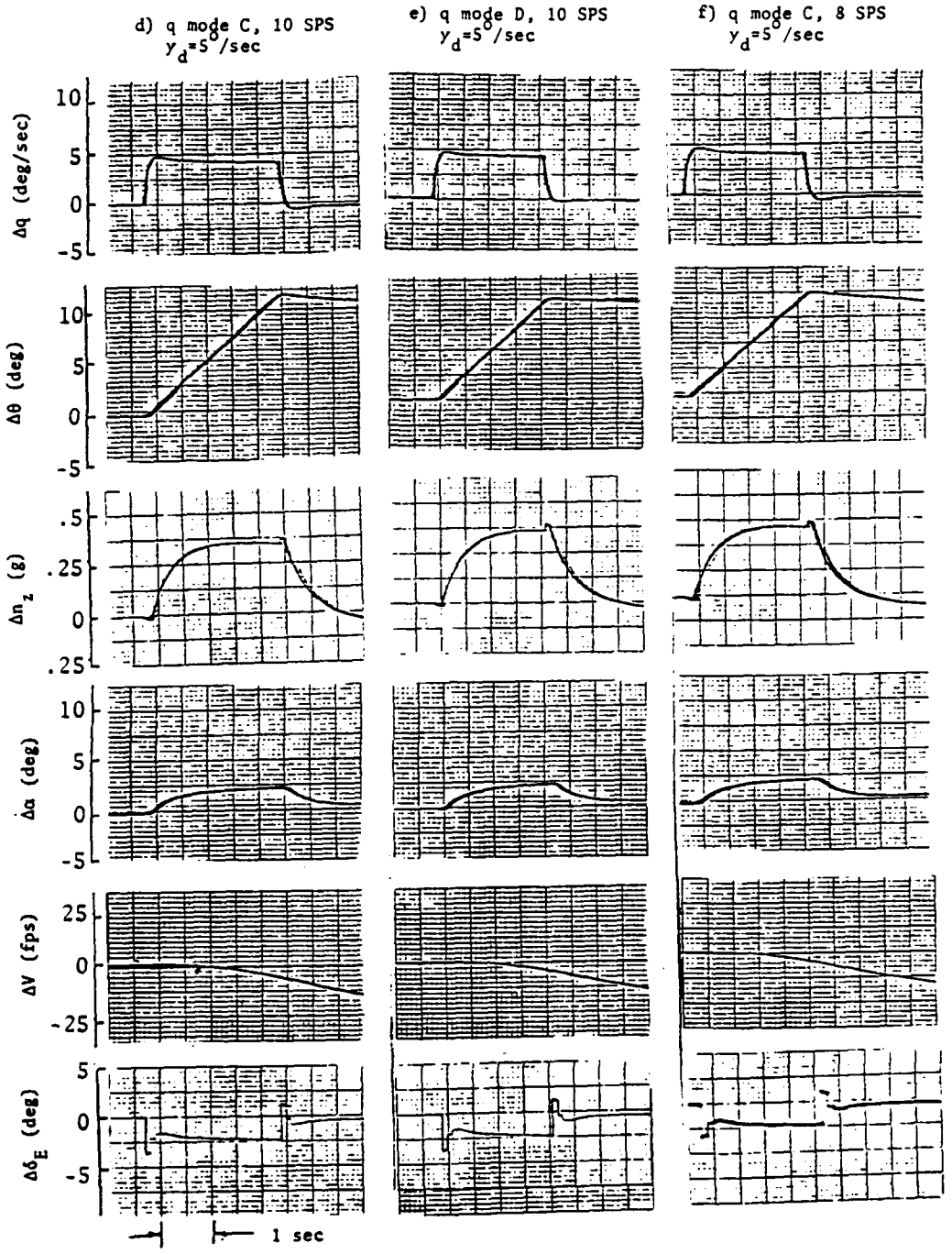

Figure 3-5. continued

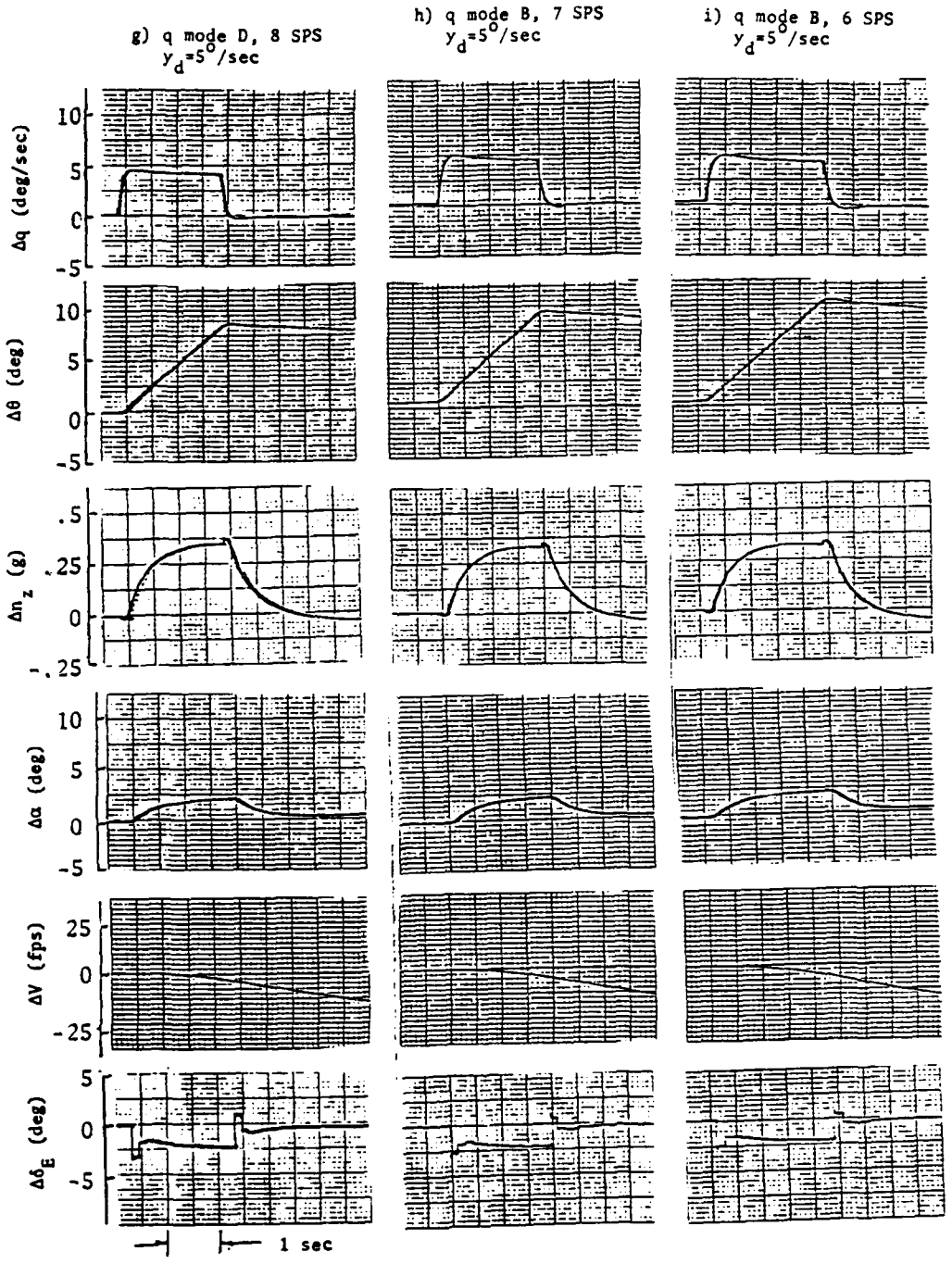

Figure 3-5. continued

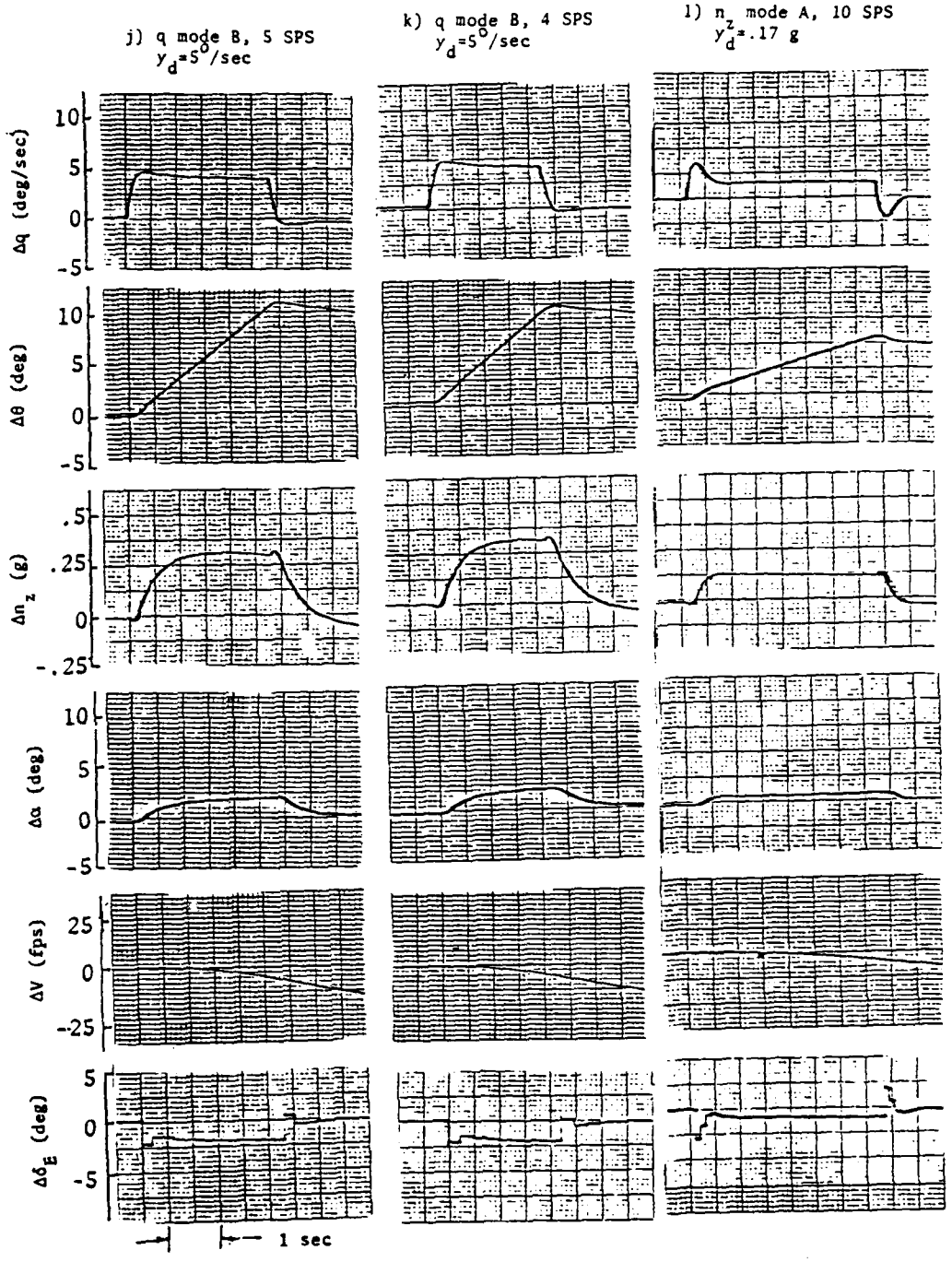

Figure 3-5. continued

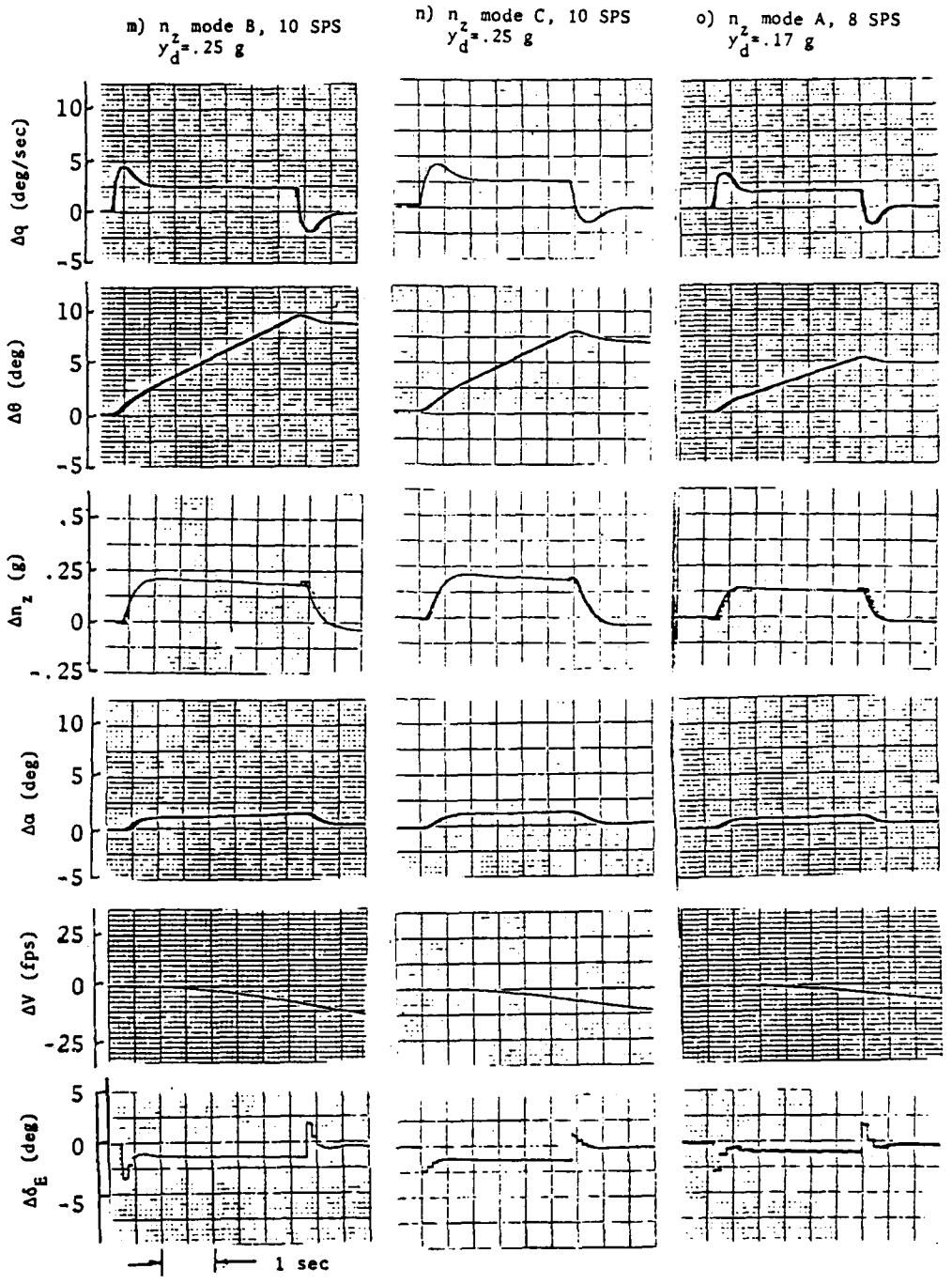

Figure 3-5. concluded

4. FLIGHT TESTING

Flight testing the Micro-DFCS is a significant element of this program, as experiment and demonstration provide the necessary bridge between theory and practice. Objectives for these tests include verification of the operation of the reduced-order LQ control laws, as well as a preliminary investigation of the effects of slow sampling rates, low quantization, and large time delay on pilot opinion of aircraft flying qualities. Test procedures are presented in Section 4.1, and initial CAS-1 results are reported in Section 4.2. Section 4.3 concentrates on sampling quantization, and delay effects primarily for the Direct Mode.

4.1 FLIGHT TEST PROCEDURES

The first objective for VRA flight testing was to verify the Micro-DFCS installation and its operation with the VRA FBW system. It was anticipated that problems due to

- Radio frequency (RF) noise
- Sensor and channel noise
- Scaling factors set incorrectly within the software
- Difficulties in using the CDU while in flight

could occur. The possibility existed that RF radiation from the telemetry or communication radios might effect the operation of the Micro-DFCS (or vice-versa). Measurement noise on the sensor signals, which was not present in the hybrid simulation, could degrade the controller's performance. Noise at high frequencies (due to structural vibrations) that normally would be filtered by the VRA's analog control system could present "aliasing" problems with the digital controller, "folding" into

the lower rigid-body frequency range. System checkout functions included verification of scale factors, effects of signal "staircasing" on aircraft actuators and safety "trip" mechanisms, and operational evaluation of the hand-held CDU.

Examination of the effects of changing gains and sampling rates for the longitudial command augmentation control laws used in the Micro-DFCS was the second major objective for testing. Factors in this phase of testing included

- Flying qualities criteria
- Pilot's opinion of controllability, responsiveness, and other noted effects
- Step response as compared to the analytic and hybrid results
- Tendency of steady turn-induced pitch rate to oppose pitch-rate feedback

The longitudinal flying qualities criteria (Ref. 17) are given in terms of ζ_{sp} and $\omega_{n_{sp}}$ versus n_z/α. Closed-loop values of these parameters for each set of gains were determined previously in the analytic study; the flight tests were intended to verify the flying qualities classification. The pilot's opinion of controllability and responsiveness is a subjective indication of flying qualities which is somewhat more comprehensive than the step response test conducted in the hybrid tests. For comparison, Δq^* and Δn_z^* commands also were produced in flight, and VRA response was telemetered to the ground for analysis. Because the longitudinal CAS being tested did not contain pitch rate "washout", it could be expected that steady turns would produce body-axis pitch rates which would oppose the pitch-rate damping feedback; the magnitude of this effect was to be demonstrated.

Preparations for each flight test included identifying the control configurations (control mode and sampling rate) to be tested

on each flight, and installing the FCCU on its VRA pallet. Prior to each flight, program modifications were made; the Micro-DFCS equipment and software were checked in the hybrid simulation to verify that all scalings and gains were set correctly.

The testing procedure for each flight was basically the same. Once the VRA had attained the proper altitude (5000 ft msl for most tests), the Micro-DFCS was engaged using the following sequence:

1) Attain straight-and-level flight at flight test condition
2) Select control configuration
3) Radio type of test to ground station
4) Engage VRA's FBW system
5) Accomplish test maneuver
6) Disengage FBW system
7) Set up for next test

The first step generally was conducted at an airspeed of 105 KIAS, although testing occurred at other speeds as well. The control law, gains, and sampling rate are selected in Step 2 by entering the requests through the CDU (see Appendix D for a detailed description for using the CDU). When a new CAS-1 control mode (different control law or set of gains) is entered, the feedback states at that instant are taken as the "set point" or nominal value about which the Micro-DFCS controls for zero δS. (Note that the CAS-1 control laws are derived for linear models and perturbation variables, but the Micro-DFCS operates with nonlinear dynamics and total variables on the VRA; hence the $\Delta(\ )$ notation is omitted in discussing flight test variables.) Therefore, it is important that the flight condition desired for the run be maintained while Step 2 is being performed. Step 3 lets the ground station operator mark the strip chart plots and tape recording with the type of run. It is done just prior to the maneuver, so that the strip chart and tape recorder do not run needlessly during the set-up. Next, the FBW system

is engaged, allowing the δE output from the Micro-DFCS to operate the elevator actuator. Up to this point in the sequence, the Micro-DFCS calculates a δE but the actuator is not enabled to follow the δE signal. When the FBW system is engaged, the Micro-DFCS δE signal is automatically biased so that it corresponds to the actual elevator position just before the engagement. This insures a smooth transition from the normal mechanical controls to the FBW controls. The maneuver is performed, and the test data for that run then is collected. The FBW system is disengaged, and the sequence is repeated for the next test run.

The tests yielded both qualitative and quantitative results. In one set of tests, the pilot performed a defined task and rated the responsiveness and controllability for each control configuration. Quantitative tests were conducted, where the response of the VRA to a step input on δS was telemetered for analysis. Figure 4-1 shows the breakdown of the test methods used.

Flight Test Methods			
Qualitative		Quantitative	
Tracking Task	Landing Approach	Analysis of Step Response	Analysis of Micro-DFCS in Banked-Turn

Figure 4-1. Breakdown of Test Methods Used.

The tracking task was conducted by engaging the Micro-DFCS and then attempting to position a "pip" mark on the windshield over an arbitrary point on the horizon. Every few seconds another point on the horizon was picked, and the pilot's success in tracking the new point was recorded as the results for that test. The pilot also was asked to

comment on his impression of the discrete elevator movements. The tracking task was performed for the Direct Mode and Pitch Rate Mode B at sampling rates of 10, 8, 7, 6, 5, and 4 sps. It also was done for all Normal Acceleration Modes and Pitch Rate Modes C and D at 10 sps.

The landing approach test was conducted in the Direct Mode because gains for both CAS modes were developed for 105 KIAS, while the normal landing speed of the VRA is in the neighborhood of 75 KIAS. The effects of sampling, quantization, and delay were examined in the landing test. The testing period for each landing began at the turn to the final approach and ended at touchdown. Sampling rates of 10, 7, 5, 3, 2, and 1 sps were used.

Response of the commanded state (either q^* or n_z^*) to a step input of δS was examined, with step inputs that were identical to those used in the hybrid tests. All control configurations presented in Section 3.3 were tested in flight. In addition, the Pitch Rate Mode B operating at 10 sps was tested in straight-and-level flight at 80 KIAS and again at 120 KIAS. The objective was to determine how the 105-KIAS gains performed at other flight speeds.

Tests were performed to determine the effects of this longitudinal controller when attempting to hold a steady coordinated turn with bank attitudes of 30 and 50 deg. The test was done using the Direct Mode and the Pitch Rate Mode B at 10 sps.

Quantization effects, in which 12 to 3 bits were used to represent full-scale elevator defection, were determined, and pure delays representing computation (or transport) lags of up to 1 sec were examined for both the tracking and landing tasks. Comparison tests were made with a simulated natural turbulence level of 3 fps rms.

4.2 FLIGHT TEST RESULTS AND ANALYSIS

The data presented in this section were collected during the first three flights. Flight 1 was used to test the components of the VRA/Micro-DFCS combination. The components did not interfere with each other's operation except in one case. Whenever the telemetry transmitter was turned off, the CPU of the Micro-DFCS was halted. It was not clear if this was due to an RF pulse or a pulse on the power lines. This did not create a problem for testing the control laws, so the matter was not pursued further.

The general operation of all but the Normal Acceleration Mode was tested on the first flight. The n_z accelerometer signal was too noisy to allow the control law to function. Stick-gearing for the Pitch Rate Modes was found to be too low for effective handling qualities evaluation. It originally was set to command 2.7 deg/sec per inch of stick deflection in the steady-state. The pilot considered this too much movement of the stick for the desired Δq. The stick-gearing was doubled, giving adequate control power at the 105 KIAS flight condition. The Normal Acceleration Mode stick-gearing also was doubled from its previous value to 0.52 g/inch. The stick-gearings were set low on Flight 1 for overflow protection; for some control modes a large stick deflection can cause the Micro-DFCS to temporarily command more than the maximum δE allowable. This causes the D/A output to overflow, resulting in a jump in output voltage, as described for the LIMIT routine in Appendix C. The routine LIMIT was added to CAS-1 after Flight 1 to prohibit D/A overflow.

Noise on the sensor channels was a problem for the n_z accelerometer. Structural vibrations with frequencies of 10-Hz or more were superimposed on the n_z signal. A first-order low-pass analog filter with 4-Hz bandwidth was added to the n_z channel before the A/D converter input. For the short-period natural frequency (f_{sp} = 0.56 Hz), this

filter causes a one-percent attenuation and an 8-deg phase lag in the n_z signal. The filter completely eliminated the effects of the structural vibration on the Micro-DFCS in the remaining test flights.

The second and third flights tested the modifications made after Flight 1 and provided data for the qualitative and quantitative tests outlined in Section 4.1. The fourth through the sixth flights are discussed in Section 4.3.

4.2.1 Tracking at Altitude

The results for the tracking task are given in Table 4-1. The pilot's comments for each control mode and sampling rate used are listed. The temperature was 17°C, the altitude was 4500 to 5500 ft msl, and sea level barometric pressure was 30.16 inches of mercury. The tests were conducted in essentially calm air. Normal Acceleration Mode A was expected to give an undesirable response because the closed-loop $\omega_{n_{sp}}$ for this mode ($\omega_{n_{sp}}$ = 8.85 rad/sec, ζ_{sp} = .73) places the flying qualities in the Level 2 region of Fig. 2-3. Figure 2-3 is presented again in Fig. 4-2 with all control modes marked. Normal Acceleration Mode B also is in Level 2 with $\omega_{n_{sp}}$ = 7.62 rad/sec. The flying qualities of n_z Mode C are in Level 1 with $\omega_{n_{sp}}$ = 5.5 rad/sec; this rating also is reflected in the pilot's comments. The discrete pulsing movements of the elevator can be felt and heard in varying degrees, depending on the sampling rate and control mode. Low sampling rates or control modes that command large initial deflections make the discrete nature of the movements very noticeable. The vibrations seem very unnatural and are likened to the sound and feel of a stall buffet. The phenomenon is annoying, and a DFCS with zero-order-hold outputs and very low sampling rate might not be tolerated in an operational design for this flight

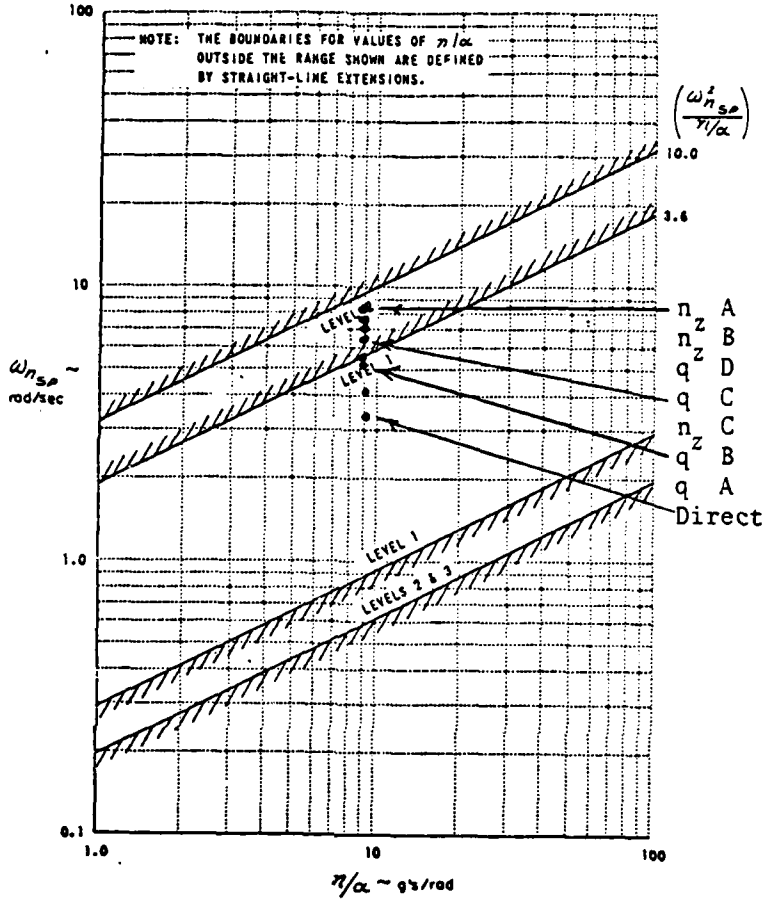

Figure 4-2. Short-Period Frequency Requirements with All Control Modes Marked.

condition using the control structure defined in Section 2.1; however, no conclusion can be reached regarding the suitability of these low sampling rates with more advanced control designs that smooth control rates.

The Direct Mode operating at 10 sps gives the normal open-loop response of the aircraft with no noticeable effects from the phase lag inherent in the sampling process. The elevator movements are noted by their "rumbling" sounds. The Pitch Rate Modes B and

TABLE 4-1

Results for Tracking Task

Sampling Rate (sps)	Control Mode	Pilots' Comments
10	n_z Mode A	Movements too abrupt. Over sensitive to command inputs. Large initial δE pulses are felt and heard. FBW system disengages on large input commands.
10	n_z Mode B	Better than Mode A, but initial response still too fast. Discrete δE deflections still noticeable.
10	n_z Mode C	Good response with "crisp" tracking. Discrete δE movements sound and feel like the stall buffet. This seems very unnatural.
10	Direct Mode	No noticeable difference from the normal continuous open-loop response except for slight rumble of δE deflection.
10	q Mode B	Good response. Easier to attain track of mark and hold then Direct Mode. Rumble from elevator about same as Direct Mode.
10	q Mode C	Seems the same as q Mode B.
10	q Mode D	Response and control the same as q Modes B and C, but rumble from elevator more noticeable. Not really distracting, but obviously present.
8	Direct Mode	The same response as Direct Mode for 10 sps. Rumble may be slightly more apparent.
8	q Mode B	The same response as q Mode B for 10 sps. Rumble may be slightly more apparent.

(continued)

TABLE 4-1. (continued)

Sampling Rate (sps)	Control Mode	Pilots' Comments
7	Direct Mode	A little overshoot noticed on tracking task but does not interfere with performance significantly. Rumble of δE movements more noticeable.
7	q Mode B	No overshooting of mark. Rumble as in the Direct Mode above.
6	Direct Mode	Continual overshoot of mark in tracking task. Very objectionable, but tolerable.
6	q Mode B	Overshoot of mark noticed, but tracking attained more quickly than Direct Mode at 6 sps. Rumble now more of a "thumping"; more noticeable than Direct Mode.
5	Direct Mode	Response seems better than Direct or q Mode at 6 sps. Thumping very noticeable (sound and vibrations).
5	q Mode B	Worse than Direct Mode. Tendency to overshoot mark, but can eventually get there. δE thumping about the same as above.
4	Direct Mode	Performance very bad. Very large overshoots in tracking task.
4	q Mode B	Pilot senses delay from command until motion, but no trouble in attaining and keeping the track. No overshoot, just a very objectionable delay. δE thumping same as 5 sps.

C at 10 sps give a better response than the Direct Mode because the overshoots and rise times in q, due to short-period model characteristics, are decreased. Pitch Rate Mode D gives a similar response, but initial elevator deflections are larger with Mode D, which causes them to be more noticeable. The flying qualities criterion set by Fig. 4-2 shows Level 2 response for Modes C and D with $\omega_{n_{sp}}$ = 6.5 rad/sec, and 7.2 rad/sec, respectively (taken from Table 2-2). The pilot's comments indicate, however, that the response and controllability are very good for these two modes. An explanation may be that when the ζ_{sp} is very high (in this case, 1.5 and 1.8), Fig. 4-2 may not necessarily apply. The Military Specification gives no necessary relationship between $\omega_{n_{sp}}$ and ζ_{sp}; possibly one is needed.

The remaining tests listed in Table 4-1 are for sampling rates 8 through 4 sps, comparing the response for the Direct Mode and Pitch Rate Mode B. As the sampling rate is decreased, the elevator vibrations get worse and are described as a "thumping" sound. The deflections also can be felt. The Pitch Rate Mode is always worse in this respect than the Direct Mode (at the same sampling rate). Down to 8 sps, the response is considered the same as for 10 sps for both the Direct Mode and Pitch Rate Mode B. At 7 sps and below, a definite degradation in performance is noted in the Direct Mode due to a tendency for the pilot to overshoot the mark. This overshoot probably is caused by the pilot expecting an immediate pitching motion that is instead delayed by the sampling interval. When the anticipated motion does not occur, the pilot moves the stick slightly more, which causes too much δE when the sampling instant does occur. Pitch Rate Mode B is better than the Direct Mode for the same sampling rate, except for the 5 sps case, a seemingly anomalous result. At 4 sps, the pilot definitely can sense a delay but comments that he has no trouble attaining and holding a track on the mark. It may be that the pilot controls overshoot better with Pitch Rate Mode B at 4 sps

because he finally realizes why he is overshooting the mark when a definite delay is sensed. The pilot probably does not recognize the problem with the Direct Mode because the overshoots in Δq due to the short-period characteristics are not suppressed as with the Pitch Rate Mode.

As mentioned above, the Direct Mode receives a better rating than the Pitch Rate Mode at the 5 sps rate. The 5 sps tests were repeated to assure that no error in set-up was made, each time with the same result. No explanation has been found for the degraded 5 sps results. Possible (unverified) causes include incorrect calculation of gains or interaction between the sampling frequency and the frequency of the pilot's inputs.

4.2.2 Landing Approach

The results for the landing approach test are given in Table 4-2. The atmospheric conditions were the same as for the tests of Table 4-1. The tests were conducted in essentially calm air. Analysis of this test shows the flare maneuver to be less sensitive to sampling rate than the short final approach or tracking task. This might be explained by examining the pilot's reaction to delayed response. In the tracking task at 105 KIAS or on short final at 70-75 KIAS, the control surfaces generate a larger moment than in the slower flare (60 KIAS). The pilot, therefore, expects an immediate response to his commanded inputs when at cruising speed or on the short final approach, but he has learned there will be slower, more sluggish movements in the flare. He anticipates a natural delay in response on the flare which in effect "masks" the delay of the sampling rate. When the aircraft does not move immediately in response to a commanded input, the pilot expects this and does not over correct with a larger command. Another possible explanation is that pitch tracking at altitude and the pitch control associated with flight path tracking on

TABLE 4-2

Results for Landing Approach Using the Direct Mode

Sampling Rate (sps)	Pilot's Comments
10	No problem: not aware of sampling effect on δE vibrations.
7	Slight overshoot in response on short final, but no problem in flare.
5	Larger overshoots on short final, but still no problem in flare.
3	Overshoots very objectionable on short final, flare still no problem.
2	The margin case: overshoots cause poor control on both short final and flare.
1	Not possible in this configuration: pilot moves stick far enough in 1 sec to send a step to δE that disengages the safety feature of the FBW system of VRA.

short final approach demand a "tight" closed loop control action by the pilot. In the flare, the pilot's control actions are more of a "programmed" or open loop control. Indeed, until near the end of the flare maneuver, visual perception of small tracking errors, which would be required to close a tight control loop, may be difficult.

4.2.3 Pitch Rate in Steady Turn

The telemetry records for the banked turn test show that the longitudinal controller does fight the execution of a coordinated, banked turn. The results are given in Table 4-3.

TABLE 4-3

Results for Banked Turn Test

Control Mode	Bank Angle (deg)	Elevator Deflection (deg)	Steady Longitudinal Stick Deflection Required, (inches)
Direct	30	-1	.24
q Mode B	30	-1	.5
Direct	50	-3	1.2
q Mode B	50	-3	1.7

More δS is needed for the Pitch Rate Mode than the Direct Mode at both bank angles. This is true because the Micro-DFCS pitch rate feedback is trying to suppress the positive Δq developed in a steady turn. The pilot is not aware of the additional deflection needed, so the longitudinal controller did not seem to degrade the lateral-directional response of the VRA in any significant way. This result is specific to this flight test and may not generalize to other aircraft in other flight conditions.

4.2.4 Step Response Analysis

The final quantitative results obtained from the flight tests are the responses to commanded step inputs. The telemetry records of the step responses are presented in Fig. 4-3. Due to a technical malfunction of the ground station, the step response runs were not recorded on tape for later analysis, so the only telemetry records available are those recorded on the strip chart recorder at the time of the actual test. The sense of these plots is opposite to that of the analytic and hybrid tests.

The analysis of the step responses from the flight and hybrid tests is done in the same manner. Since there is a corresponding

hybrid plot for each flight test plot (except for the 120- and 80-KIAS cases), and the hybrid plots were discussed in Section 3.3, only the difference in important aspects of the flight test plots are mentioned here. Pitch Rate Mode A response is similar to that of the Direct Mode. Modes B, C, and D (Fig. 4-3c,d,e) at 10 sps improve the Δq response by essentially the same amount. Mode D commands a larger initial $\Delta\delta E$ deflection, as expected. As the sampling rate is decreased for Pitch Rate Mode B (Fig. 4-3g,h,i,j,k,), the q response stays the same, but the initial δE deflections are smaller, to account for the decrease in sampling rate. In Fig. 4-3k it is easy to see the 0.25-sec sampling interval in δE. Comparing plots from Fig. 4-3 l and m to Fig. 4-3c, there is not much difference in q response from speeds of 80 and 120 KIAS. At 80 KIAS it is apparent, however, that more δE is needed to hold the commanded q as velocity falls to even lower values.

There are two important differences between the Pitch Rate Mode plots of the hybrid and flight tests. The first is the presence of small disturbances on the latter. Low turbulence levels at the wing tips are picked up by the α sensors; the α signal feeds to the elevator, which in turn causes small perturbations in q. In this case, however, the pilot is not aware of these small perturbations and gives the Pitch Rate Modes B-D good ratings at 10 sps. The second difference is that the 10-Hz bandwidth of the VRA's elevator actuator was not modeled in the hybrid tests but was experienced in flight.

The Normal Acceleration Modes have plots in Fig. 4-3 similar to the hybrid plots. With y_d = .25g, the Normal Acceleration Mode A has an initial δE deflection that disengages the FBW system. Consequently, Normal Acceleration Mode A was tested with a commanded input of y_d = .17g. The large overshoots in q are present, as expected, while n_z response is rapid and well damped.

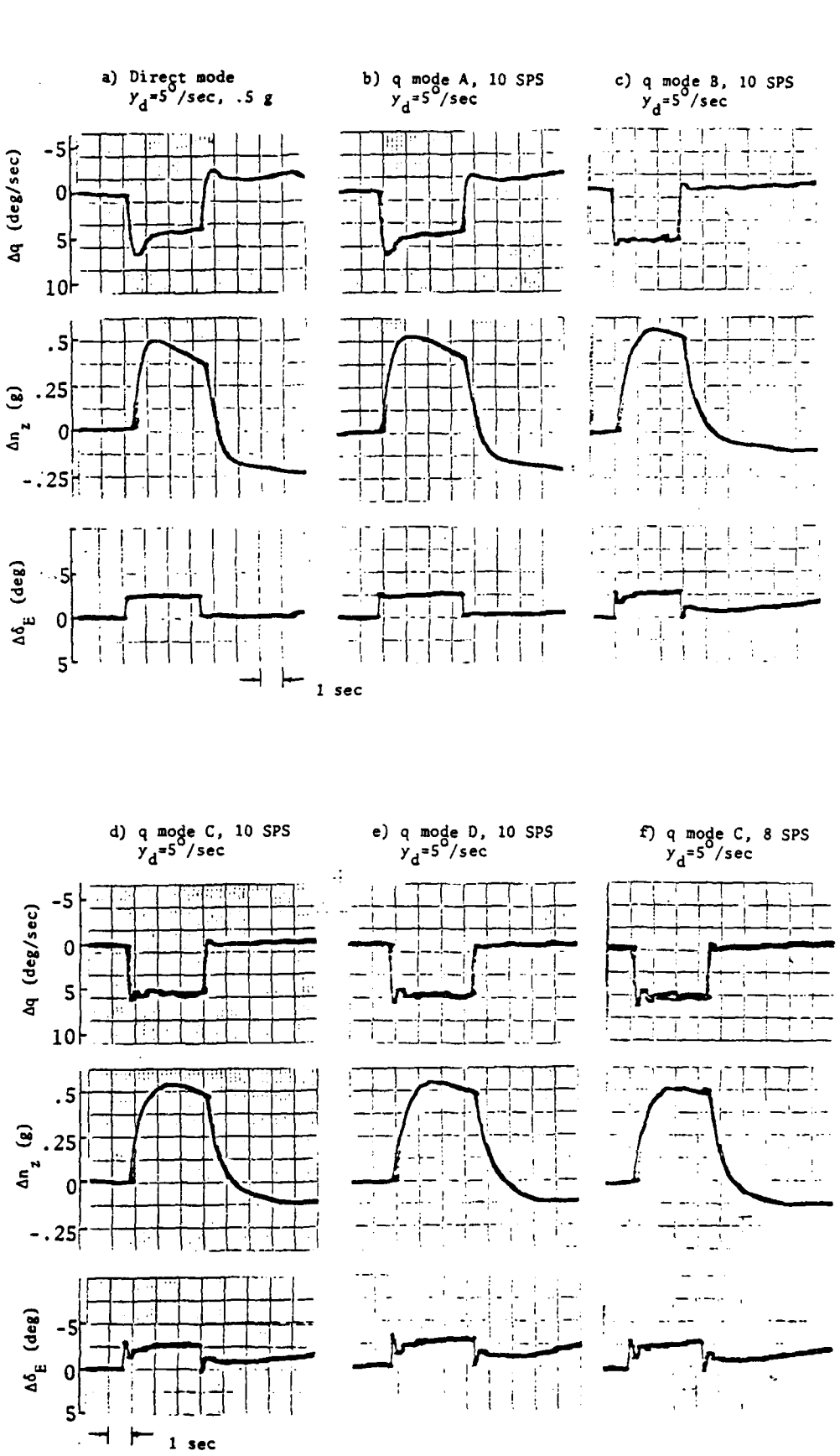

Figure 4-3. Flight Test Step Responses.

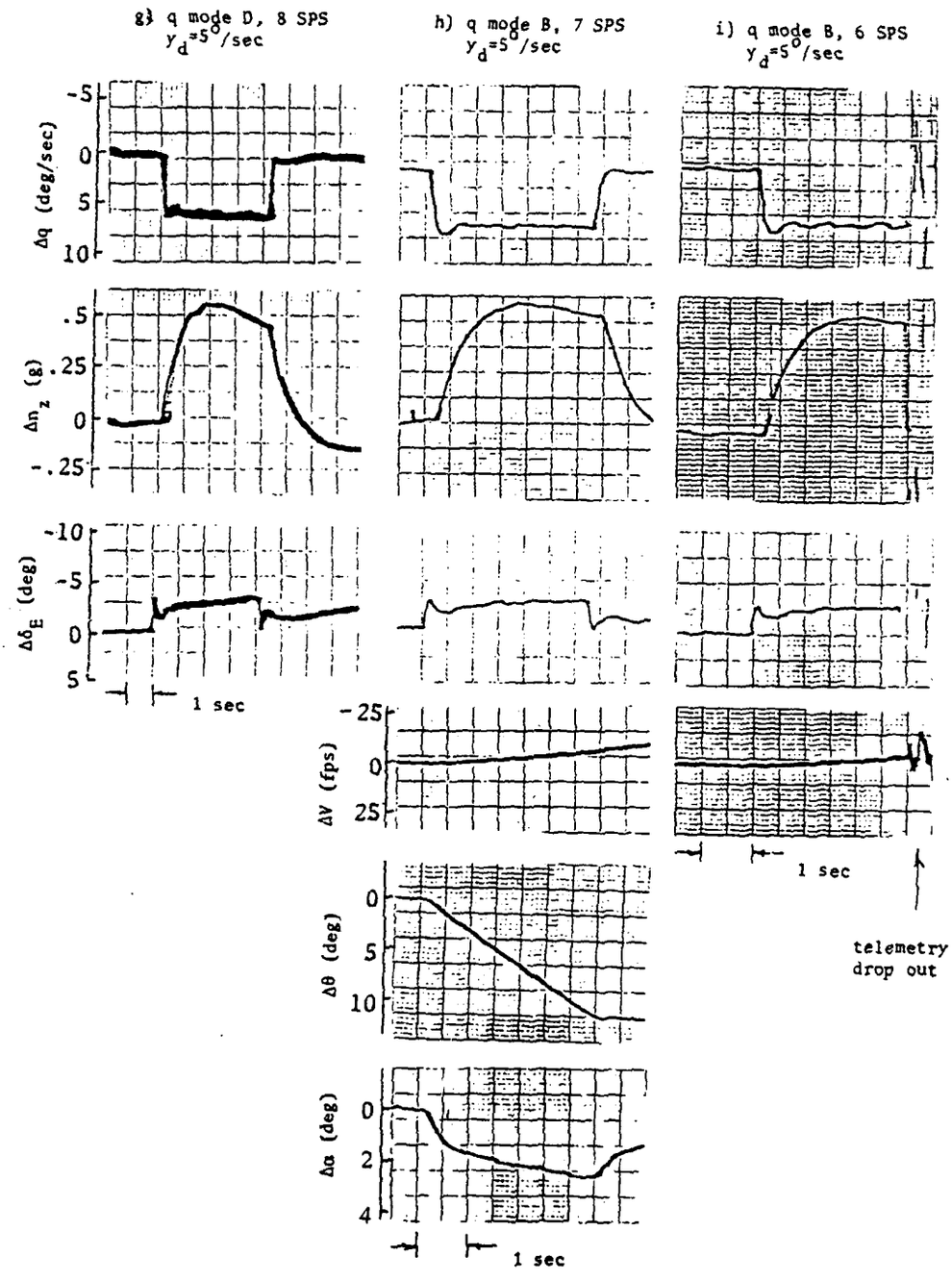

Figure 4-3. continued

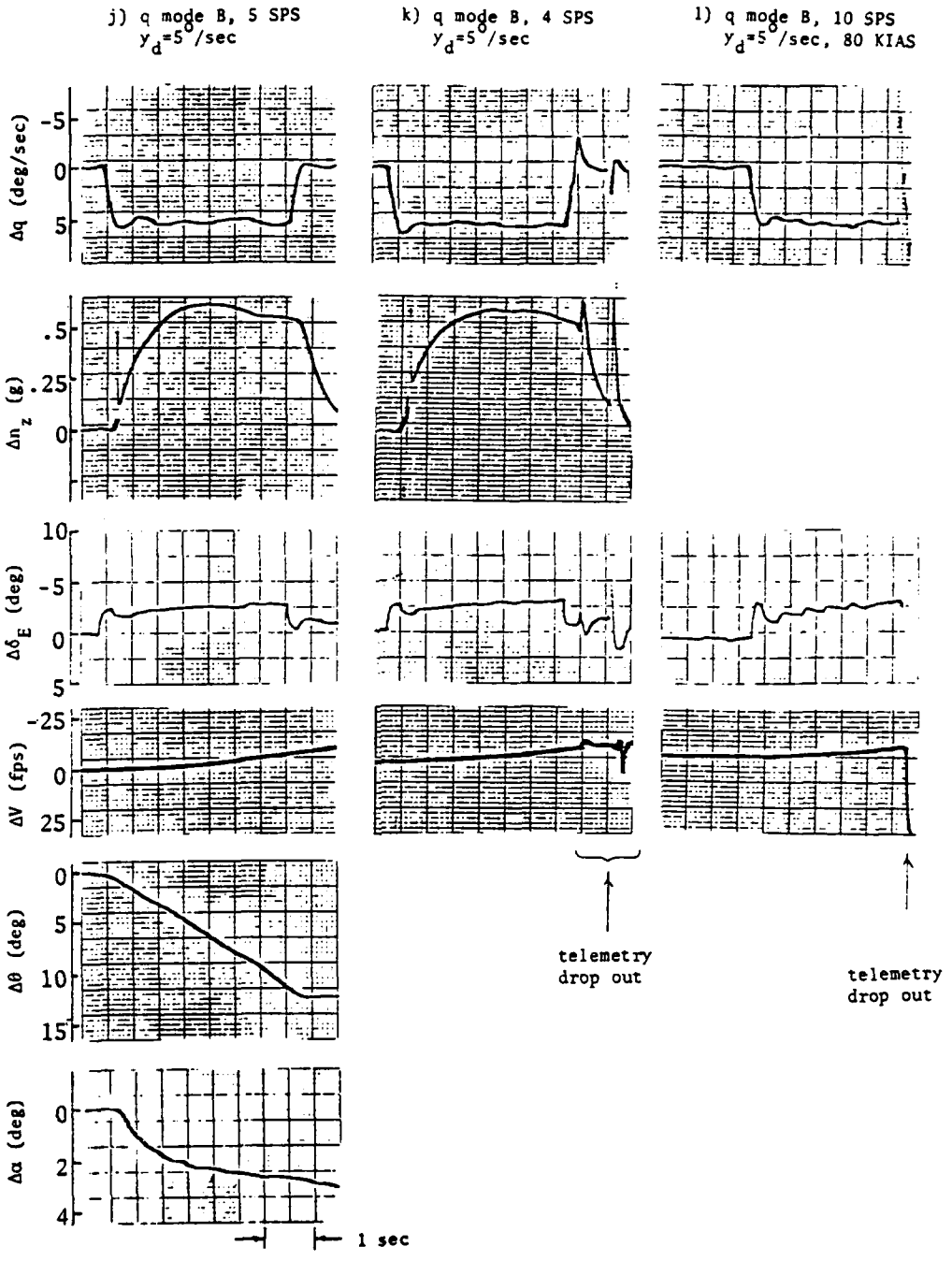

Figure 4-3. continued

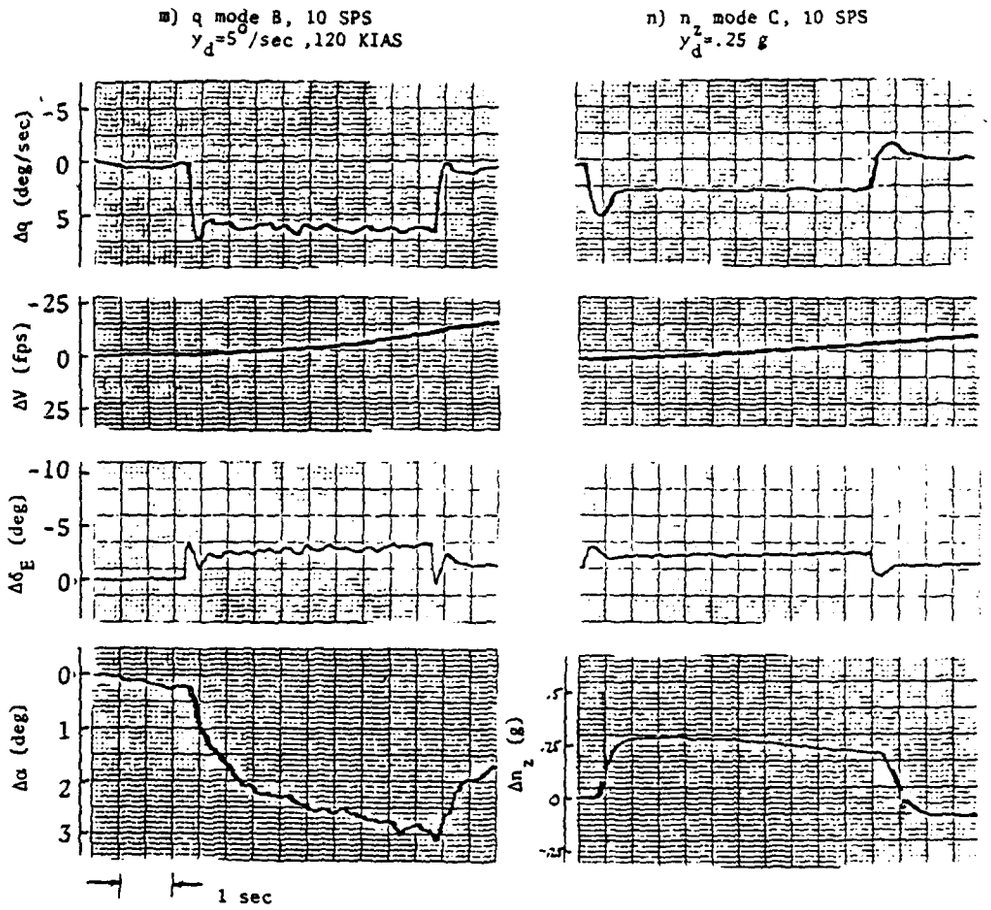

Figure 4-3. continued

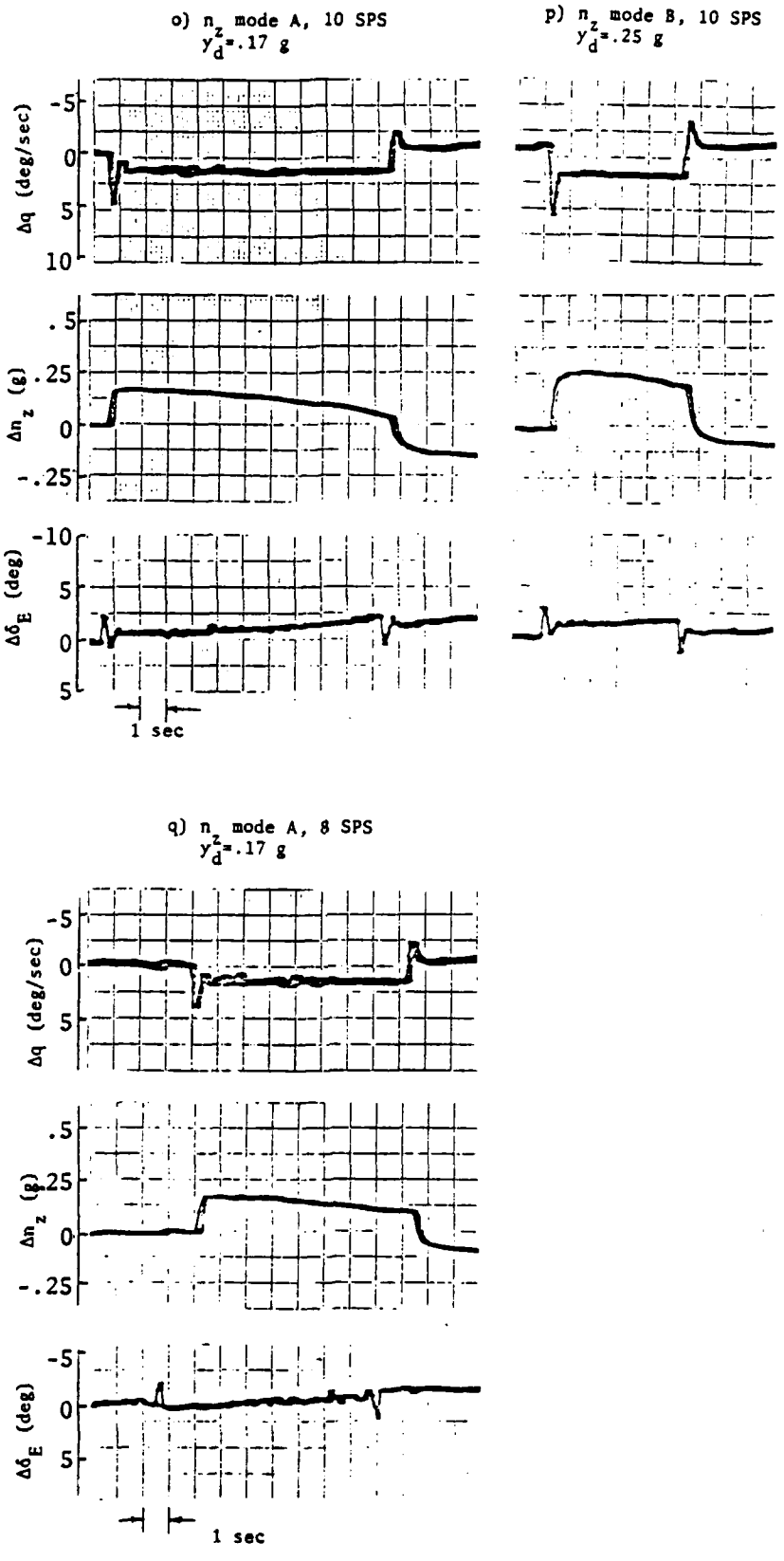

Figure 4-3. concluded.

4.3 FLIGHT TESTS OF DIGITAL PROCESSING EFFECTS

Digital flight control systems possess several characteristics which rarely have occurred in the analog flight control systems of past aircraft. Digital computation is sequential in nature; there is a finite lag between the time an input is received from the pilot and an output is transmitted to the control actuator. Consequently, digital flight control systems always possess a pure time delay, however large or small, which depends on the flight control computer's mean cycle time, program complexity, coding efficiency (Appendix C), and so on. Digital flight control systems also possess an additional "equivalent time delay" as a consequence of the sampling process itself. Rather than operating the control actuator on a continuous basis, pilot commands are sampled at finite instants and held constant until the next sampling instant. The effect is to introduce an equivalent delay equal to half the sampling interval. In addition to these delays, a digital control system has an output with some degree of discreteness or "granularity" depending on the precision of the computations (quantization) and the resolution of sensor inputs and control outputs.

Qualitative data on the above effects were obtained during the fourth through sixth flights. The evaluation pilot for these flights had a general aviation experience background. In addition to his commentary, the pilot usually gave a rating based on the Cooper-Harper pilot rating scale (Ref. 19). To expedite the tests, the CAS-1 program was enlarged to provide rapid selection (through the CDU) of the computation time delay, sampling interval, and control surface resolution. The flight tasks and procedures were essentially the same as those used on previous flights, except that the comparisons between configurations in the tracking task were made without going through the entire set-up procedure described in Section 4.1; the new configuration was merely typed into the CPU. A total of 42 landings and approximately 35 tracking runs (about 5 minutes each) were made during these latter three flights.

4.3.1 Pure Time Delays

Pure time delays greater than the 5-msec delay inherent in the Direct Mode were investigated on Flights 4, 5, and 6. For convenience, the additional delay was made a multiple of the sample interval. Both pitch tracking at altitude and landings were investigated, with and without a simulated turbulence level of 3 fps rms. The data for all three flights are summarized in Table 4-4.

It long has been known that pure time delays between the pilot's commands and the actuation of the control surfaces can degrade the flying qualities, and the tests confirmed this tendency. However, the findings presented herein must be considered tentative. There is evidence that the pilot was adapting to the pure time delay. Also, no quantitative measures, such as touchdown accuracy or sink rate, were made in these preliminary tests. Perhaps the most significant finding was that the turbulence disturbances did not seem to further degrade the flying qualities for the large pure time delay cases.

4.3.2 Control Surface Resolution

The effect of quantization errors represented as an equivalent control surface resolution was investigated during Flights 4 and 5. The normal default value of surface resolution of 12 bits, is altered through the CDU command "R", followed by a two-digit decimal number. The implementation of this command is by bit stripping or masking of the input to the D/A hardware unit. This method reduces the range of the output and introduces a "bias". Only the bias is corrected in the present software program; consequently, there is a change in gain factor as the resolution is reduced. The reduction in the output can be computed by the following expression:

TABLE 4-4

Results for Pure Time Delays

Equivalent Time Delay msec	Pure Time Delay msec	Pilot's Comments
a)	Tracking Task, Direct Mode	
55	5	Good tracking, I can hear and feel the digital control inputs but the performance seems the same as the basic aircraft system. Pilot rating = 2.
155	105	The delay is noticeable. I can get the final precision on attitude so it is not too bad, it is only bothersome for fast tracking where I get some overshooting and some induced oscillation. Pilot rating = 3.
255	205	There is a slight pilot-induced oscillation (PIO) when making larger corrections. I can still get the required precision in attitude. Pilot rating = 3.
355	305	There is a definite tendency to PIO; it takes a conscious effort to relax the controls to keep from losing control. If you use slow motions, you can still achieve precesion in final attitude, the PIO tendency is very strong but the motions damp rapidly if you release the controls. Pilot rating = 6.
b)	Landing Task, Direct Mode	
55	5	Good. Pilot rating = 2.
155	105	Some slight compensation is required because of the delay. Pilot rating = 3.
255	205	Tendency to PIO after the flare. Pilot rating = 4.

TABLE 4-4. (continued)

Equivalent Time Delay msec	Pure Time Delay msec	Pilot's Comments
355	305	Very PIO prone; if I'm careful, its not too bad up until the flare. My landings all were successful (four for this configuration), but I still feel there is an element of luck involved. Pilot rating = 5.5.
455	405	Controllable in the approach by using slow, open loop like inputs. Can not be landed using conventional techniques. Pilot rating = 7.
c)	Landing Task, Turbulence, Direct Mode	
55	5	Slightly worse than the no turbulence case, mostly in the lateral-directional mode. Pilot rating = 3.
155	105	I can see the effect of the delay but it is not affecting my performance. My rating is primarily due to the turbulence. Pilot rating = 3.
255	205	Pilot rating = 3.5.
255	305	Not too bad on the flare; no PIO. I'm compensating for the delay by using slow inputs. Pilot rating = 4.
455	405	I don't seem to mind the delay as much with turbulence, or I'm learning and changing my technique. My rating is based on the fact that all my landings were successful. Pilot rating = 5.

$$\frac{A^*}{A} = 1 - \frac{1}{2^B} \tag{63}$$

where A is the nominal range

A* is the actual range

b is the number of bits

The control surface resolution, R, may be expressed by

$$R = \frac{A^*}{2^B - 1}$$

$$R = \frac{A}{2^B} \tag{64}$$

The current authority (A) of the DFCS is 30 deg of elevator. Flight tests are possible with a resolution of as low as 3 bits, corresponding to a surface resolution of 3.75 deg. At this resolution the control gains, if not corrected, are reduced by the factor 0.875, and the control authority is reduced to 26.25 deg. Lower resolution values result in safety disengage of the VRA variable response control system. The larger control steps create differences between the actual and commanded elevator position which exceed the threshold value chosen to protect against "hard over" electronic failures.

The pilot commentary data is summarized in Table 4-5. In the Direct Mode, reductions in control surface resolution to 7 or 6 bits did result in some performance degradation in the tracking task; (6-bit resolution corresponds to elevator increments of .47 deg); however, no closed-loop stability problems were encountered with progressively lower values.

Landings were made with resolutions as low as 3 bits (3.75-deg elevator resolution) with much less difficulty than might be expected.

The pilot is able to readily compensate for these lower resolution cases by increasing the frequency of his inputs. With the Pitch Rate Mode B command augmentation system, reductions in resolution were less bothersome. Landings were readily performed and the pilot compared the airframe motions resulting from the 3.75-deg elevator steps at 3-bit resolution to flying through light turbulence. Consequently, in the presence of simulated turbulence, reductions in control surface resolution were not noticeable (except for airframe/structural shaking).

TABLE 4-5

Results for Control Surface Resolution

Bit Resolution	Minimum Surface Increment, deg	Pilot's Comments
a)	Tracking Task, Direct Mode	
12	.007	Good. Pilot rating = 2.
8	.12	Difference not noticeable. Pilot rating = 2.
6	.47	Definite degradation in tracking performance. I can't get the precision expected, but it is OK for normal flying. Pilot rating = 4 for tracking.
5	.94	Very noticeable degradation. Even with higher frequency inputs, I have trouble holding the desired precision pitch attitude. Even normal flying performance is less than desired. Pilot rating = 5.5 for tracking.
4	1.88	Tracking performance is very poor; I can't achieve the desired attitude even with continuous inputs. I'm always passing through the desired attitude. Pilot rating = 7.
5	.94	(With an increase of sample rate from 10 sps to 30 sps). This helped quite a bit. Pilot rating = 4.5.
b)	Landing Task, Direct Mode	
8	.12	Same as basic before. Pilot rating = 2.
6	.47	No problem, no performance loss. Pilot rating = 2.
4	1.88	It seems like turbulence; I can't get a good long-term trim, but task performance is OK. Pilot rating = 4.

TABLE 4-5. (continued)

Bit Resolution	Minimum Surface Increment, deg	Pilot's Comments
3	3.75	The long term trim is bad but the problem is not bad on approach and landing. I tend to overflare and have some trouble "finding" the ground. Not as bad as I expected. Pilot rating = 5.
c)		Landing Task, Turbulence, Direct Mode
12	.007	The problems are chiefly lateral-directional due to turbulence. Not much different in the pitch axis. Pilot rating = 3.
6	.47	About the same. Pilot rating = 3.
4	1.88	I can't see the effect yet. Pilot rating = 3.
3	3.75	No big problems in pitch. Pilot rating = 3.5.
d)		Landing Task, Pitch Rate Mode B
12	.007	Better performance than the basic aircraft (Direct Mode). Improved open loop response, good speed control. Pilot rating = 1.5.
8	.12	Still OK, no significant change (after a second run). Pilot rating = 2.0.
6	.47	I still rate this as 2.0 or better, I can't see the effect in performance.
5	.94	Still OK on aircraft response. Pilot rating = 2.0.
4	1.88	I now notice the effect in terms of aircraft response. Pilot rating = 3.0.
3	3.75	A lot of airframe shake, some pitching motion, not much worse than previous run in terms of performance. My main concern is with airspeed control. Aircraft motions are similar to flying in turbulence. Pilot rating = 3.5.

AD-A089 147 PRINCETON UNIV NJ DEPT OF MECHANICAL AND AEROSPACE --ETC F/G 1/4
DIGITAL FLIGHT CONTROL RESEARCH USING MICROPROCESSOR TECHNOLOGY--ETC(U)
MAY 80 R F STENGEL, J C SEAT, G E MILLER N00014-78-C-0257
UNCLASSIFIED MAE-1425 ONR-CR-300-003-1 NL

2 OF 2
AD A089147

END
DATE FILMED
10-80
DTIC

4.3.3 Sampling Delays

Although the sampling process introduces an equivalent delay equal to half the sampling interval, the effect is not necessarily directly equivalent to a pure time delay from the pilot's control standpoint. For comparison, two configurations having the same equivalent time delay of 225 msec were tested, as shown in Table 4-6.

TABLE 4-6

Time Delay Comparison Configurations

Configuration	Pure Time Delay, msec.	1/2 x Sample Interval, msec.	Sample Rate, sps	Equivalent Delay, msec.
A	205	50	10	255
B	5	250	2	255

The average delay chosen for the test was based on the previous pure time delay results for the tracking task. The equivalent time delay of 255 msec appeared to be at the "knee" of the pilot's rating curve where differences might be more noticeable.

The pilot commented that the significant difference was the closed-loop response to a rapid step tracking task, although both cases were characterized by an overshoot and short PIO in stabilizing on the new attitude. With configuration A the overshoot and (PIO) oscillations were always larger. Put another way, Configuration B appeared to have a higher closed-loop damping ratio.

4.3.4 Concluding Tests

On Flight No. 6, the Micro-DFCS lateral and directional Direct Mode was operational. A preliminary assessment of the effects of pure time delay and resolution with regard to lateral/directional control aspects was made.

Again, control surface resolution of 8 bits was not noticeable, and somewhat lower levels could be tolerated without performance degradation. Time delays seem more critical. Delays of .25 sec and greater were found to be very PIO prone. Landings were made with the three-axis Micro-DFCS in the Direct Mode with delays of up to 355 msec on both pitch and roll axes.

5. CONCLUSIONS

A number of conclusions can be drawn as a consequence of this research relating to flight control hardware, software, control law design, and flying qualities of digitally controlled aircraft. Flying qualities conclusions are based on a limited number of flights and are of a preliminary nature. All conclusions are summarized below, and additional details can be found in the text.

- Currently available microcomputer components and system-development software provide flexible tools for digital flight control research. Equipment available during 1978 proved itself fully capable of executing comprehensive control laws at reasonable sampling rates in the Micro-DFCS.

- Digital flight control research clearly is facilitated by several existing features of the Variable-Response Research Aircraft (VRA), principally its sensors, control actuators, analog logic, safety circuits, and dual-pilot operation (with mechanical backup flight control). The variable-stability control system's DC analog signal levels were compatible with the Micro-DFCS's A/D and D/A converters, so digital-analog interface was a relatively easy matter.

- Linear-quadratic (LQ) sampled-data regulator theory provides a powerful, practical technique for digital flight control design. This was verified by the progression from digital analysis through hybrid simulation to actual flight. The analysis provided an accurate prediction of flight test results, and the LQ control synthesis algorithms achieved design objectives.

- Pitch rate (q) and normal acceleration (n_z) control laws based on reduced-order (2-state) aircraft models both improve the VRA's flying qualities, although the latter seemed a little too abrupt (or "crisp"), commanding higher bandwidth elevator motions. Such results are, of course, subject to cost function weightings.

- Flying qualities of the direct digital mode at 10 sps were indistinguishable from conventional direct control. The principal indication of digital control was a rumble reminiscent of stall buffet, the result of "staircased" control motions.

- Decreasing the direct mode sampling rate led to gradually increasing control overshoots, as perceived by the evaluation pilot. Degraded tracking first became noticeable at 7 sps, control overshoots on short final approach became objectionable at 5 sps, but flare (in still air) was "no problem" down to 3 sps. It was possible to land the VRA at 2 sps in still air conditions with no constraint on touchdown point. Safety disconnects engaged during 1-sps approach, making touchdown impossible; however, the evaluation pilot felt that 1 sps is beyond the "critical limit" for the landing task.

- For tracking at altitude, the pitch rate mode tended to smooth the perceived effects of decreasing sampling rate down to at least 4 sps. There was an anomalous point at 5 sps, where the direct mode appeared smoother than the pitch rate mode.

- Because the control contains neither "washout" nor "feed-forward" compensation, the pitch rate mode opposed steady turns, but the effect was not particularly objectionable in these tests.

- Pure time delays have a greater impact on flying qualities than equivalent sampling delays (half the sampling interval) of equal value. It is concluded tentatively that the pilot finds adaptation to sampling delay to be the easier task. Relatively short time delays (less than 0.1 sec) can be sensed by the pilot and are considered objectionable but acceptable. There is sharp degradation in pilot opinion for pure time delays in excess of 0.2 sec.

- Quantization errors (resolution or "granularity") have the appearance of light turbulence to the pilot and do not degrade stability in a major way. The pilot tends to compensate by "dithering" his control inputs. Eight-bit resolution in control surface commands can not be distinguished from 12-bit resolution in still air. Moderate difficulty was experienced in performing landings with 3-bit (3.75 deg) elevator resolution and 10-sps sampling rate. Simulated 3-fps (rms) turbulence tended to mask quantization errors.

This program has demonstrated the utility of microprocessor technology in conducting digital flight control research, allowing certain fundamental questions of pilot acceptance and aircraft flying qualities to be answered for the first time. This research is expected to contribute to a better understanding of how to build superior flight control systems for future aircraft.

APPENDIX A

RESEARCH SYSTEMS

A.1 VARIABLE-RESPONSE RESEARCH AIRCRAFT (VRA)

The VRA is a highly modified Navion equipped with inertial, air data, and navigation sensors, as well as six independent force and moment controls. The VRA, shown in Fig. A-1, has been used to conduct a broad range of experiments in aircraft flying qualities, human factors and control in the past. The aircraft has played a major role in establishing current military and civil flying qualities criteria, and with the addition of the Micro-DFCS, the VRA is equipped to expand this type of research, as well as to investigate advanced digital control concepts.

Independent control of three forces and three moments is provided by commands to the elevator, ailerons, rudder, throttle, direct-lift flaps, and side-force panels (Fig. A-2). The control surfaces are driven by hydraulic servos originally fitted to the B-58 aircraft. The modified VRA units incorporate solenoid-actuated valves with force-override features for quick disengagement. Characteristics of the control effectors are summarized in Table A-1. Surface rate limits are seen to range from 60 to 110 deg/sec. Bandwidths are given for flat response and 6 db attenuation (in

Figure A-1. Variable-Response Research Aircraft (VRA).

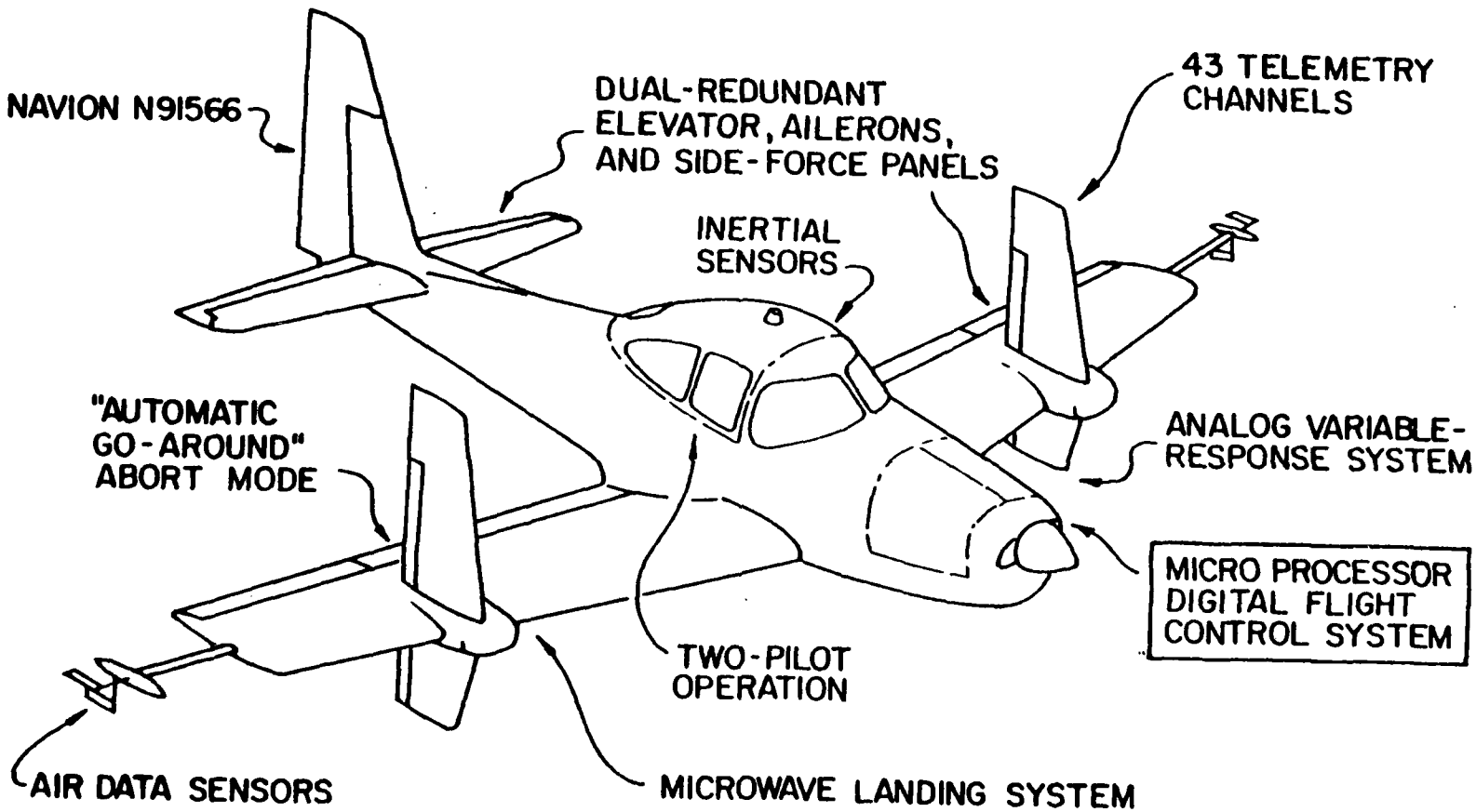

Figure A-2. Major Components of VRA.

parentheses), except that thrust bandwidth is specified by the frequency for 3 db attenuation. The aircraft's normal operating speed range is 65 to 120 kt; maximum specific forces and moments ("control power") are given for 70-kt airspeed. At IAS = 105 kt, maximum direct lift and side-force accelerations are 1g and 0.5g, respectively.

The sensors used for most flight testing include angular rate gyros and linear accelerometers for all three axes, vertical and heading gyros, dual angle-of-attack and sideslip-angle vanes, radar altimeter, indicated airspeed, control surface positions, and cockpit control positions. Several other signals (e.g., air temperature, barometric altimeter, altitude rate, and TALAR microwave landing system signals) are available for system feedback or telemetry recording. The present telemetry system allows 42 data channels to be multiplexed and transmitted to the FRL ground station described below.

TABLE A-1

VRA Control Characteristics

Control	Displacement Limit, deg	Rate Limit, deg/sec	Bandwidth, H_z	Maximum Specific Force or Moment (IAS = 70kt)
Roll	30.	70.	5 (10)	4.1 rad/sec^2
Pitch	-30. +15	70.	5 (10)	4.4 rad/sec^2
Yaw	15.	70.	5 (10)	1.9 rad/sec^2
Thrust	-	-	0.6	0.1 g
Side Force	35.	60.	2 (3)	0.25 g
Normal Force	30.	110.	2 (3)	0.5 g

The aircraft is flown by a two-man crew during all research. This provides a number of advantages in comparison to single-pilot operation from the standpoint of flight safety and experimental efficiency. The instrument panel and controls are shown in Fig. A-3. The conventional mechanical aircraft system is flown by the safety pilot in the left seat, while the fly-by-wire aircraft system used for research is flown by the evaluation pilot seated at the right. This system includes the Micro-DFCS and redundant aileron, elevator, and side-force actuators for protection against system failures. The evaluation pilot's station is tailored to the experiment; for the Micro-DFCS program, this station includes a center control stick, thumb switches for trim and direct force modes, rudder pedals,

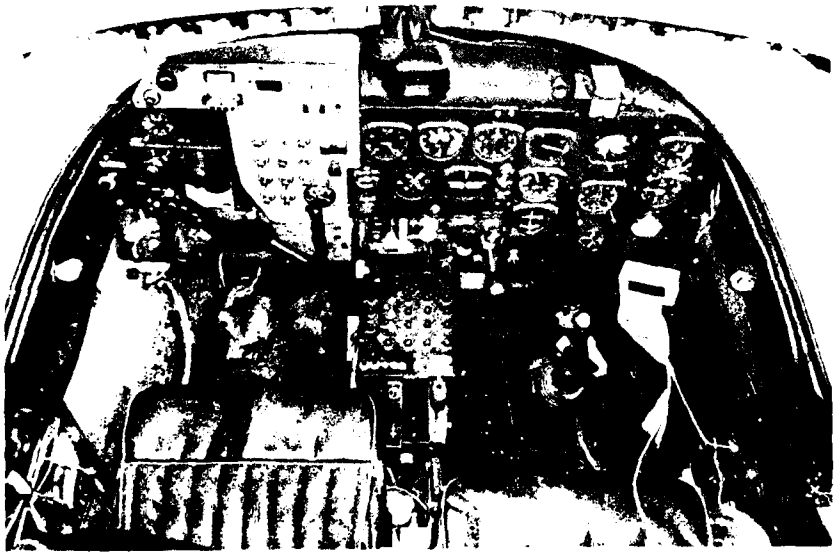

Figure A-3. Instrument Panel and Controls of VRA.

sideslip and side-force-panel meters, and conventional instruments.

The safety pilot is the in-flight test conductor, monitoring systems and adjusting all experimental parameters. He has several electrical and hydraulic mechanisms for disengaging the Micro-DFCS and the variable-response system in the event of a malfunction, as well as an "automatic go-around" abort mode which makes safe experimentation through touchdown possible. The abort mode commands a 20-deg flap setting and climb power when activated; at 70-kt (36 m/s) airspeed on a 6-deg glideslope, an up-flap "hardover" failure can be corrected and climbout can be initiated with a maximum altitude loss of 10 ft (3 m).

A.2 EXPERIMENTAL FACILITIES

The VRA is operated from the flight test facility at Princeton University's James Forrestal Campus. The facility includes the FRL hangar, laboratories, and shops, plus a 3000-ft Basic Utility II runway. TALAR 3 and 4 fixed-beam microwave landing systems (MLS) furnish precision approach-path guidance.

The ground station (Fig. A-4) at the FRL is used to receive, record, and analyze the telemetered data from the VRA. It includes a Honeywell seven-channel tape recorder, an FM or AM receiver presently operating at 1458 MHz in the FM mode, a telemetry demultiplexer with five translators, an EAI TR-48 analog computer, a radio telephone, and a six-channel paper strip chart recorder. The PDM

telemetry system provides 42 data channels, each sampled at a rate of 20 sps. The telemetry data from the receiver can be recorded on tape and demultiplexed five channels at a time for plotting on the strip chart recorder. The analog computer scales and buffers all input channels from the translators to the strip chart recorder.

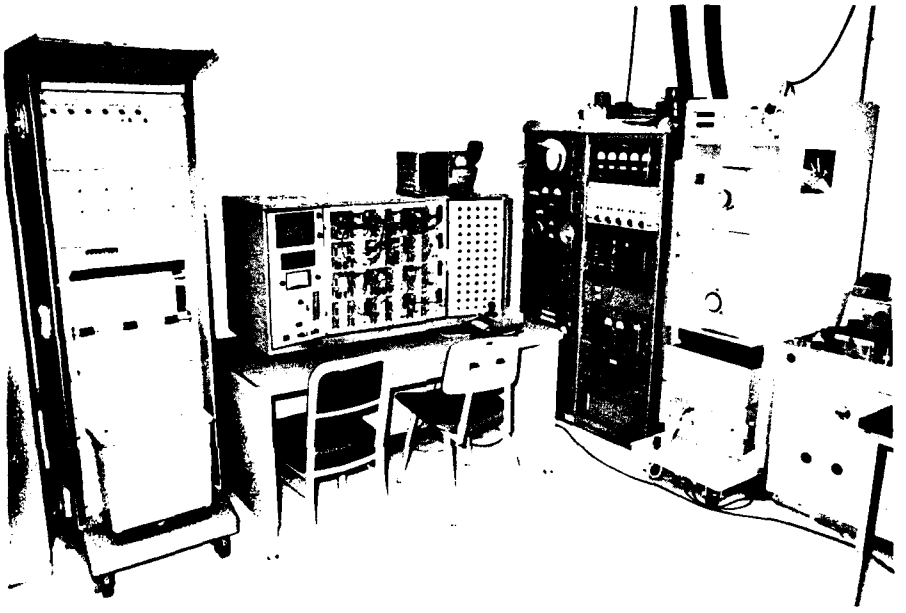

Figure A-4. FRL Ground Station.

In addition to the analog computer's function in analyzing telemetered data, it is also used for ground-based simulations of the VRA and other dynamic systems. In the Micro-DFCS study, it is used to model the VRA for ground testing the microcomputer software. The schematic and corresponding potentiometer settings are presented in Fig. A-5 and Table A-2, respectively.

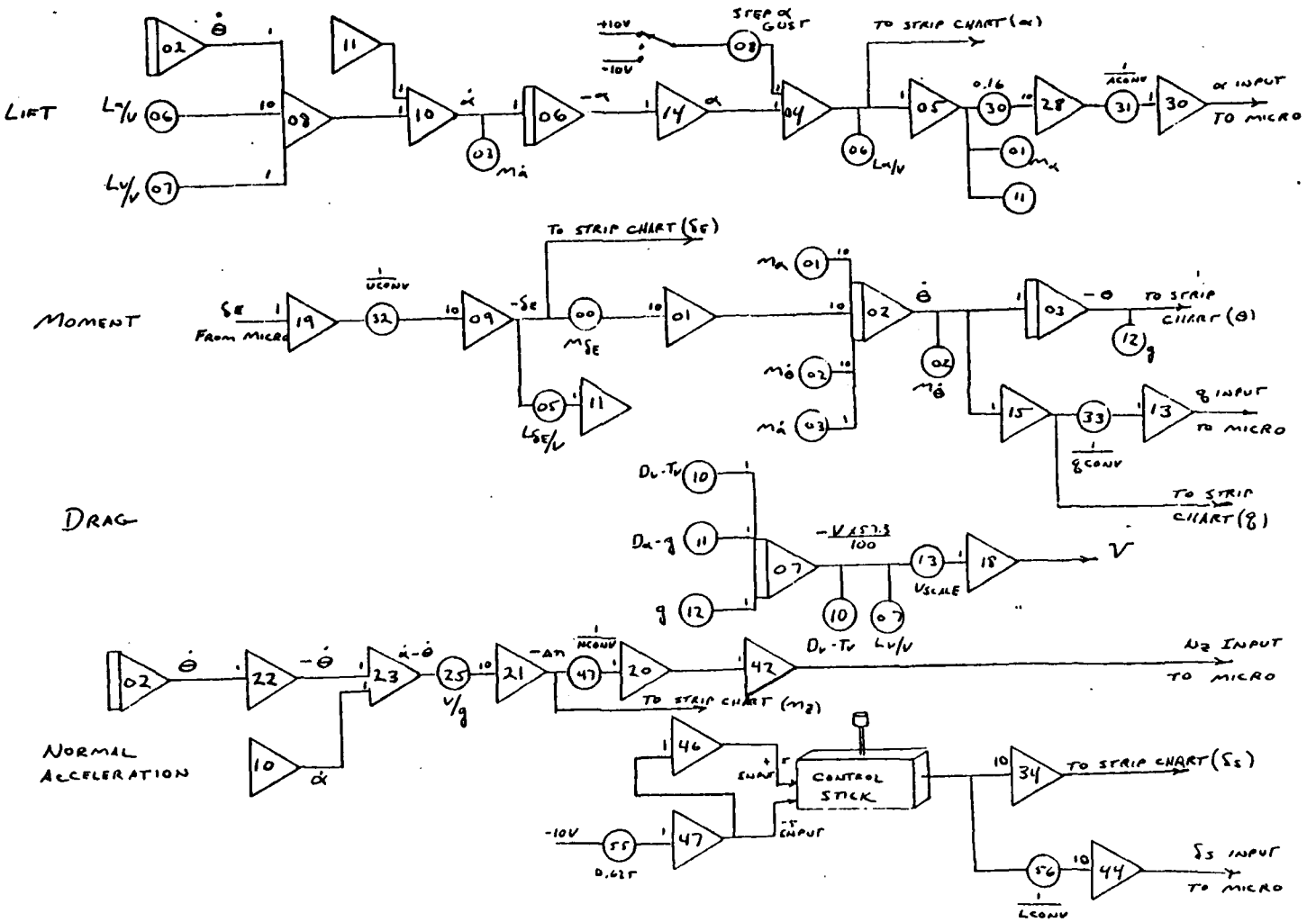

Figure A-5. Schematic of Simulated VRA at 105 KIAS With Scaling for Microcomputer Interface.

TABLE A-2

COMPUTER POTENTIOMETER SETTINGS
FOR VRA LONGITUDINAL MODEL (105 KIAS)

Pot	Parameter	Scaling	Setting
00	M_{δ_E}	$M_{\delta_E}/100$	.125
01	M_α	$M_\alpha/10$	.835
02	$M_{\dot{\theta}}$	$M_{\dot{\theta}}/10$	.208
03	$M_{\dot{\alpha}}$		.910
05	L_{δ_E}/V		.125
06	L_α/V	$L_{\alpha/V}/10$	.200
07	L_V/V	$100\ L_{V/V}$	.200
08	Step Gust Scaling		.100
10	D_V-T_V		.073
11	D_α-g	D_{α}-g/100	.060
12	g	g/100	.322
13	V_{scale}	$\frac{100}{57.3x5}$	.349
25	V/g	$V/g \times \frac{2x10}{57.3}$	.190
30	α_M scaling error	$\alpha_{MSE}/10$	.160
31	$\frac{1}{ACONV}$		.345
32	$\frac{1}{UCONV}$	$\frac{1}{UCONVx10}$	.144
33	$\frac{1}{QCONV}$		.225
47	$\frac{1}{NCONV}$		.188
55	Stick Range		.625
56	Stick Scaling		.592

Nominal Scaling: 1 volt = 1^o, 1^o/sec, 5 ft/sec, .05 g's

APPENDIX B

DESCRIPTION OF APL FUNCTIONS FOR GENERATING OPTIMAL GAINS AND TIME HISTORIES

The equations from modern control theory (given in Section 2) are coded in APL functions. The functions are listed in Table B-1. A short description of each function is given below:

FCLOOP - Calculates the closed-loop F matrix for a second-order system given Φ, Γ, and the gains, k. F_{CL} is returned in variable FCL. Uses Eq. 46.

FCL4 - Calculates the closed-loop F matrix for a fourth-order system given the fourth-order Φ and Γ, and the second-order gains, k. F_{CL} is returned in variable FCL.

FOLLOW - Calculates continuous-time Q, M, and R for implicit model-following given the matrix F of the model, matrices F and G of the VRA and a weighting matrix, W. Uses Eqs. 57-59.

GAIN - Calculates optimal gains using Eq. 29. Gains are passed to variable k. The dimension of k is changed in k4 for use in FCL4.

GAMMA - Calculates the discrete control effects matrix, Γ, for a second-order system. It is a monadic operator that uses the second-order Φ(STM). Variable GAM holds the result. Uses Eq. 12.

GAMMA4 - Calculates fourth-order Γ. It is a monadic operator that uses the fourth-order Φ(STM4).

GENSTM - Generates 100 Φ matrices using time intervals in 1 percent increments of the sampling interval. These matrices are for use in function QMR for calculating discrete weighting matrices.

IDENT - Forms an identity matrix. A monadic operator that uses the matrix dimension as the argument. Result returned in variable I.

QMR - Calculates discrete weighting matrices $\hat{Q}$, $\hat{M}$, and $\hat{R}$ from continuous Q and R. Uses simple Euler integration in 100 steps. Uses Eqs. 26-28.

QMRF - Calculates discrete weighting matrices $\hat{Q}$, $\hat{M}$, and $\hat{R}$ from continuous Q, M, and R. Uses simple Euler integration in 100 steps. Uses Eqs. 60-62.

RICCATI- Solves Riccati equation (Eq. 30). Result returned in variable P.

SONETWO- Calculates relation between $\Delta\underline{y}_d$ and $\Delta\underline{x}^*$: S_{12}. It uses the result from STWOTWO. Uses Eq. 18.

STMDYN - Calculates Φ given sampling interval and F matrix. Result is returned to variable specified by using the "back arrow." Uses Eq. 11.

STWOTWO- Calculates relation between $\Delta\underline{y}_d$ and $\Delta\underline{u}^*$: S_{22}. Uses Eq. 19.

SYSMODEL-Generates a time history for the second-order system. The function will ask if a printed table is desired (answer yes or no). The time history will run for 5 sec. unless 'BREAK' is depressed. The time history is stored in vectors ΔQ, ΔALPHA, TIME, and DELU. Vector ΔQ contains elements $\Delta\underline{x}_{1_k}$, ΔALPHA contains $\Delta\underline{x}_{2_k}$, TIME contains the time instances spaced by the sampling interval, and DELU contains $\Delta\underline{u}_k$. These vectors are used in the 10 LINPLOT functions to plot the time histories. Uses Eqs. 10 and 22.

SYSMOD4-Same as SYSMODEL except 4th-order time history is generated using the 2nd-order gains. Additional vectors for plotting are Δv and ΔGAM. Vector Δv contains $\Delta\underline{x}_{3_k}$ and ΔGAM contains $\Delta\underline{x}_{4_k}$.

```
      ∇FCLOOP[□]∇
      ∇ FCLOOP;SM;R;FACTOR;INDEX;I;IFCL
[1]   A CALCULATES C.L. F MATRIX FOR SECOND ORDER SYSTEM
[2]    R←(⍴,STM)×0.5
[3]    I←(⍳R)∘.=⍳R
[4]    N←0
[5]    FCL←I-I
[6]    STMCL←STM-GAM+.×K
[7]    STMI←I
[8]   LO:N←N+1
[9]    STMI←(STMCL-I)+.×STMI
[10]   FACTOR←((¯1)*N+1)×STMI
[11]   IFCL←FCL+FACTOR÷N
[12]   INDEX←(+/|,FCL-IFCL)÷R*2
[13]   FCL←IFCL
[14]   →(N=100)/STP
[15]   →(INDEX>0.00001)/LO
[16]   →CONT
[17]  STP:'DID NOT CONVERGE ON C.L.F  MATRIX IN 100 ITERATIONS.'
[18]  CONT:FCL←FCL÷DT
      ∇
      ⋄


      ∇FCL4[□]∇
      ∇ FCL4;SM;R;FACTOR;INDEX;I;IFCL
[1]   A CALCULATES C.L. F MATRIX FOR FOURTH ORDER SYSTEM
[2]    R←(⍴,STM4)×0.5
[3]    I←(⍳R)∘.=⍳R
[4]    N←0
[5]    FCL←I-I
[6]    STMCL←STM4-GAM4+.×K4
[7]    STMI←I
[8]   LO:N←N+1
[9]    STMI←(STMCL-I)+.×STMI
[10]   FACTOR←((¯1)*N+1)×STMI
[11]   IFCL←FCL+FACTOR÷N
[12]   INDEX←(+/|,FCL-IFCL)÷R*2
[13]   FCL←IFCL
[14]   →(N=100)/STP
[15]   →(INDEX>0.00001)/LO
[16]   →CONT
[17]  STP:'DID NOT CONVERGE ON C.L.F  MATRIX IN 100 ITERATIONS.'
[18]  CONT:FCL←FCL÷DT
      ∇
      ⋄


      ∇FOLLOW[□]∇
      ∇ FOLLOW
[1]   A CALCULATES CONTINUOUS TIME Q, M, R
[2]   A FOR IMPLICIT MODEL-FOLLOWING GIVEN
[3]   A THE MATRIX F OF THE MODEL.
[4]    Q←(⌹F-FM)+.×W+.×F-FM
[5]    M←(⌹G)+.×W+.×F-FM
[6]    R←(⌹G)+.×W+.×G
      ∇
```

Table B-1. Listing of APL Functions.

```
      ∇GAIN[□]∇
      ∇ GAIN
[1]   ⍝ CALCULATES OPTIMAL FEEDBACK GAINS
[2]    K←(⌹RH+(⍉GAM)+.×P+.×GAM)×((⍉GAM)+.×P+.×STM)+⍉MH
[3]    K4← 1 4 ⍴(0,0,K)
       ∇
       ⋄

       ∇GAMMA[□]∇
       ∇ GAMMA STM
[1]   ⍝  CALCULATES GAMMA MATRIX
[2]    GAM←STM+.×(⌹F)+.×(I-(⌹STM))+.×G
       ∇
       ⋄

       ∇GAMMA4[□]∇
       ∇ GAMMA4 STM
[1]   ⍝  CALCULATES 4TH ORDER GAMMA MATRIX
[2]    GAM4←STM+.×(⌹F4)+.×(I-(⌹STM))+.×G4
       ∇
       ⋄

       ∇GENSTM[□]∇
       ∇ GENSTM;STEP
[1]   ⍝ GENERATES 100 TRANSITION MATRICES FOR QMR
[2]    T←STEP←DT÷100
[3]    GSTM←I
[4]   AGAIN:STMI←T STMDYN F
[5]    GSTM←GSTM,STMI
[6]    →(T=DT)/0
[7]    T←T+STEP
[8]    →AGAIN
       ∇
       ⋄

       ∇IDENT[□]∇
       ∇ I←IDENT N
[1]   ⍝  MAKES IDENTITY MATRIX OF SIZE N
[2]    I←⍳N
[3]    I←I∘.=I
       ∇
       ⋄
```

Table B-1. continued

```
      ∇QMR[□]∇
      ∇ QMR;STEP
[1]   A  CALCULATES Q HAT, M HAT , R HAT
[2]    MH←GAM-GAM
[3]    QH←I-I
[4]    RH←0
[5]    T←STEP←DT÷100
[6]    C←1
[7]   LOOP:C←C+2
[8]    D←C+1
[9]    STATETM← 2 2 ⍴GSTM[1;C],GSTM[1;D],GSTM[2;C],GSTM[2;D]
[10]   GAMMA STATETM
[11]   IQ←STEP×(⍉STATETM)+.×Q+.×STATETM
[12]   QH←QH+IQ
[13]   IM←STEP×(⍉STATETM)+.×Q+.×GAM
[14]   MH←MH+IM
[15]   IR←STEP×R+(⍉GAM)+.×Q+.×GAM
[16]   RH←RH+IR
[17]   →(T=DT)/0
[18]   T←T+STEP
[19]   →LOOP
       ∇
       ⋄

      ∇QMRF[□]∇
      ∇ QMRF;STEP
[1]   A  CALCULATES Q HAT, M HAT , R HAT
[2]   A FROM CONTINUOUS Q, M, R
[3]    MH←⍉GAM-GAM
[4]    QH←I-I
[5]    RH←0
[6]    T←STEP←DT÷100
[7]    C←1
[8]   LOOP:C←C+2
[9]    D←C+1
[10]   STATETM← 2 2 ⍴GSTM[1;C],GSTM[1;D],GSTM[2;C],GSTM[2;D]
[11]   GAMMA STATETM
[12]   IQ←STEP×(⍉STATETM)+.×Q+.×STATETM
[13]   QH←QH+IQ
[14]   IM←STEP×((⍉GAM)+.×Q+.×STATETM)+M+.×STATETM
[15]   MH←MH+IM
[16]   IR←STEP×R+((⍉GAM)+.×Q+.×GAM)+2×M+.×GAM
[17]   RH←RH+IR
[18]   →(T=DT)/STOP
[19]   T←T+STEP
[20]   →LOOP
[21]  STOP:MH←⍉MH
       ∇
```

Table B-1. continued

```
      ∇RICCATI[□]∇
      ∇ RICCATI
[1]   ⍝ CALCULATES SS P FROM RICCATI EQUATION
[2]    P←QH
[3]    COUNT←0
[4]    ERROR←0.001
[5]   ⍝
[6]    GAMMA STM
[7]    GAMT←⍉GAM
[8]    MT←⍉MH
[9]   LOOP:GPS←MT+.×P+.×STM
[10]   NP←QH+((⍉STM)+.×P+.×STM)-(⍉GPS)+.×(⌹RH+GAMT+.×P+.×GAM)+.×GPS
[11]   COUNT←COUNT+1
[12]   DIFF←NP-P
[13]   P←NP
[14]   A←(|DIFF)>ERROR
[15]   B←+/A
[16]   C←+/B
[17]   →(COUNT=100)/STOPS
[18]   →(C≥1)/LOOP
[19]   →0
[20]  STOPS:'DID NOT CONVERGE ON RICCATI SOLUTION IN 100 ITERATIONS.'
[21]   →0
      ∇
      ∘

      ∇SONETWO[□]∇
      ∇ SONETWO
[1]    S12←-(⌹STM-I)+.×GAM+.×S22
      ∇
      ∘

      ∇STMDYN[□]∇
      ∇ PHI←DT STMDYN A;R;N;FACTOR;INDEX
[1]   ⍝ CALCULATES TRANSITION MATRIX
[2]    R←(⍴,A)*0.5
[3]    I←(⍳R)∘.=⍳R
[4]    N←0
[5]    PHI←I
[6]    FACTOR←I
[7]   L0:N←N+1
[8]    FACTOR←FACTOR+.×A×DT÷N
[9]    PHI←PHI+FACTOR
[10]   INDEX←(+/|,FACTOR)÷R*2
[11]   →(INDEX>EPS)/L0
      ∇
```

Table B-1. continued

```
      ∇STWOTWO[□]∇
      ∇ STWOTWO
[1]   S22←⌹((-HX+.x(⌹(STM-I))+.xGAM)+HU)
      ∇
```

```
      ∇SYSMODEL[□]∇
      ∇ SYSMODEL YD
[1]   A  GIVES RESPONSE OF 2ND ORDER SYSTEM TO INPUT YD
[2]   A  AND STORES TIME HISTORY FOR GRAPHING
[3]   A  NOTE: ANSWER WITH 'NO' IF TABLE IS NOT DESIRED.
[4]    T←ΔQ←TIME←DELU←ΔALPHA←0
[5]    ΔX← 2 1 ⍴ 0 0
[6]    'IS A PRINTED TABLE DESIRED?'
[7]    →('N'=1↑ANS←□)/LOOP
[8]    'TIME                    ΔQ                    ΔALPHA          ΔU'
[9]   LOOP:ΔU←(-(K+.x(ΔX-S12xYD)))+S22+.xYD
[10]   →('N'=1↑ANS)/SKIP
[11]   T,ΔX[1;],ΔX[2;],ΔU
[12]  SKIP:ΔX←(STM+.xΔX)+GAMxΔU
[13]   →(T=5)/STOP
[14]   T←T+DT
[15]   ΔQ←ΔQ,ΔX[1;]
[16]   ΔALPHA←ΔALPHA,ΔX[2;]
[17]   TIME←TIME,T
[18]   DELU←DELU,ΔU
[19]   →LOOP
[20]  STOP:DELU←1↓,DELU
      ∇
```

```
      ∇SYSMOD4[□]∇
      ∇ SYSMOD4 YD
[1]   A GIVES RESPONSE OF 4TH ORDER SYSTEM TO INPUT YD
[2]   A  AND STORES TIME HISTORY FOR GRAPHING
[3]   A  NOTE: ANSWER WITH 'NO' IF TABLE NOT DESIRED.
[4]    T←ΔQ←TIME←DELU←ΔALPHA←ΔGAM←ΔV←0
[5]    ΔX← 4 1 ⍴ 0 0 0 0
[6]    'IS A PRINTED TABLE DESIRED?'
[7]    →('N'=1↑ANS←□)/LOOP
[8]    'TIME       ΔQ            ΔALPHA          ΔU                  ΔV
[9]   LOOP:ΔQALF← 2 1 ⍴ΔX[3;],ΔX[4;]
[10]   ΔU←(-(K+.x(ΔQALF-S12xYD)))+S22+.xYD                        ΔGAM'
[11]   →('N'=1↑ANS)/SKIP
[12]   T,ΔX[3;],ΔX[4;],ΔU[1;],ΔX[1;],ΔX[2;]
[13]  SKIP:ΔX←(STM4+.xΔX)+GAM4xΔU
[14]   →(T=5)/STOP
[15]   T←T+DT
[16]   ΔQ←ΔQ,ΔX[3;]
[17]   ΔALPHA←ΔALPHA,ΔX[4;]
[18]   TIME←TIME,T
[19]   DELU←DELU,ΔU
[20]   ΔV←ΔV,ΔX[1;]
[21]   ΔGAM←ΔGAM,ΔX[2;]
[22]   →LOOP
[23]  STOP:DELU←1↓,DELU
      ∇
```

Table B-1. concluded

There are two separate methods for finding the optimal gains using these functions. The first method involves changing the weighting matrices in the cost functional to obtain the desired response. The sequence for using the APL functions in this manner is given in Fig. B-1. For example, say the gains are to be found for a pitch rate controller using the second-order model given in Eq. 39. It can be specified as a pitch rate controller by letting

$$H_x = [1\ 0] \quad \text{and} \quad H_u = 0 \tag{B-1}$$

The weightings for this example will be

$$Q = \begin{bmatrix} 25 & 0 \\ 0 & 25 \end{bmatrix}, \quad R = 33 \tag{B-2}$$

and a sampling interval of 0.1 sec is used.

The public workspace 3 EIGENVAL is copied for use in calculating eigenvalues from F_{CL}. Following the sequence of Fig. B-1:

```
)APL

      V S  A P L

CLEAR WS
      )LOAD OPTIMAL
SAVED 12:21:33 08/03/78
      )COPY 3 EIGENVAL
SAVED 23:49:23 08/18/77
      •


      F←2 2⍴¯2.08 ¯8.35 1 ¯2
      •

      G←2 1⍴¯12.5 0
      •

      HX←1 2⍴1 0
      HU←0
      •

      I ←IDENT 2
      •

      DT←.1
      •

      STM←.1 STMDTN F
      •



      STM
 0.7784429646  ¯0.6714762106
 0.08041631265  0.7848762696
      •

      GAMMA STM
      •

      GAM
¯1.113699322
¯0.05424770696
      •
```

```
      STWOTWO
      •

      S22
¯0.5004
      •

      SONETWO
      •

      S12
1
0.5
      •


      GENSTM
      •

      R←33
      •

      Q←2 2⍴25 0 0 25
      •

      QMR
      •

      RICCATI
      •

      GAIN
      •

      K
¯0.4264245713  0.3235125049
```

```
      SYSMODEL .1
IS A PRINTED TABLE DESIRED?
YES
TIME                  ΔQ                    ΔALPHA              ΔU
  0                   0                     0                   -0.07650683188
  0.1                  0.0852056068          0.004150320196     -0.04151574802
  0.2                 0.1097769243          0.01236154268      -0.03369436764
  0.3                 0.114679987           0.02035797915      -0.03419052844
  0.4                 0.1136798987          0.02705539419      -0.03678368817
  0.5                 0.1112922323          0.03237228587      -0.03952192871
  0.6                 0.1089129806          0.03650192393      -0.04187248965
  0.7                 0.1069057333          0.03967936074      -0.04375636978
  0.8                 0.1053077085          0.04211403623      -0.04522545477
  0.9                 0.1040650297          0.04397614249      -0.04635777823
  1                   0.1031083829          0.0453991598       -0.04722607982

      FCLOOP
      .

      FCL
-11.45888255    -5.925957372
  1.090881488   -1.958250392
      .

      .001 EIGVAL FCL
-10.72116982    0
 -2.69596312    0
      .

      F4+4 4F-.073 -32.2 0 0 .002 0 0 2 .002 0 -2.08 -8.35
      .
                                                -.002 0 1 -2

      F4
-0.073 -32.2      0        0
 0.002   0        0        2
 0.002   0       -2.08    -8.35
-0.002   0        1       -2
      .
```

```
      G4←4 1ρ0 0 ¯12.5 0
      •


      G4
  0
  0
¯12.5
  0
      •


      ⍝TM4←.1 STMDTN F4
      •

      GAMMA4 STM4
      •

      FCL4
      •


      .001 EIGVAL FCL
¯10.72048909      0
 ¯2.680229258     0
 ¯0.0444667675    0.1392138386
 ¯0.0444667675   ¯0.1392138386
```

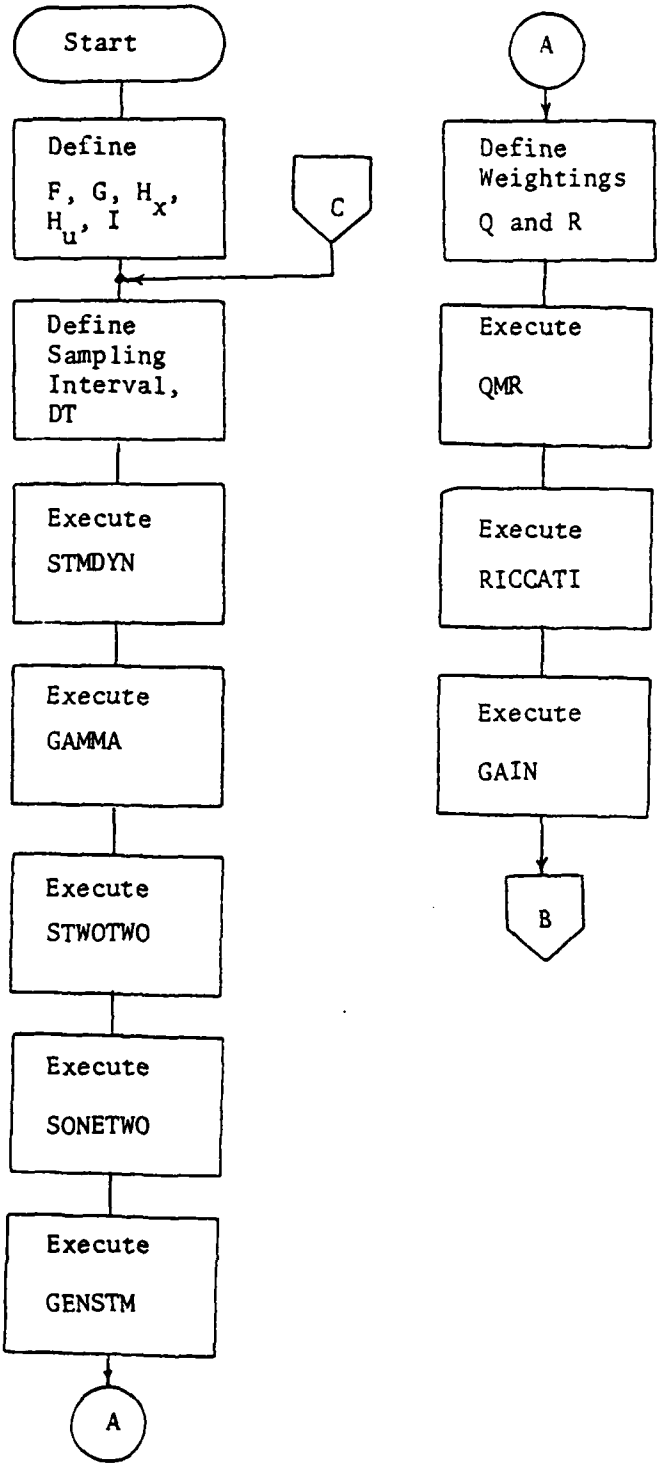

Figure B-1. Sequence for Calculating Gains by Changing Weighting Matrices.

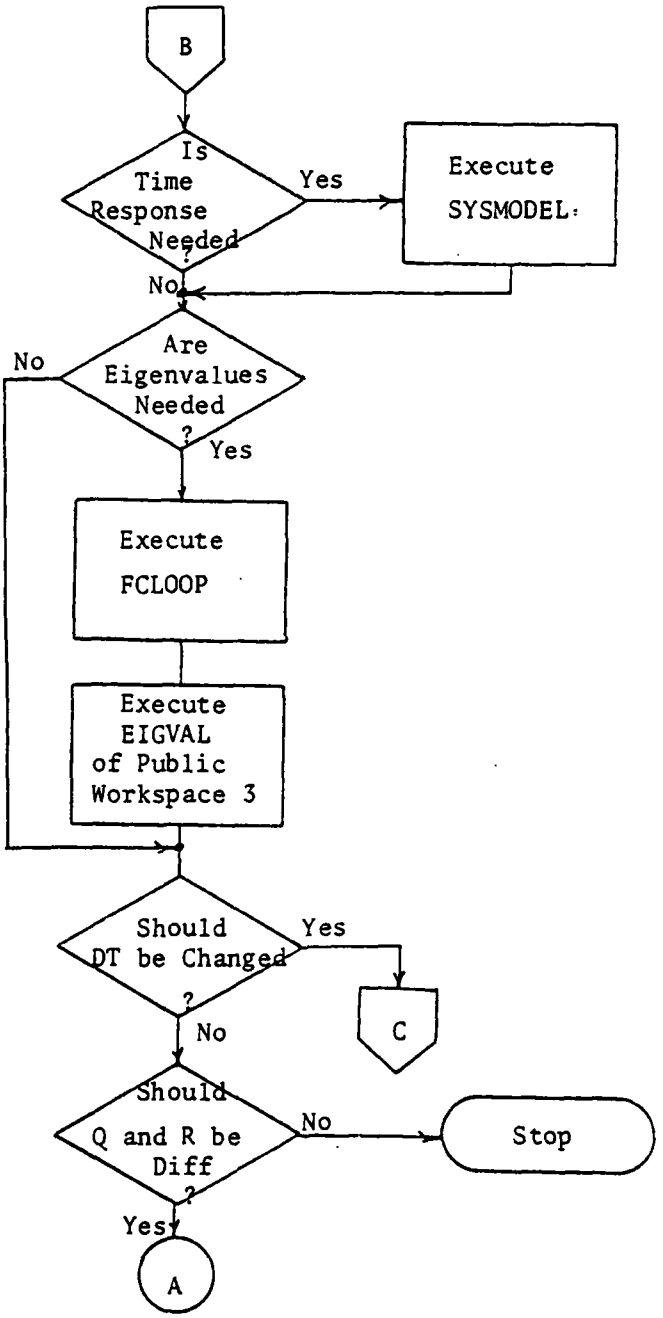

Figure B-1. continued

The second method for calculating gains uses implicit model-following. For instance, say the VRA is to match the short-period modal characteristics of an aircraft with the reduced second-order model

$$\Delta\dot{\underline{x}} = \begin{bmatrix} -.5 & -6 \\ 1 & -2 \end{bmatrix} \begin{bmatrix} \Delta q \\ \Delta\alpha \end{bmatrix} + \begin{bmatrix} M_{\delta_E} \\ 0 \end{bmatrix} \Delta_{\delta_E} \quad . \tag{B-3}$$

A weighting matrix, W, should initially be set to the identity matrix. Following the sequence given in Fig. B-2:

```
F←2 2⍴¯2.08 ¯8.35 1 ¯2
•

G←2 1⍴¯12.5 0
•

FM←2 2⍴¯.5 ¯6 1 ¯2
•

DT←.1
•

STM← .1 STMDYN F
•

GAMMA STM
•

GENSTM
•

W←I
•

FOLLOW
•
```

```
      QMRF
      .

      RICCATI
      .

      GAIN
      .

      K
0.1304705484 0.1334808096

      FCLOOF
      FCL
¯0.5054028136 ¯5.983308109
 1.001310358  ¯2.011826687
      .
```

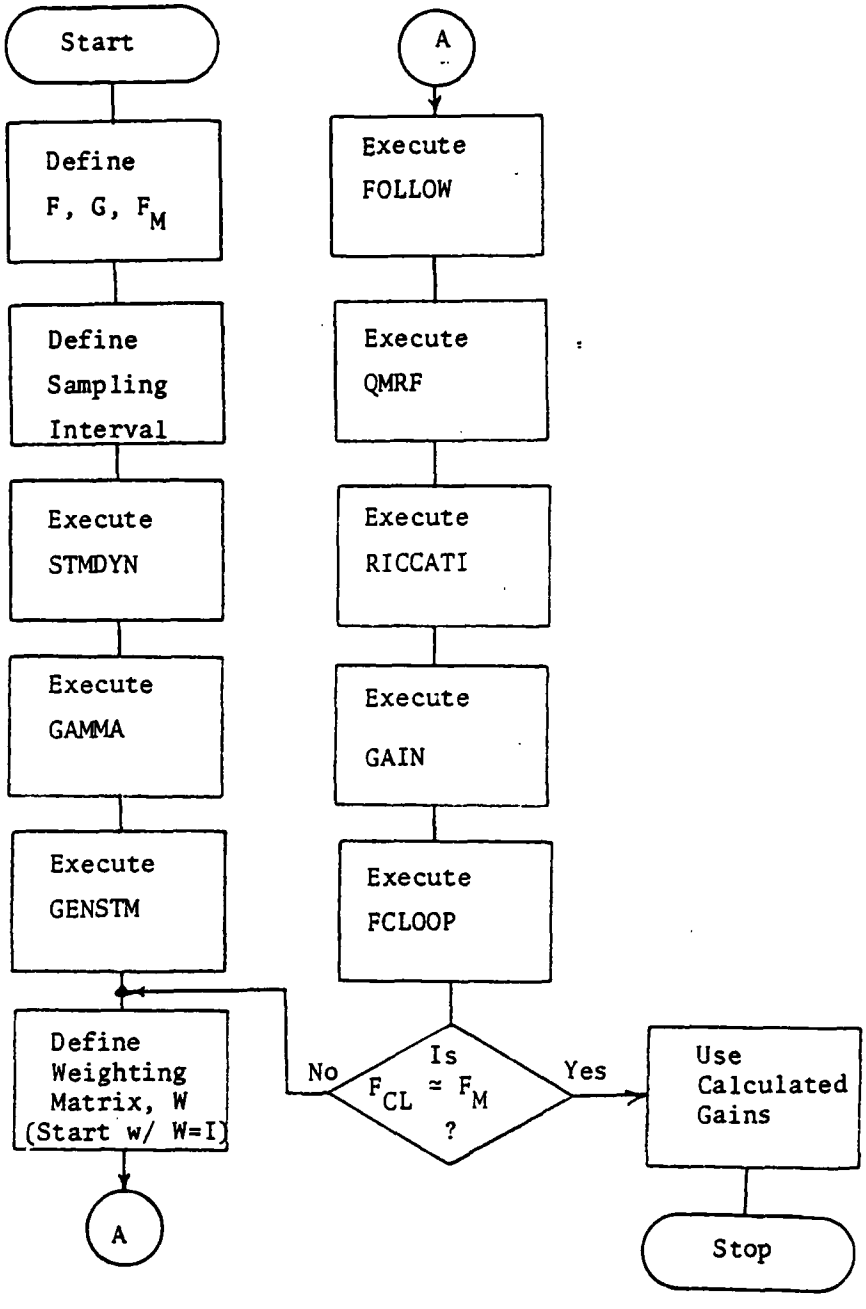

Figure B-2. Sequence for Calculating Gains Using Implicit Model-Following.

APPENDIX C

THE MICRO-DFCS SOFTWARE

C.1 DESCRIPTION OF CAS-1 ROUTINES

The routines of CAS-1 are divided into three categories, depending on their function: Executive, Utility and Flight Control. Each of these routines has detailed documentation included in the source listing consisting of line comments and a header. The header explains the purpose of the routine, how variables should be passed to it, and what parameters of the microcomputer are effected by the routine's execution.

A brief explanation of the major elements of CAS-1 is given below.

EXECUTIVE ROUTINES - Initialization, CDU interface, and one of the three error detection methods are contained in this section (Fig. C-1). INITIALIZATION involves setting up the mathematics unit, the analog board, the parallel I/O ports, the serial port, the hardware interrupt timer, the registers to be used as counters and flags, and clearing storage area in RAM. CDU INTERFACE routine allows the user to set the operation of CAS-1 by inputs from the keyboard. MEMORY CHECK is one of two software error detection methods employed in the program. Every 50 samples, the entire contents of CAS-1 is summed in an 8-bit register (ignoring overflow) and compared to the known sum. If the two differ, some part of

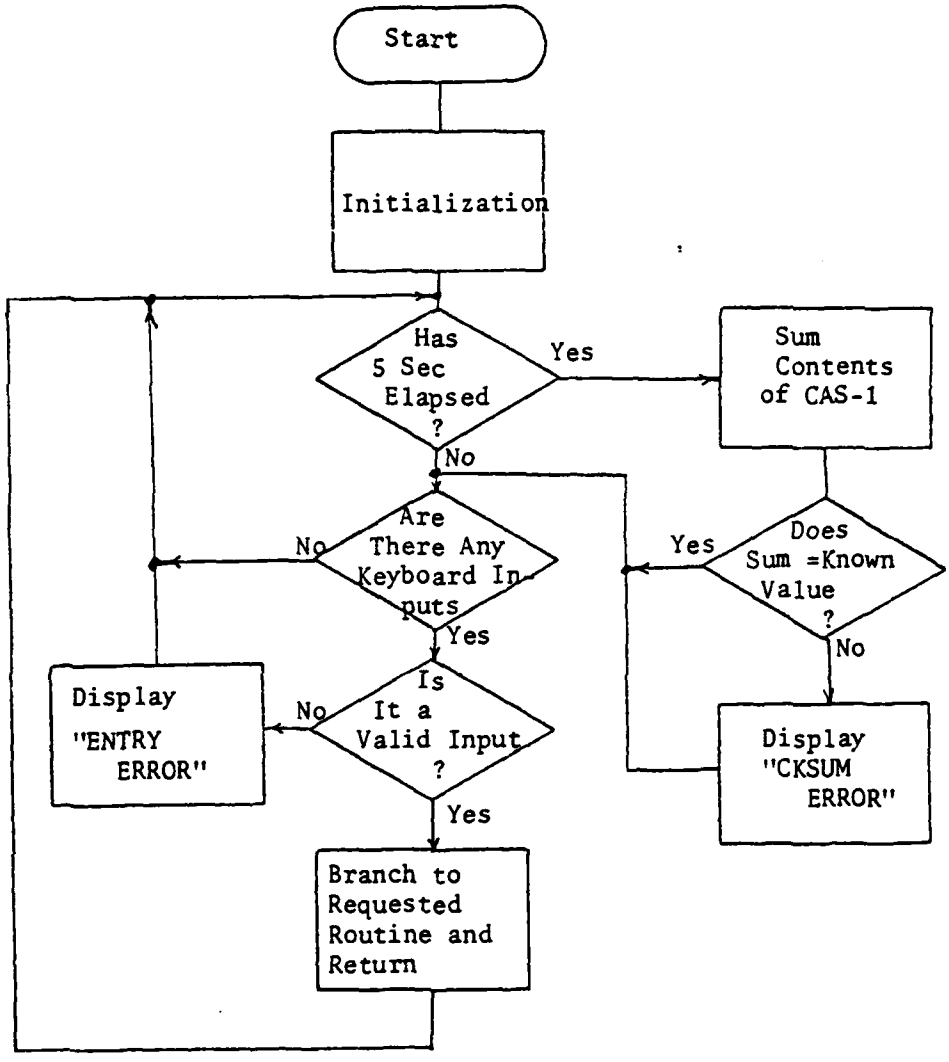

Figure C-1. Flowchart of Executive for CAS-1.

the program has changed; this condition is displayed on the CDU, and sent via telemetry to the ground station.

UTILITY ROUTINES - The routines CLEAR LINE, CONSOLE OUTPUT, NUMERIC INPUT, ENTRY ERROR, and SERIAL OUTPUT are used for displaying and entering data on the CDU. BLINK is part of the hardware error detection method that flashes a light on the safety pilot's instrument panel to indicate that the flight control function of CAS-1 is running. BLINK is called once in every flight control interrupt service routine. ANALOG TO DIGITAL CONVERSION selects the proper analog input channel, initiates the conversion, and stores the results. COUNT-UP DISPLAY generates an increasing sequence of numbers 1-9 (reset each 10 sec) on the bottom line of the CDU. This is to indicate that the hardware interrupt (used for timing purposes) is working, the program has initialized correctly, and the D/A channels are operational. An increasing sequence of voltage outputs from a D/A channel is telemetered to the ground station to indicate in what mode the Micro-DFCS is operating. INTERRUPT COUNT increments a counter every time an interrupt service routine is executed. This counter is used for timing purposes in routines such as MEMORY CHECK (which must execute every 50 samples). LIMIT ANALOG OUTPUT prevents the analog output channels from instantly switching from +10 volts to -10 (or vice versa). This condition occurs when the control law calculates a value for control surface deflection which corresponds to a voltage greater than 10 volts or less than -10 volts. It is due to the method used for converting floating point numbers to fixed point format. This routine was not added until after flight

testing had begun. MODE CHANGE allows the user to select 1 of 20 possible flight control modes. Presently only six modes are defined; four pitch rate command modes with different feedback gains, one normal acceleration command mode, and one direct mode where longitudinal stick is fed directly to the elevator through a stick gearing factor. MATH UNIT DRIVER loads the high-speed mathematics unit with the two arguments to be operated on, initiates the mathematical operation, and stores the results in RAM. It is very general and slow (normally 230 μsec). Therefore, it should not be used for time critical functions; i.e. not in flight control interrupt service routines. MATH ERROR PROCESSOR is the second software error detection method. It is used to check for errors that occur in the mathematics unit (such as divide by zero or an overflow condition). The type of error that has occurred and the number of mathematics unit uses since the last interrupt service routine began execution is displayed on the CDU. The type of error is also sent to the ground station via telemetry. This information should allow the user to find which mathematical operation is causing the problem, should one exist. CALIBRATED STEP INPUT allows the pilot to apply a step input on any one of the analog input channels. After entering the desired step value, the input is initiated by depressing the CDU's "carriage return" key. The step input is nulled by depressing any CDU key.

FLIGHT CONTROL ROUTINES - These are of two types: control set-up routines and the timed interrupt service routines. The control set-up routines are called from MODE CHANGE and set the

parameters necessary for the interrupt service routines to operate. A set-up routine will store the starting location of a service routine in the timed interrupt branch point, and it will set the optimal gains for the control law. A set-up routine will also store the nominal values of all analog inputs for use in calculating perturbation values by the service routine. The microcomputer status channel is set to indicate what flight control mode the computer is executing.

The flight control interrupt service routines are executed on every timed interrupt. They contain the control logic that calculates the control inputs, $\Delta \underline{u}$, for every sampling interval. Once a set-up routine has set the timed interrupt branch point to execute a particular service routine on every timed interrupt, then that service routine has the highest priority over all other routines and will be executed on every timed interrupt, regardless of where the program is running at the time.

The DIRECT INTERRUPT SERVICE ROUTINE takes in commands from longitudinal stick, adds the step bias, multiplies this input by a stick gearing factor, and sends this value to the elevator actuator. The stick gearing used for flight tests was three degrees elevator deflection per inch of longitudinal stick, δ_s, deflection. At 105 KIAS, this corresponds to a steady-state Δq of 5.3 deg/sec per inch or a steady-state Δn_z of 0.52g per inch of δ_s.

The PITCH RATE INTERRUPT SERVICE ROUTINE calculates an elevator command, δ_E, for measured values of δ_s, α, and q. The inputs

must be formatted and scaled before the control law can begin its calculation (Fig. C-2). First the analog voltage signal for a particular input is converted to a 12-bit fixed-point binary number, which is then converted to a 32-bit floating-point representation. The nominal value for the channel (stored by the control set-up routine) is subtracted from the current input value to form the perturbation value. At this point, if a step bias value has been specified for a particular input channel by CALIBRATED STEP INPUT, that value is added to the input. The control law must be calculated with the inputs scaled to the proper units. A scaling factor that converts units of voltage to the proper units of motion is the last step before actual calculation of $\Delta \underline{u}$. In the case of the pilot's inputs, this scaling factor can be thought of as a stick gearing. For $\Delta\alpha$, there is one more scaling to be done that takes into account the difference between the α vane deflection and the aircraft's actual α. The output from the control law is converted from units of radians to volts, converted to fixed-point notation, then converted to an analog voltage, and sent to δ_E.

The control law is calculated using Eq. 22 where the mathematical operations are performed by calling MATH UNIT DRIVER. This mathematics routine is actually too slow and general for calculating the control law. The PITCH RATE INTERRUPT SERVICE ROUTINE takes, on the average, 19 msec to execute including all formating and scaling. The normal acceleration command version of this routine is written not using MATH UNIT DRIVER in order to decrease execution time.

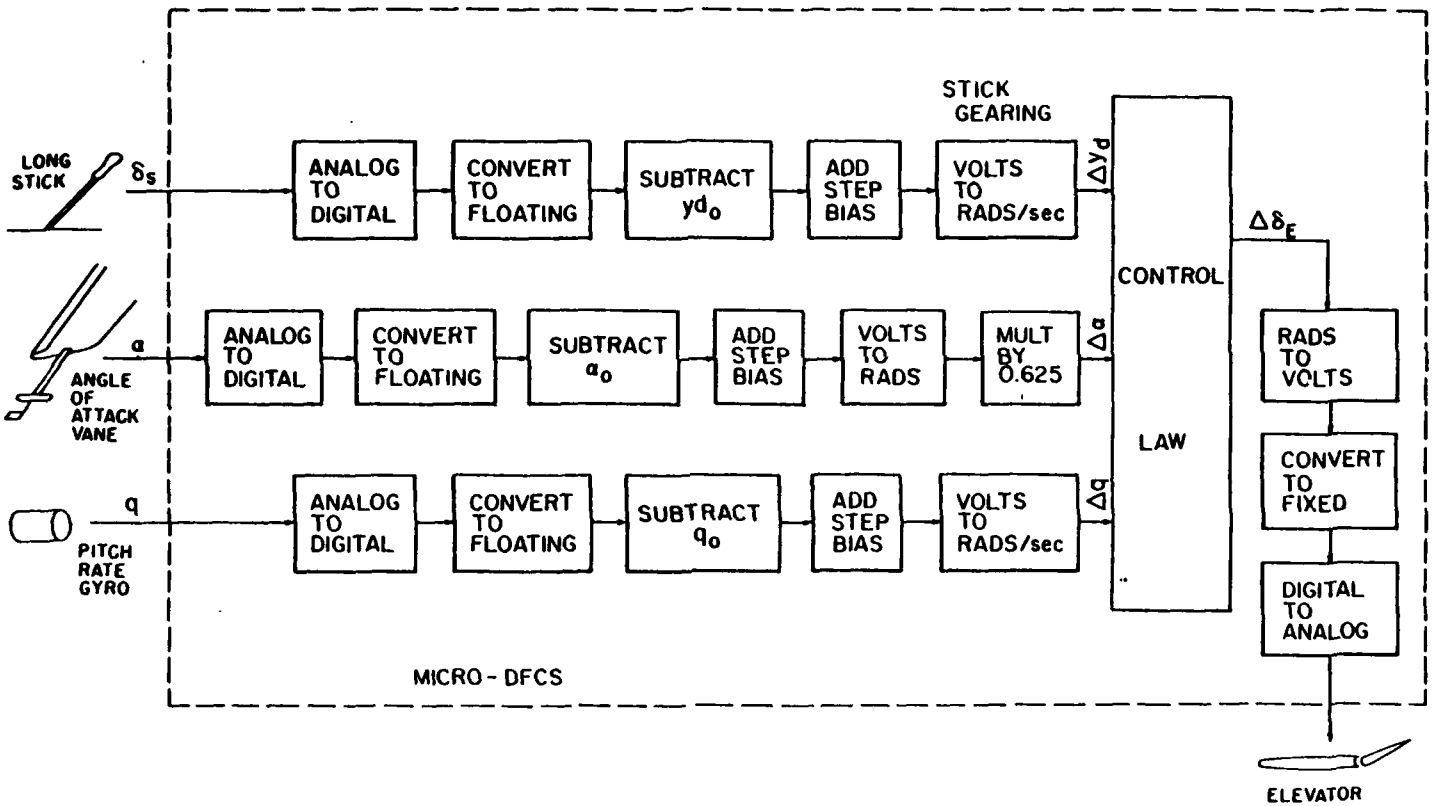

Figure C-2. Formating and Scaling of Sensor and Pilot Inputs.

The NORMAL ACCELERATION INTERRUPT SERVICE ROUTINE calculates a δ_E command for measured values of δ_S, n_z, and q. The task of this routine is similar to the pitch rate service routine, but the method of making calculations is fundamentally different in two ways. First, the MATH UNIT DRIVER is not used to perform the calculations. Instead, this service routine sets up the mathematics unit and initiates the mathematical operations itself. While the mathematics unit is doing the calculation, the service routine gets the next calculation ready. Also, only one argument is loaded to the mathematics unit per calculation because the answer from the last calculation is always used as the second argument. By comparison, MATH UNIT DRIVER always loads two arguments and stores the answer regardless of the next operation to be performed. By not using MATH UNIT DRIVER, this service routine takes more storage but each calculation is speeded up by a factor 1.7 (137 μsec per calculation). The second difference in calculations comes from using a reduced form of Eq. 22 for the control law. The equation can be rearranged to the form

$$\Delta \underline{u}_k = (S_{22} + CS_{12})\, \underline{y}_{d_k} - C\, \Delta \underline{x}_k \qquad \text{(C-1)}$$

For the two-state feedback and single pilot input CAS studied here, this breaks down further to

$$\Delta \delta_{E_k} = c_1\, \Delta \delta_s - c_2\, \Delta q - c_3\, \Delta\, n_z \qquad \text{(C-2)}$$

which only takes five mathematical operations to calculate compared to nine for Eq. 22. By not using MATH UNIT DRIVER and using this for the control law, execution time of the NORMAL ACCELERATION INTERRUPT SERVICE ROUTINE is reduced to 6 msec. PITCH RATE INTERRUPT SERVICE ROUTINE could also be rewritten to run at this speed because it has the same number of calculations as the normal acceleration routine. The scaling factors for the inputs and outputs can be incorporated in the control gains to speed up the service routines even more. This was not done in CAS-1 to help isolate any problems that might have occurred in its initial use.

C.2 SOFTWARE DEVELOPMENT

Each routine for the Micro-DFCS software was developed using the method shown in Fig. C-3. The routines are written in the assembly language for the Intel 8085 CPU. This language consists of 80 different mnemonics that represent the machine operation codes. The assembly language is cross-assembled to the machine language and loaded to the microcomputer for debugging. Initially, the routines are tested separately, i.e., without the other program modules. This procedure helps identify problems that may occur when the routines are combined to operate in the program.

C.3 ADDING FLIGHT CONTROL ROUTINES TO CAS-1

New or modified Flight Control routines can easily be added to CAS-1. The procedure consists of 1) defining a new mode in the Mode Branch Table of CAS-1, 2) writing an appropriate mode set-up

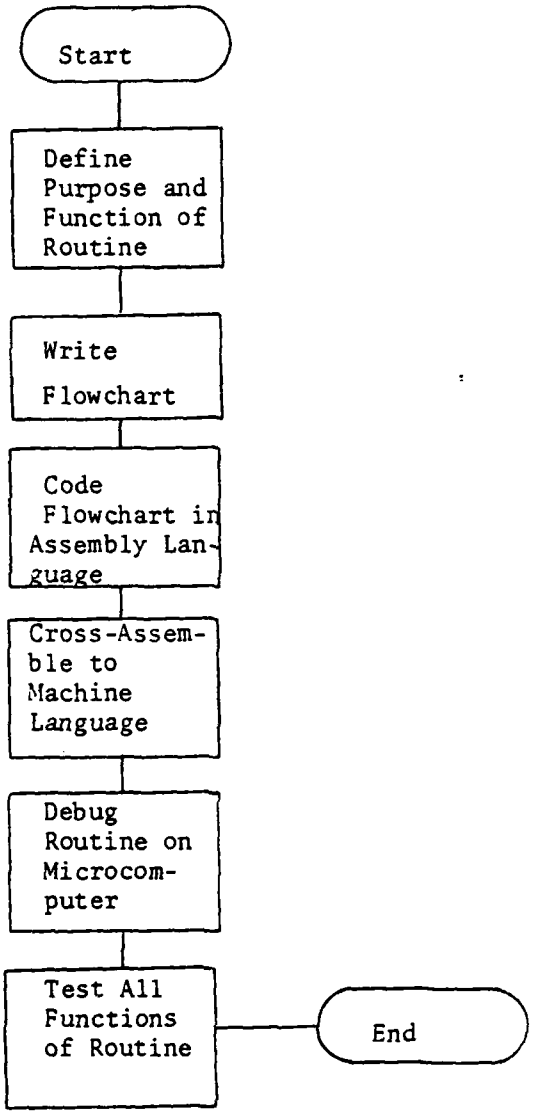

Figure C-3. Sequence for Developing Micro-Computer Routines.

routine, and 3) writing the flight control interrupt service routine in a form that makes it compatible with the operation of CAS-1. Step one is the only modification necessary to the coding of CAS-1. It consists of replacing the operand "BADEN" at the correct location in the Mode Branch Table with the label for the new mode set-up routine.

In the second step, the mode set-up routine is written to set the timed interrupt branch point and store parameters for the interrupt service routine. The branch point for the timed interrupt starts at 3FECH in RAM. A typical mode set-up routine is structured as in Fig. C-4. All registers are saved to insure the routine does not change any parameters for CAS-1. The interrupt is disabled so the interrupt service routine does not execute before the gains and other parameters can be changed. The mode type (e.g. OPEN LOOP, PITCH RATE, etc.) is displayed on the bottom line of the display and a corresponding voltage level is set on the analog status channel. After storage is set for the service routine, all registers are restored and the interrupt is enabled to allow the newly specified service routine to execute on the occurence of each timed interrupt.

The third step of the procedure is to structure the flight control interrupt service routine as shown in Fig. C-5. The interrupt is disabled to guarantee the routine completes before the next service routine starts. All registers are saved because the timed interrupt may break the program flow of CAS-1 at any point, and therefore the status of the program at the break must be saved.

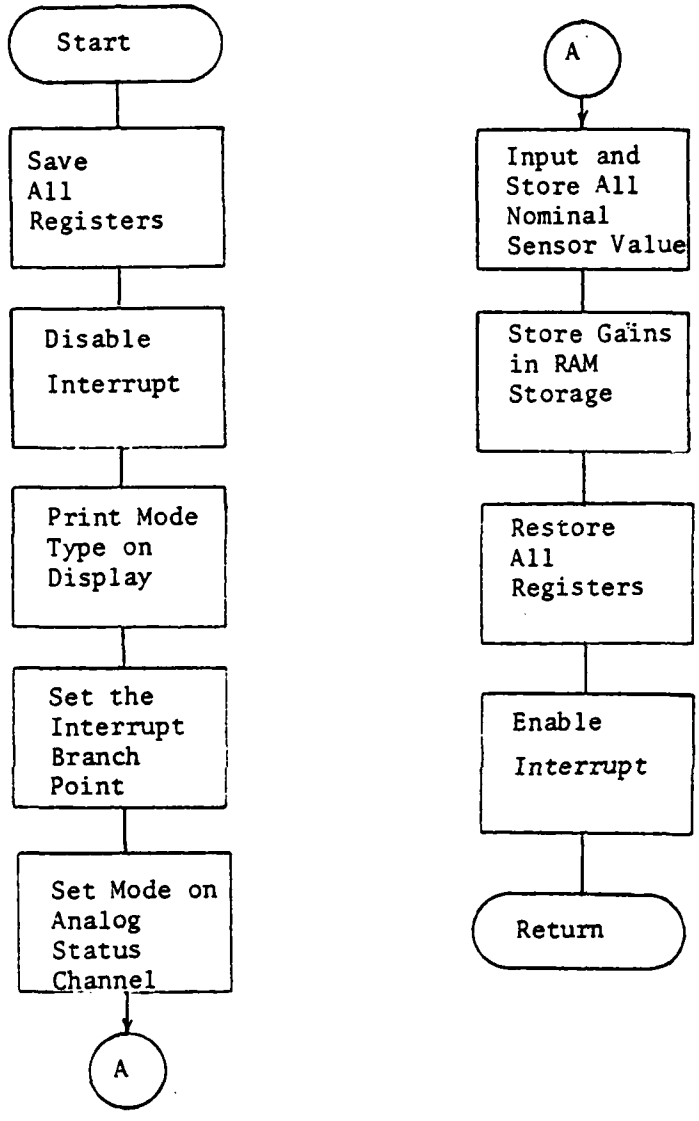

Figure C-4. Flowchart for Typical Mode Set-Up Routine.

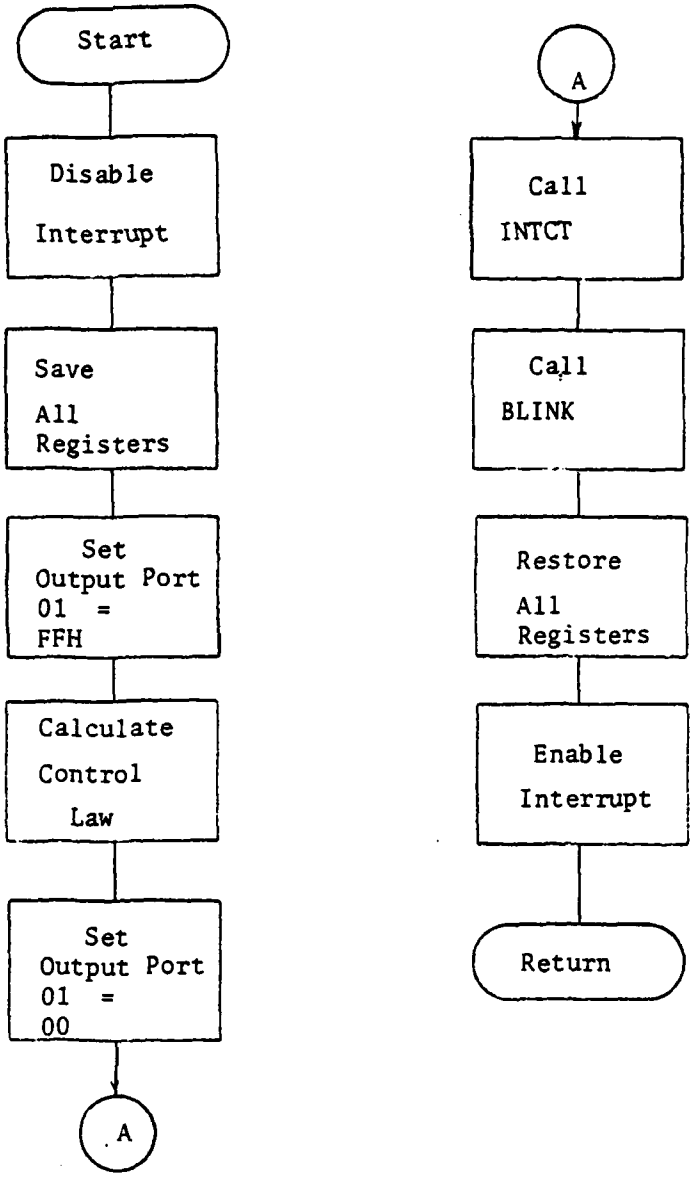

Figure C-5. Flowchart for Typical Flight Control Interrupt Service Routine.

Output port 01 is set to FFH to indicate the start of the control law inputs and calculations. The port is set to 00 to mark the end of the calculations. The time of the calculations can be measured by connecting an oscilloscope to this output port and observing the pulse length. The routine INTCT is called to increment a counter that keeps track of interrupts. The routine BLINK is called to flash the instrument panel light at one-tenth the sampling rate.

There is basically only one restriction on the Flight Control routine for the proper operation of CAS-1. The routine must complete execution within the sampling interval or no other routines will run. In such a case, there would be no available time for keyboard inputs, display outputs, or memory checks. See the CAS-1 source listing (not included in the thesis) for detailed examples of using mode set-up and flight control interrupt service routines.

APPENDIX D

THE MICRO-DFCS HARDWARE

D.1 DESCRIPTION OF MICROCOMPUTER COMPONENTS

In addition to the brief description of the microcomputer equipment given in Chapter 3, the following information is provided. The CPU board has 22 parallel lines of input and output (I/O), 4.5k of memory and one hardware interval timer which may be wired to an interrupt line of the 8085. The timer's time interval may be changed under software control. The mathematics unit does 16- and 32-bit fixed-point and 32-bit floating-point operations, where the typical time needed to do one floating-point operation (including the time to pass arguments to the mathematics unit) is 137 μsec. The mathematics unit provides the computational speed necessary to calculate the control law within the sampling interval. The main memory contains 24K words of RAM and PROM and also provides an interface for the CDU. The battery back-up memory allows programs and data to be stored with the power off for up to 96 hours. This board is used to transfer the microcomputer programs from the software development system to the FCCU mounted in the VRA. The analog I/O boards provide 16 (expandable to 32) input channels and 6 output channels each with 12-bits of resolution. The A/D has a conversion rate of 28KHz and can be interrupt- or software-driven. The CDU provides input for all ASCII characters and can display two lines of 12 characters each.

It is functionally equivalent to a conventional 1200-baud keyboard/ display terminal, although its display is limited, and multiple key strokes are required to enter most characters.

The FCCU consists of the six computer circuit boards and two 4-board cardcages into which the boards plug. It is housed in an RF-shielded, shock-mounted aluminum box. The mount is located in the cockpit behind the two pilots. The FCCU therefore experiences the same environment the pilots do, and no special provisions are made in using these commercially available microcomputer components. The Micro-DFCS components installed in the VRA, including the power supplies, costed approximately $6900 when purchased in February, 1978. There are four cables that interface the FCCU with the rest of the VRA's FBW system. One cable supplies the $\pm$5 and $\pm$12 volts necessary to operate the Intel SBC boards. These voltages are obtained by regulating the VRA's primary 28vdc. A second connector links the CDU to the FCCU. A two-position switch and program monitor light mounted on the pilot's instrument panel each have connections made through a third cable. One position of the switch resets the computer's program counter, and the other position gives the CPU program control. The light is part of an error detection system. When the light flashes at a steady rate, it indicates that the control law is being calculated every sampling interval. The fourth cable supplies the inputs from the motion sensors and pilot controls, and the outputs to the control surface actuators. The voltage range of these signals ($\pm$10v) is compatible with that used by the A/D and D/A converters of the microcomputer.

The status of the Micro-DFCS is output on one of the D/A channels and this information is sent on a telemetry channel. This status channel indicates what control mode is running (if any) and also flags any errors found by the two software error detection methods described in Section 3.2. The telemetered data can be recorded and plotted on a strip chart recorder.

The components of the Micro-DFCS and development system are pictured in Fig. D-1. The FCCU and CDU are at the upper left, resting on the ground chassis and power supply. The keyboard-CRT terminal, acoustic coupler, and telephone extension are to the right of the chassis. A keyboard-printer unit (not shown in Fig. D-1) is used to obtain copies of program listings and other computer output.

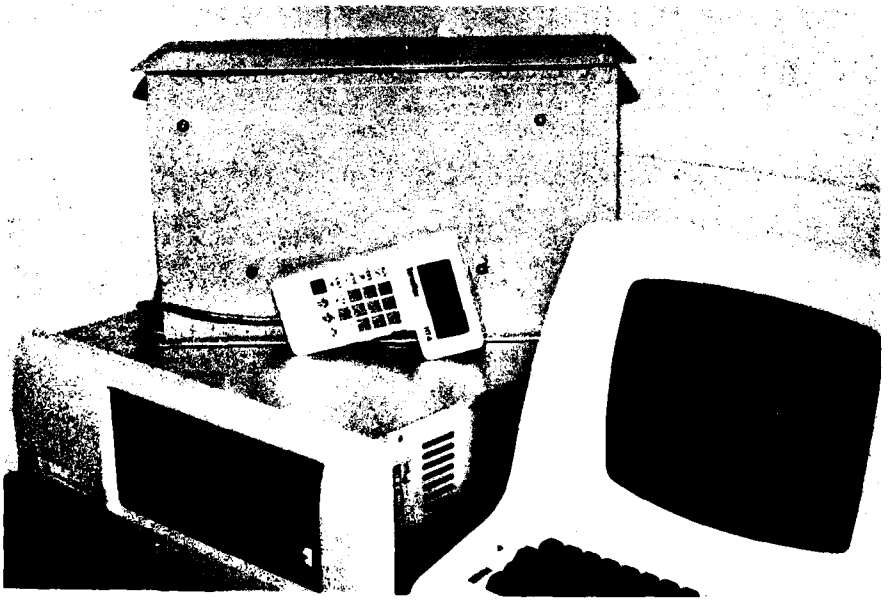

Figure D-1. Components of the Micro-DFCS and Software Development System.

D.2 DIRECTIONS FOR USING CONTROL DISPLAY UNIT

The Control Display Unit (CDU), shown in Fig. D-2, allows the pilot to monitor the Micro-DFCS and input commands. The display is two lines of 12 characters each. The keyboard allows all 128 ASCII characters to be entered; most by multiple key strokes.

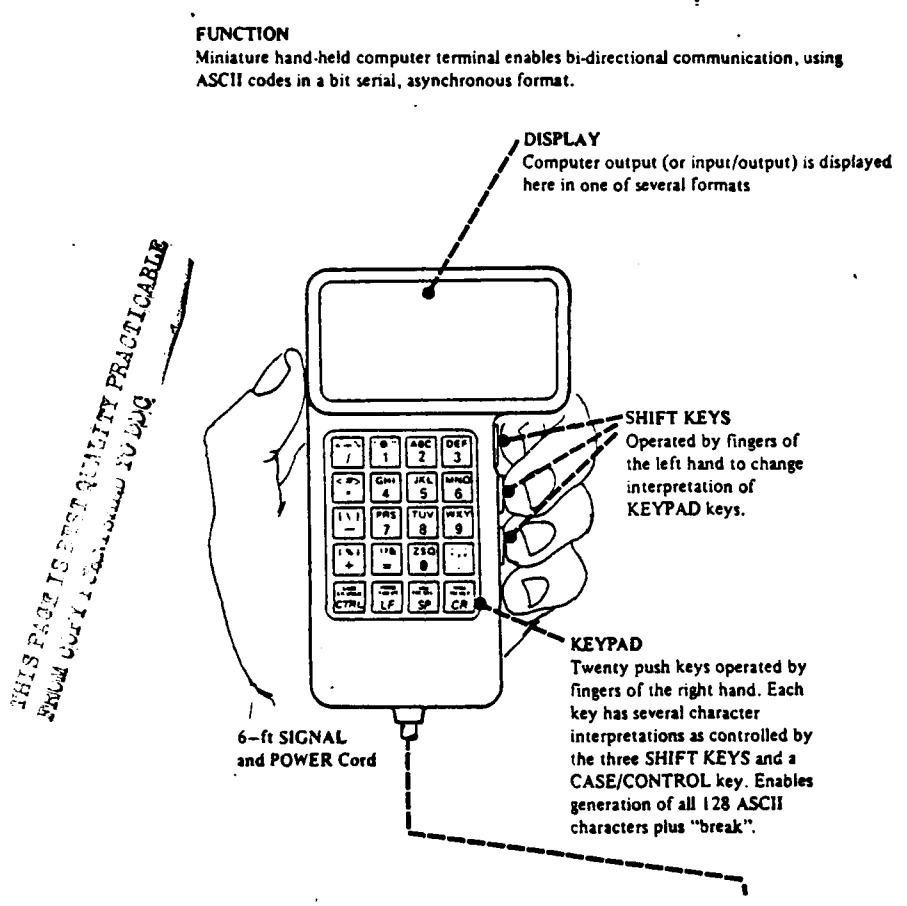

Figure D-2. Control Display Unit (CDU).

There are three levels of entry on the CDU (Fig. D-3). The System Monitor level is entered by flipping the two-position switch on the instrument panel (marked RESET/RUN) to the RUN position. The

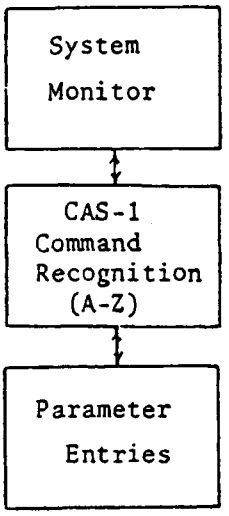

Figure D-3. Levels of Entry on CDU.

CDU display will show "80/05 MON" indicating the first entry level. Any of the normal 80/05 System Monitor commands outlined in the Intel SBC 80P05 User's Guide can be used at this level.

The second level of entry may be entered by jumping to location 8000H. This is accomplished by pressing the keys:

G, 8, 0, 0, 0, CR

where CR is the CDU's "carriage return". This starts execution of CAS-1 and enters the CAS-1 Command Recognition level. Twenty-six different commands may be entered at this level, each selected by pressing a key with a letter of the alphabet. Seven commands are presently defined in CAS-1: HALT, INITIALIZE, MODE CHANGE, STEP INPUT, DELAY, RESOLUTION, AND TIMER.

The third level sets parameters necessary to complete the command entered at the second level. For example, if MODE CHANGE was entered by pressing "M", then the third entry level is automatically set and the next two key strokes will specify which mode is selected (a number 00-19). Once the mode number is entered, then the CDU again operates at the second entry level waiting for another command. STEP INPUT also requires the third entry level after the "S" is pressed. The analog channel to be stepped (00-15) is entered followed by the voltage this channel is to be stepped (in the format ±DD.DD, where D represents some base ten number).

The upper line of the display shows the mode CAS-1 is operating in at all times. In the case where CAS-1 is first entered, the mode is Initialization and the top display line reads "8085 READY". If the mode is changed by using the MODE CHANGE command, the new mode is displayed on the upper line (e.g. "OPEN LOOP", PITCH RATE", or "NORMAL ACC"). The entries made at the second level are displayed on the bottom line. If an entry error is made at any time while using the CDU, "ENTRY ERROR" will be displayed on the bottom line for ten sampling intervals.

To reenter the System Monitor level, the switch on the instrument panel is placed in the RESET position and then back to RUN.

APPENDIX E

DERIVATION OF DISCRETE WEIGHTING MATRICES FROM CONTINUOUS IMPLICIT MODEL-FOLLOWING WEIGHTING MATRICES

The discrete weighting matrices, $\hat{Q}$, $\hat{M}$, and $\hat{R}$ derived in Ref. 12 use the continuous cost functional of Eq. 23. The implicit model-following presented in Section 2.6 calculates Q, M, and R matrices for the continuous cost functional of Eq. 56. In order to use the implicit model-following technique for a digital system, a transformation from Q, M, and R to $\hat{Q}$, $\hat{M}$, and $\hat{R}$ is needed. This relation is derived below with the same assumptions used for the derivations of Ref. 12.

The objective is to minimize the continuous-time cost functional, so it is necessary to find $\hat{Q}$, $\hat{M}$, and $\hat{R}$ that satisfies the relation

$$J = \int_{t_o}^{t_N} [\underline{x}^T(t)\ Q\ \underline{x}(t) + 2\ \underline{u}^T(t)\ M\ \underline{x}(t) + \underline{u}^T(t)\ R\ \underline{u}(t)]dt \qquad \text{(E-1)}$$

$$= \sum_{i=0}^{N-1} \left(\underline{x}_i^T\ \hat{Q}\ \underline{x}_i + 2\ \underline{u}_i^T\ \hat{M}\ \underline{x}_i + \underline{u}_i^T\ \hat{R}\ \underline{u}_i \right)$$

N = number of samples

i = index

given the system dynamics, Q, M, and R. The continuous J can be decomposed into a sum of N integrals:

$$J = \sum_{i=0}^{N-1} \int_{t_i}^{t_{i+1}} (\underline{x}^T Q \underline{x} + 2 \underline{u}^T M \underline{x} + \underline{u}^T R \underline{u}) \quad dt \tag{E-2}$$

where the time dependency is understood. Setting Eq. 64 equal to the bottom line of Eq. 63 and making a substitution with

$$\underline{x}(t) = \Phi(t,t_i) \underline{x}_i + \Gamma(t,t_i) \underline{u}_i \tag{E-3}$$

the derivation proceeds as follows:

$$\begin{aligned} &\underline{x}_i^T \hat{Q} \underline{x}_i + 2 \underline{u}_i^T \hat{M} \underline{x}_i + \underline{u}_i^T \hat{R} \underline{u}_i \\ &= \int_{t_i}^{t_{i+1}} [(\Phi \underline{x}_i + \Gamma \underline{u}_i)^T Q(\Phi \underline{x}_i + \Gamma \underline{u}_i) + 2 \underline{u}_i^T M(\Phi \underline{x}_i + \Gamma \underline{u}_i) \\ &\quad + \underline{u}_i^T R \underline{u}_i] \quad dt \end{aligned} \tag{E-4}$$

$$\begin{aligned} &= \int_{t_i}^{t_{i+1}} (\underline{x}_i^T \Phi^T Q \Phi \underline{x}_i) dt + 2 \int_{t_i}^{t_{i+1}} (\underline{u}_i^T \Gamma^T Q \Phi \underline{x}_i \\ &\quad + \underline{u}_i^T M \Phi \underline{x}_i) dt + \int_{t_i}^{t_{i+1}} [\underline{u}_i^T R \underline{u}_i + \underline{u}_i^T \Gamma^T Q \Gamma \underline{u}_i \\ &\quad + 2 (\underline{u}_i^T M \Gamma \underline{u}_i)] \, dt \end{aligned} \tag{E-5}$$

Because $\underline{x}_i$ and $\underline{u}_i$ are not functions of the integration variable, t, they may be taken outside the integrals. Matching like variables from both sides of the equation we have the desired relation:

$$\hat{Q} = \int_{t_i}^{t_{i+1}} \Phi^T(t,t_i)\ Q\ \Phi(t,t_i)\ dt \qquad \text{(E-6)}$$

$$\hat{M} = \int_{t_i}^{t_{i+1}} [\Gamma^T(t,t_i)\ Q\ \Phi(t,t_i) + M\ \Phi(t,t_i)]\ dt \qquad \text{(E-7)}$$

$$\hat{R} = \int_{t_i}^{t_{i+1}} [R + \Gamma^T(t,t_i)\ Q\ \Gamma(t,t_i) + 2\ M\ \Gamma(t,t_i)]\ dt \qquad \text{(E-8)}$$

REFERENCES

1. Motyka, P. R., Rynaski, E. G., and Reynolds, P. A., "Theory and Flight Verification of the TIFS Model-Following System", Journal of Aircraft, Vol. 9, No. 5, May 1972, pp. 347-353.

2. Gallagher, J. T., Saworotnow, I., Seeman, R., and Gosset, T., "A Model-Following Variable Stability System for the NASA ARC X-14B", Journal of Aircraft, Vol. 9, No. 7, July 1972, pp. 461-469.

3. Stein, G., Hartmann, G. L., and Hendrick, R. D., "Adaptive Control Laws for F-8 Flight Test", IEEE Transactions on Automatic Control, Vol. AC-22, No. 5, Oct 1977, pp. 758-767.

4. Stengel, R. F., Broussard, J. R., and Berry, P. W., "Digital Controllers for VTOL Aircraft", IEEE Transactions on Aerospace and Electronic Systems, Vol. AES-14, No. 1, Jan 1978, pp. 54-63.

5. Tobie, H. N., and Ramby, K. W., "A Practical Solution to Automatic Landings Using Digital Flight Control Computers", AIAA Paper No. 70-1032, Aug 1970.

6. Mathews, M. A., Jr., "SAAB Digital Flight Control", AIAA Paper No. 74-26, Jan 1974.

7. Osder, S. S., Mossman, D. C., and Devlin, B. T., "Flight Test of a Digital Guidance and Control System in a DC-10 Aircraft", AIAA Paper No. 75-567, April 1975.

8. Yechout, T. R., and Oelshlaeger, D. R., "Digitac Multimode Flight Control System", AIAA Paper No. 75-1085, Aug 1975.

9. Rediess, H. A., and McIver, D. E., ed., "Avionics and Controls Research and Technology", NASA CP-2061, 1979.

10. Stengel, R. F., Broussard, J. R., and Berry, P. W., "The Design of Digital-Adoptive Controllers for VTOL Aircraft", NASA CR-144912, March 1976.

11. Stengel, R. F., and Berry, P. W., "Stability and Control of Maneuvering High-Performance Aircraft", NASA CR-2788, April 1977.

12. Dorato, P, and Levis, A. H., "Optimal Linear Regulators: The Discrete-Time Case", IEEE Transactions on Automatic Control, Vol. AC-16, No. 6, Dec. 1971, pp. 613-620.

13. Mrazek, J. G., and Rubertus, D. P., "Considerations in the Design of a Digital Flight Control Function for a High Performance Aircraft", NAECON '74 Record, Dayton, June 1974.

14. Berman, H., and Gran, R., "Design Principles for Digital Autopilot Synthesis", Journal of Aircraft, Vol. 11, No. 7, July 1974, pp. 414-422.

15. Anderson, B. D. O., and Moore, J. B., Linear Optimal Control, Prentice-Hall, Inc., Englewood Cliffs, 1971.

16. Harvey, C. A., and Stein, G., "Quadratic Weights for Asymptotic Regulator Properties", IEEE Transactions on Automatic Control, Vol. AC-23, No. 3, June 1978, pp. 378-387.

17. Anon., "Flying Qualities of Piloted Airplanes", MIL-F-8785B(ASG), USAF/USN, August 1969.

18. Tyler, J. S., Jr., "The Characteristics of Model-Following Systems as Synthesized by Optimal Control", IEEE Transactions on Automatic Control, Vol. AC-9, No. 4, Oct 1964, pp. 485-498.

19. Harper, R. P., Jr., and Cooper, G. E., "The Use of Pilot Rating in the Evaluation of Aircraft Handling Qualities", NASA TND-5153, April 1969.

DISTRIBUTION LIST

Office of Naval Research
800 N. Quincy St.
Arlington, VA 22217
D. Siegel, Code 211 4
S. L. Brodsky, Code 432 1

Office of Naval Research
Branch Office
495 Summer Street
Boston, MA 02210 1

Office of Naval Research
Branch Office
536 South Clark St.
Chicago, IL 60605 1

Office of Naval Research
Branch Office
1030 E. Green St.
Pasadena, CA 91106 1

Naval Research Laboratory
Washington, DC 20375
Code 2627 3

Naval Air Systems Command
Washington, DC 20361
G. Tsaparas, AIR 340D 1
R. C. A'Harrah, AIR 53011 1

Naval Air Development Center
Warminster, PA 18974
C. R. Abrams, Code 6072 1
C. Mazza, Code 6053 1

Naval Material Command
Washington, DC 20360
Code 08T23 1

Naval Weapons Center
China Lake, CA 93555
B. Hardy, Code 3914 1

Naval Surface Weapons Center
Silver Spring, MS 20910
J. Wingate, Code R44 1

Naval Air Test Center
Antisubmarine Aircraft
Test Directorate
Patuxent River, MD 20670
R. Detrick 1

Naval Air Test Center
Strike Aircraft Test Directorate
Patuxent River, MD 20670
W. Branch 1

Naval Coastal Systems Center
Hydromechanics Division
Panama City, FL 32407
D. Humphreys, Code 794 1

David Taylor Naval Ship R&D Center
Bethesda, MD 20084
Technical Library 1

Naval Post Graduate School
Monterey, CA 93940
Technical Reports Library 1

Defense Technical Information
Center
Building 5
Cameron Station
Alexandria, VA 22314 12

Air Force Office of Scientific
Research
Building 410
Bolling Air Force Base
Washington, DC 20332
C. L. Nefzger 1

Air Force Flight Dynamics Laboratory
Wright-Patterson Air Force Base
Dayton, OH 45433
R. Anderson, Control Dyn. Br. 1
F. George, Control Dyn. Br. 1

Army Armament R&D Command
Building #18
Dover, NJ 07801
N. Coleman, DRDAR-SCFCC 1

NASA Langley Research Center
Hampton, VA 23665
Technical Library 1

Scientific Systems, Inc.
Suite No. 309-310
186 Alewife Brook Parkway
Cambridge, MA 02138
R. K. Mehra 1

Systems Technology, Inc.
13766 South Hawthorne Blvd.
Hawthorne, CA 90250
R. Whitbeck 1

The Analytic Sciences Corp.
6 Jacob Way
Reading, MA 01867
C. Price 1

University of Michigan
Dept. of Naval Architecture &
Marine Engr.
Ann Arbor, MI 48109
M. G. Parsons 1

Nielsen Engineering & Research, Inc.
510 Clyde Ave.
Mountainview, CA 94043
J. N. Nielsen 1

University of Notre Dame
Dept. of Electrical Engineering
Notre Dame, IN 46556
M. K. Sain 1

The C. S. Draper Laboratory, Inc.
555 Technology Square
Cambridge, MA 02139
R. V. Ramnath 1

Honeywell, Inc.
Systems and Research Center
2600 Ridgway Parkway
Minneapolis, MN 55413
C. A. Harvey 1

Calspan Corp.
P. O. Box 400
Buffalo, NY 14225
E. G. Rynaski 1

Systems Control Inc.
1801 Page Mill Road
Palo Alto, CA 94306
E. Hall 1

National Transportation Safety
Board
Bureau of Technology
Laboratory Services Division
800 Independence Ave., S.W.
Washington, DC 20594
R. von Husen 1